Pharmacological modulation of inflammation in mouse models of experimental diabetic retinopathy

Inaugural Dissertation

zur

Erlangung des Doktorgrades

Dr.nat.med.

der Medizinischen Fakultät

und

der Mathematisch-Naturwissenschaftlichen Fakultät

der Universität zu Köln

vorgelegt von

Urbanus Muthai Kinuthia

aus Machakos, Kenia

Hundt druck GmbH, Köln

2024

Betreuer:	Prof. Dr. Thomas Langmann
Referenten:	Prof. Dr. Henning Walczak
	Prof. Dr. Gunther Döhlemann
Datum der mündlichen Prüfung:	15.04.2024

Dedicated to my dear parents, Boniface and Theresia Kinuthia, my brother Joseph and my sister Ann.

"*Research is to see what everybody else has seen, and to think what nobody else has thought*." - Albert Szent-Györgyi

SUMMARY

Microglia are the immune sentinels of the central nervous system including the retina, where they play crucial roles in innate immunity and maintenance of retina CNS tissue homeostasis. Mild reactivity of microglia is important in mounting an inflammatory response, termed parainflammation, which is an important function of tissue macrophages. However, chronic activation of microglia due to sustained tissue stress leads to dysfunction of microglia-specific immune checkpoints, which aggravates cell reactivity with increased secretion of cytokines and chemokines. The overt activation of microglia is a key feature of retinal degenerative diseases and ocular retinopathies including diabetic retinopathy (DR). Indeed, mounting evidence in mice and human patients has shown that neuroinflammation precedes the clinically detectable microvascular complications of DR. This highlights microglia, resident immune macrophages of the retina, not only as drivers of inflammation but also as targets for therapeutic intervention. Indeed, immunomodulation of microglia reactivity has been studied in various degenerative diseases of the eye and showed improved disease outcomes. However, immunomodulation had not been studied in the models of neural and vascular complications reminiscent of human DR where loss of pericytes is associated with breakdown of the blood retina barrier. The PDGFB/PDGFRβ signalling is vital for adequate pericyte coverage of endothelial cells, proper retention of PDGFB in retinal endothelium. However, the lack of adequate disease models that recapitulate key features of human disease has precluded understanding of the cellular and molecular factors of DR.

Therefore, the aim of the present study was to investigate whether pharmacological modulation of inflammation with minocycline limits disease progression and confers protection to the retina. Minocycline is a second-generation tetracycline that has anti-inflammatory effects besides its use as a bacteriostatic drug. Moreover, this thesis aimed at identifying the cellular and molecular phenotype of activated microglia and its response to minocycline during disease pathogenesis.

By using mouse models of attenuation of the PDGFB/PDGFRβ signalling in the postnatal retina, we show that microglia reactivity is an early feature of the disease and it was sustained in the mature mouse retina. The early activation of microglia was associated with an inflammatory gene signature marked by CCL2, TSPO, LGALS3, AIF-1 and morphological changes reflecting an inflammatory state. Minocycline effectively downregulated the expression of microglia activation factors and angiogenic factors including VEGFA, ICAM-1 and PGF. Transcriptomic analyses of the mature retina of the pericyte inhibition model revealed FGF2, EDN2, GLYCAM-1, AIF-1 and CASP-1 as key inflammatory factors in the late stage of disease. In the mature retinas of the PDGFB depletion model, we observed an

upregulation of VEGFA, FGF2, TSPO, LGALS3 and VWF. Besides reactive gliosis, leaky vasculature was observed in the mature mouse retinas. Notably, minocycline suppressed the expression of the inflammatory and angiogenic factors, reduced reactive gliosis and limited microglia activation and migration into the nuclear layers and subretinal space. Furthermore, we show that minocycline mediates its protective effect, at least in part, at a transcriptional level by downregulation of STAT3. Taken together, the present findings show that treatment with minocycline dampened microglia reactivity attenuated retinal inflammation and microvascular abnormalities in mice with an ocular phenotype reminiscent of diabetic retinopathy.

ZUSAMMENFASSUNG

Mikroglia sind ein zentraler bestandteil des angeborenen Immunsystems im Zentralnervensystem, einschließlich der Netzhaut, wo sie eine entscheidende Rolle bei der Aufrechterhaltung der Homöostase des Nervengewebes spielen. Eine milde Reaktivität der Mikroglia ist wichtig für die Einleitung einer Entzündungsreaktion, die als Parainflammation bezeichnet wird und eine wichtige Funktion von Gewebsmakrophagen ist. Eine chronische Aktivierung der Mikroglia durch anhaltenden Gewebestress führt jedoch zu einer Fehlfunktion der mikroglia-spezifischen Immun-Checkpoints, was wiederum mit einer erhöhten Sekretion von Zytokinen und Chemokinen einhergeht. Die Aktivierung von Mikroglia ist ein Hauptmerkmal von degenerativen Erkrankungen der Netzhaut und anderen neuronalen Vaskulopathien, einschließlich der diabetischen Retinopathie (DR). In der Tat gibt es immer mehr Beweise bei Mäusen und Patienten, dass die Neuroinflammation den klinisch erkennbaren mikrovaskulären Komplikationen der DR vorausgeht. Dies macht deutlich, dass die Mikroglia, die in der Netzhaut ansässigen Immunmakrophagen, nicht nur Entzündungen auslösen, sondern auch Ziele für therapeutische Maßnahmen darstellen. In der Tat wurde die Immunmodulation der Mikroglia-Reaktivität bereits bei verschiedenen degenerativen Augenerkrankungen untersucht und zeigte eine Verbesserung des Krankheitsverlaufs. Die Immunmodulation wurde jedoch nicht in Modellen für neurale und vaskuläre Komplikationen untersucht, die die menschliche DR erinnernnachbilden, bei der der Verlust von Perizyten mit einem Zusammenbruch der Blut-Retina-Schranke verbunden ist. Der PDGFB/PDGFRβ-Signalweg ist entscheidend für eine angemessene Ummantelung der Endothelzellen durch Perizyten und die korrekte Retention von PDGFB im Netzhautendothel. Das Fehlen geeigneter Krankheitsmodelle, die die wichtigsten Merkmale der menschlichen Erkrankung rekapitulieren, hat jedoch bisher das Verständnis der zellulären und molekularen Faktoren der DR verhindert.

Ziel der vorliegenden Studie war es daher zu untersuchen, ob die pharmakologische Modulation der Entzündung mit Minocyclin das Fortschreiten der Krankheit eindämmt und der Netzhaut Schutz bietet. Minocyclin ist ein Tetracyclin der zweiten Generation, das neben seiner Verwendung als bakteriostatisches Medikament auch entzündungshemmende Wirkungen hat. Darüber hinaus zielte diese Arbeit darauf ab, den zellulären und molekularen Phänotyp der aktivierten Mikroglia und ihre Reaktion auf Minocyclin während der Krankheitsentstehung zu identifizieren.

Anhand von Mausmodellen, bei denen der PDGFB/PDGFRβ-Signalweg in der postnatalen Netzhaut gestört wurde, zeigen wir, dass die Mikroglia-Reaktivität ein frühes Merkmal der Krankheit ist und in der reifen Mausnetzhaut erhalten bleibt. Die frühe Aktivierung der

Mikroglia war mit einer entzündungsassoziierten Gensignatur verbunden, die durch CCL2, TSPO, LGALS3, AIF-1 und morphologische Veränderungen gekennzeichnet war, die einen entzündlichen Zustand widerspiegeln. Durch Minocyclin wurde die Expression von Mikroglia-Aktivierungsfaktoren und angiogenen Faktoren wie VEGFA, ICAM-1 und PGF wirksam herunterreguliert. Transkriptomische Analysen der reifen Netzhaut des Perizyteninhibitionsmodells ergaben FGF2, EDN2, GLYCAM-1, AIF-1 und CASP-1 als wichtige Entzündungsfaktoren im Spätstadium der Erkrankung. In den reifen Netzhäuten des PDGFB-Depletionsmodells beobachteten wir eine Hochregulierung von VEGFA, FGF2, TSPO, LGALS3 und VWF. Neben reaktiver Gliose wurden in den reifen Mäusenetzhäuten auch undichte Gefäße beobachtet. Minocyclin unterdrückte die Expression der entzündlichen und angiogenen Faktoren, reduzierte die reaktive Gliose und begrenzte die Aktivierung der Mikroglia und ihre Migration in die Körnerschichten und den subretinalen Raum. Darüber hinaus zeigen wir, dass Minocyclin seine schützende Wirkung zumindest teilweise auf transkriptioneller Ebene durch die Herunterregulierung von STAT3 vermittelt. Insgesamt zeigen die vorliegenden Ergebnisse, dass die Behandlung mit Minocyclin die Mikroglia-Reaktivität dämpfte und die Entzündung der Netzhaut sowie die mikrovaskulären Anomalien bei Mäusen mit einem okulären Phänotyp, der die diabetische Retinopathie nachbildet, verringerte.

TABLE OF CONTENTS

List of Tables

List of Figures

List of abbreviations and acronyms

AIF1	Allograft inflammatory factor 1
ANGPT2	Angiopoietin 2
ANOVA	Analysis of variance
APB5	rat-anti-mouse platelet derive growth factor (clone APB5)
BRB	Blood retinal barrier
C1qa	Complement component 1q subunit a
C4b	Complement component 4b
CCL2	Chemokine ligand 2
CD31	Cluster of differentiation 31
Clec7a	C-Type lectin domain containing 7A
CNS	Central nervous system
DME	Diabetic macula edema
DR	Diabetic retinopathy
ECs	Endothelial cells
EDN2	Endothelin 2
FA	Fluorescein angiography
FGF2	Fibroblast growth factor 2
GCL	Ganglion cell layer
GFAP	Glial fibrillary acidic protein
GS	Glutamine synthatase
GYLCAM1	Glycosylation-dependent cell adhesion molecule 1
IB4	Isolectin b4
Iba1	Ionized calcium-binding adapter molecule 1
ICAM1	intercellular cell adhesion molecule 1
iECKO	inducible endothelial cell conditional knock out
IgG	Immunoglobulin G
IL-1β	Interleukin 1 beta
INL	Inner nuclear layer
iNOS	inducible nitric oxide synthase
IPL	Inner plexiform layer

ISH	In situ hybridization
LGALS3	Galectin 3
Mino	Minocycline
NFL	Nerve fiber layer
NG2	Nerve glial antigen 2
ONL	Outer nuclear layer
OPL	Outer plexiform layer
OS	Outer segments
PCs	Pericytes
PDGFB	Platelet derived growth factor polypeptide B
PDGFRβ	Platelet derived growth factor receptor beta
PGF	Placental growth factor
RGCs	Retinal ganglion cells
ROS	Reactive oxygen species
RPE	Retinal pigment epithelium
SD-OCT	Spectral domain-optical coherence tomography
SEMA3G	Semaphorin 3G
SPP1	Secreted phosphoprotein 1
SRS	Subretinal space
STAT	Signal transducer and activator of transcription
TNF-α	Tumor necrosis factor-α
TNF-α	Tumor necrosis factor alpha
TSPO	Translocator protein (18 kDa)
VEGF	Vascular endothelial growth factor
vSMCs	Vascular smooth muscle cells

1. INTRODUCTION

1.1 Diabetic Retinopathy

Diabetic retinopathy (DR) is a complication of diabetes mellitus (DM) and a leading cause of vision loss. Diabetes mellitus is one of the world's fastest growing chronic diseases with an estimated prevalence of 1 in 11 adults. Hyperglycemia, a hallmark of DM, activates the production of advanced glycation end products (AGE), hypoxia and a cascade of pathways leading to damage of the microvasculature in the inner retina (Mengstie et al., 2022; Xu et al., 2018). The consequences are occlusions of capillaries, which cause circulatory disorders in the retina. In addition, the microvasculature may become permeable and lead to hemorrhage in the retina (Figure 1). There are two main classes of diabetic retinopathy: nonproliferative and proliferative. Nonproliferative diabetic retinopathy (NPDR) is the early stage of the disease, characterized by vascular hyperpermeability, retinal hemorrhage, capillary obstruction, hard exudates, basement membrane thickening and loss of pericytes. Pericyte loss has consequences on capillary remodeling and may be responsible for the initial abnormalities in the diabetic retina that can be detected clinically. Proliferative diabetic retinopathy (PDR) is an advanced stage characterized by pathological neovascularization, vitreous hemorrhage and retinal detachment leading to vision loss. A key pathologic feature that manifests itself in both NPDR and PDR is diabetic macula edema (DME) characterized by fluid accumulation in the neural retina and retinal thickening. DME is a consequence of the breakdown of the blood-retina barrier (BRB) and is the most common cause of vision loss among DR patients (Duh et al., 2017). DME and PDR are vision-threatening endpoints of diabetes linked to prolonged duration of disease and poor glycemic control.

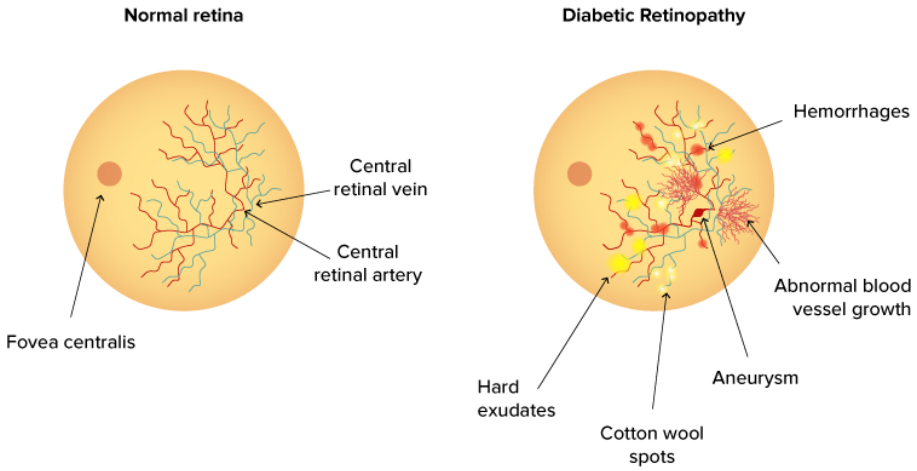

Figure 1: Schematic representation of healthy human eye versus clinical manifestation of diabetic retinopathy. Image source: https://afamilyoptician.co.uk/diabetic-retinopathy/

Although type 1 DM is a predisposing factor for the development of DR, type 2 DM is the most common underlying disorder that leads to DR among the working-age population globally. In

2019, the International Diabetes Federation estimated the global diabetes prevalence at 9.3%, representing 463 million people and expected to affect 700 million people by 2045 (Saeedi et al., 2019; Sun et al., 2022). Furthermore, the most recent global estimate on the prevalence of DR stands at 22.7% with the global burden expected to remain high through 2045 (Teo et al., 2021). Prevention of diabetic retinopathy includes controlling blood sugar levels, maintaining a healthy blood pressure, and not smoking. Regular eye exams are also crucial for early detection and treatment.

The existing treatment options for DR include laser photocoagulation of leaky aneurysms and anti-vascular endothelial growth factor (VEGF) therapy, which is effective in regressing retinal neovascularization. Unfortunately, these treatment options are not beneficial to 40-50% of the patients thus necessitating the search for additional therapeutic options that would benefit the remaining patients (Duh et al., 2017; Glassman et al., 2020; Wells et al., 2016). Although DR has been traditionally regarded as a microvasculature complication, mounting evidence suggests that changes in the neural retina precede retinal microvasculopathy (Jonsson et al., 2016; Lynch & Abràmoff, 2017; Sohn et al., 2016). The scientific focus has now shifted towards the retinal neurons and glia, particularly retinal microglia.

1.2 The Retina

The retina is the light-sensitive part of the eye that receives light photons and converts them to electrical signals that are relayed to the brain through the optic nerve. The mammalian retina consists of approximately 60 functionally distinct cell types (Masland, 2001). Just like other tissues of the central nervous system (CNS), a majority of these cells are neurons (Masland, 2001). Structurally, the retina is well organized into 10 layers comprising three nuclear layers separated by two synaptic layers also known as the plexiform layers. The nuclear layers namely; the ganglion cell layer (GCL), inner nuclear layer (INL) and outer nuclear layer (ONL) whereas the plexiform layers are the inner plexiform layer (IPL) and outer plexiform layer (OPL). The murine retina is well characterized and extensively utilized in studying developmental and pathologic angiogenesis and thus invaluable in the understanding and development of therapies for vision-threatening human diseases (Stahl et al., 2010). Although the murine retina lacks a macula, it possesses some structural feature including increased photoreceptor density in that correspond to the peripheral part of the human macula (Volland et al., 2015).

1.3 Retinal vascularization and blood-retina barrier formation

Neurovascular unit (NVU) refers to the intricate coupling of neurons and vascular cells. The term NVU was first applied to the blood-brain barrier and later to the retina (Gardner & Davila, 2017; Metea & Newman, 2007). In the retina, the NVU is composed of several neuronal cell

types (horizontal cells, bipolar cells, ganglion cells and amacrine cells, glia (microglia, Müller and astrocytes) and vascular cells (pericytes, endothelial cells and vascular smooth muscle cells). Endothelial cells form the tube structure of capillaries that are then covered by pericytes. The development of the primary vascular plexus of the mouse retina is associated with the astrocyte endfeet that emerge from the optic nerve (Huxlin et al., 1992; Watanabe & Raff, 1988). In this process, the tip endothelial cells express filopodia which they use to migrate and guide capillary outgrowth along the pre-existing astrocyte template (Dorrell et al., 2002). The astrocytes in the avascular retina highly express vascular endothelial growth factor (VEGF-A) which controls angiogenesis (Provis et al., 1997). Indeed, similar research established that VEGF is a guiding cue for angiogenesis following the endothelial tip concept (Gerhardt et al., 2003). Other factors such as VEGF-C have also been shown to contribute to angiogenesis through binding to their receptors VEGFR2/3, which are expressed on the surface ECs.

The formation of an extensive vascular network requires repetitive steps of sprouting and tube formation (Phng & Gerhardt, 2009; Roca & Adams, 2007). This angiogenic process is tightly controlled and not all the ECs acquire vascular sprouting properties. Only a subset of ECs at the vascular front sprouts whereas the other stalk cells are committed to maintenance of structural integrity of vessels formed. The endothelial tip cells express a distinct molecular signature that is different from ECs on other parts of the vasculature. For example, PDGFB, Apelin, delta-like 4 (DLL4), VEGFR2, CXCR4, ESM1 and netrin receptor Unc5b are highly expressed on the endothelial tip cells (Blanco & Gerhardt, 2013; Chow & Gu, 2017; De Bock et al., 2013; Fruttiger, 2007; Rocha et al., 2014; Strasser et al., 2010).

Although genetic signals such as the Notch1 and VEGF signalling are known to control vessel sprouting and migration of superficial tip cells (Blanco & Gerhardt, 2013), it has also been demonstrated that ECs rely on ATP produced via glycolysis for vessel formation. Indeed, phosphofructokinease-2/fructose-2,6-bisphosphatase 3 (PFKFB3), an isoenyzyme of PFKFB and glycolytic regulator is known to control the formation of tip cell filipodia and directional migration in association with F-actin (De Bock et al., 2013). However, the mechanisms guiding vascular sprouting into the deep layers of the retina are not well known.

Unlike in humans where the retina is vascularized during embryonic development, the formation of the superficial plexus in mice begins at postnatal day 1 (P1) with a radial outgrowth of vessels from the optic nerve to the periphery. At P7, the capillaries start growing vertically into the deep plexus and lastly, the intermediate plexus, completing the vascularization of the three retinal layers at P12. The intermediate plexus is formed within the inner plexiform layer whereas the deep plexus forms within the outer plexiform layer (Stahl et al., 2010).

Both vasculogenesis and angiogenesis are complex biological processes that rely on cellular associations with adhesive substrates and regulatory molecules. These substrates include cadherins and integrin while the factors include growth factors and receptors, extracellular matrix proteins, cell-cell and cell-matrix receptors and angiopoietins (Rupp & Little, 2001). Genetic changes in some of these factors and molecules may lead to embryonic death as has been demonstrated with gene deletion studies (Carmeliet et al., 1996; Ferrara et al., 1996; Fong et al., 1995; Radice et al., 1997). Cadherins are vital for cell-cell adhesion whereas integrins are involved in cell-matrix adhesion. Although their effects seem different, it was demonstrated with inducible and endothelial-specific gene targeting that beta 1 (β1) integrin controls the localization of vascular endothelial cadherin (Ve-cadherin) and thereby vessel stability (Yamamoto et al., 2015). In addition, another protein, α-Parvin was shown to be indispensable for vascular sprouting and vessel integrity. Endothelial-specific deletion of α-Parvin in mice results in embryonic lethality characterized by hemorrhage and hypovascularization (Fraccaroli et al., 2015; Pitter et al., 2018). Also, the loss of α-Parvin leads to an elevated RhoA and Rho-kinase-mediated signalling, stimulation of myosin light chain II and actomyosin hypercontraction in vascular smooth muscle cells (vSMCs) (Montanez et al., 2009; Qi et al., 2020).

Ve-cadherin belongs to the family of classical cadherins and its expression is specific to ECs. As an endothelial-specific adhesion molecule located at the junction of ECs, its promoter may be used to target the vascular endothelium of transgenic mice (Gavard, 2014; Gory et al., 1999). Ve-cadherin is important for maintaining EC contacts, regulating cellular processes like proliferation and apoptosis and functionality of the VEGFR2. The mechanisms that control the adhesive properties of Ve-cadherin also regulate EC permeability and leukocyte extravasation (Lagendijk & Hogan, 2015; Vestweber, 2008). Ve-cadherin is also known to regulate signalling by limiting the nuclear translocation of β-catenin and factors involved in cell transcription (Giampietro et al., 2015; McCrea et al., 2015). Furthermore, Ve-cadherin acts as a master regulator of endothelial cell-cell junctions by its regulation of mRNA levels and localization of claudin-5 and N-cadherins among other junctional proteins (Giampietro et al., 2012; Taddei et al., 2008). Although Ve-cadherin is not directly involved in vessel sprouting, its loss or absence in mice leads to death at mid-embryonic development due to disassembly of nascent vessels (Crosby et al., 2005; Vittet et al., 1997). Inducible inactivation of the *Cdh5* gene encoding Ve-cadherin in the murine retina was found to enhance angiogenic sprouting (Abraham et al., 2009). Furthermore, studies using gain and loss of function in mutant mice revealed that binding of p120-catenin to the cytoplasmic tail of Ve-cadherin is paramount for vessel stability (Grimsley-Myers et al., 2020). Ve-cadherin harbors three distinct tyrosine phosphorylation sites, Y758, Y685 and Y731 (Potter et al., 2005; Wallez et al., 2007). Phosphorylation of Y658

and Y685 occurs in veins but not in arteries and it is mainly driven by hemodynamic forces (Orsenigo et al., 2012). Phosphorylation of Y658 leads to the displacement of p120 catenin bound to Ve-cadherin, whereas, the inflammatory cytokine and VEGFA-triggered phosphorylation of Y685 and Y731 regulate vascular leakage and leukocyte extravasation, respectively (Conway et al., 2017; Wessel et al., 2014). In a recent study, the tyrosine-protein kinase Yes was identified as essential for EC junction plasticity and barrier integrity through the regulation of phosphorylation of Ve-cadherin (Jin et al., 2022). Indeed, sufficient retention of Ve-cadherin in EC junctions is essential to maintain EC junction plasticity, pericyte coverage of ECs and blood-retina barrier integrity.

1.4 Mural cells

Mural cells include non-endothelial vessel-associated cells such as vSMCs and pericytes. They play critical roles in the regulation of growth and homeostasis of both embryonic and adult vasculature. During development, mural cells regulate vascular growth and maturation via secretion of factors such as fibroblast growth factor (FGF), VEGF, and transforming growth factor beta (TGFβ). In adult CNS, brain and retina, mural cells maintain vascular integrity, and vascular tone thereby regulating blood flow.

1.4.1 Pericytes

Pericytes are produced during embryonic development and postnatal lifespan (Winkler et al., 2011). Ontogenically, pericytes are ascribed to possess both mesenchymal and neuroectodermal origin. In the retina, pericytes cover capillaries and share the same basement membrane with ECs. Pericytes are recruited to growing ECs via the PDGFB/PDGFRB paracrine signalling. Mechanistically, PDGFRβ-expressing pericytes are attracted to PDGFB-secreting ECs (Lindahl et al., 1997). Even though pericytes are required at the initial angiogenic steps of retinal vascularization, they are paramount for stabilizing the vasculature and maintaining a functional BBB and BRB. Pericytes are more abundant in the retina than in other tissues and organs in the body. It is estimated that the ratio of pericytes to ECs in the retina is 1:1, clearly showing the need for a tight BRB in a region of high blood flow. During developmental angiogenesis, PDGFRβ is predominantly expressed by pericytes and may be detected with various molecular markers. However, in the adult retina, PDGFRβ is less or hardly detectable. Although there exists no pan-pericyte marker, several markers including nerve glial antigen 2 (NG2), PDGFRβ, αSMA, and desmin, have been shown to detect pericytes as reviewed elsewhere (Pfister et al., 2013; Trost et al., 2019). Although PDGFRβ and NG2 have been used successfully for the identification of pericytes on retinal capillaries *in vivo* (Trost et al., 2013), aSMA identifies pericytes and vSMCs *in vitro* but does not identify pericytes *in vivo* (Hill et al., 2015; Trost et al., 2013). That implies the existence of antigen

variation *in vitro* and *in vivo* and the need for at least two markers for the identification of pericytes. Furthermore, the location of pericytes on ECs is also beneficial for the discrimination of pericytes from vSMCs. Inadequate coverage of capillaries by pericytes may result in microaneurysms and leaky vasculature. Indeed, pharmacological inhibition or genetic ablation of PDGF-B or PDGFRβ at embryonic or postnatal development leads to a significant reduction in mural cell coverage, vessel dilation and hemorrhage reminiscent of DR (Ogura et al., 2017; D. Y. Park et al., 2017). However, Park and colleagues demonstrated that neither loss of PDGF-B nor pericyte depletion in the adult retina leads to pericyte detachment or retinal vascular leakage, respectively (D. Y. Park et al., 2017).

1.4.2 PDGFB/PDGFRβ signalling

The PDGFB/PDGFRβ signalling in pericytes in the brain and retina is critical for the formation and maintenance of BBB and BRB, respectively. PDGF-B belongs to the PDGF family of growth factors implicated in angiogenesis, vascular inflammation, organogenesis, tissue fibrosis and carcinogenesis as described elsewhere (Andrae et al., 2008). The PDGF family has four members, PDGF-A, PDFG-B, PDGF-C and PDGF-D encoded by four different genes. In this family, only PDGF-A and PDGF-B polypeptides have been studied extensively. The four polypeptide chains assemble into homo- or heterodimer via disulfide bonds, and five isomers have been documented, PDGF-AB, PDGF-BB, PDGF-CC, PDGF-DD (Fredriksson et al., 2004). The polypeptide chains contain a highly conserved growth factor domain and an N- and C-terminal that regulate the biological activity of each factor. The growth factor domain is also denoted as the PDGF/VEGF domain composed of almost 100 amino acids with eight conserved cysteine residues that form a motif via disulfide linkage of the polypeptides (Fredriksson et al., 2004).

During development, PDGFB is prominently expressed in the microvascular endothelium and its retention is paramount for attraction and organization of pericytes in the retina (Lindblom et al., 2003). The sprouting ECs secrete PDGFB that acts as a mitogen and creates a concentration gradient thereby attracting PDGFRβ expressing mural cells. It's worth noting that pericytes may be initially recruited in the absence of PDGFB but they fail to increase in density and population and thus fail to cover the microvessels (Armulik et al., 2005; Hellström et al., 1999). Therefore, the PDGFB/PDGFBRβ signalling is not only fundamental for the recruitment of pericytes but also for the migration expansion of the pericyte pool along blood vessels during angiogenesis.

1.5 Microglia in the central nervous system

Microglia are the tissue-resident macrophages of the CNS including brain, spinal cord and retina. Microglia are embryonically derived from the yolk sac and restore their populations by

self-renewal (Ginhoux et al., 2010; Kierdorf et al., 2013). Although microglia first enter the murine brain and retina at embryonic day E8.5 – 9.5 and E11.5, respectively (Ginhoux et al., 2010; Santos et al., 2008) a second wave of microglia colonization of the brain and retina has been documented just before the anatomical completion of the blood-brain and retina barriers (L. Chen et al., 2002; De et al., 2018). Within the CNS, microglia play critical roles in the maintenance of CNS tissue homeostasis and responding to infection and injury and participate in both innate and adaptive immune responses in the CNS. In the healthy brain and retina, microglia are constantly surveilling the brain parenchyma and retina tissue using their long arm-like processes/protrusions. The development and survival of microglia within the CNS are dependent on several factors including the interferon regulatory factor 8 (IRF8), colony-stimulating factor 1 receptor (CSF1R) and transcription factor Spi-1 Proto-oncogene (PU.1) (Kierdorf et al., 2013). The CSF1R signalling is vital for the survival and maintenance of microglia because mice lacking the receptor have reduced populations of microglia and other tissue macrophages. It was recently reported that microglia occupy the brain by clonal expansion of highly proliferative microglia progenitors and that specific clones have different expansion capacities (Barry-Carroll et al., 2023).

1.5.1 Microglia in the developing retina

Microglia enter the retina during the differentiation of retina neurons: photoreceptors, bipolar cells, amacrine cells, horizontal cells and retinal ganglion cells. Microglia cells comprise 0.2% of the retinal cell population and occur alongside two other glial cells; Müller cells and astrocytes (Schlamp et al., 2013). Upon maturation, the retinal neurons are strategically ordered into the three cellular and two synaptic layers of the mature retina whereas microglia occupy the synapse layers. The retinal synapse begins to form at around E17 as an immature IPL where microglia are localized (Sernagor et al., 2001) until postnatal day 3 (P3) when microglia are also observed in the ganglion cell layer. At P7, the OPL is formed and becomes occupied by microglia and at P10, both retinal synapse layers are refined. During the developmental phase, microglia reside in the nerve fiber layer/ganglion cell layer, the synapse layers, and the inner nuclear layer but not the outer nuclear layer. Within the synapse layers, microglia actively participate in synaptic pruning. Indeed, the number of postnatal microglia in the IPL and OPL correlates with the extent of synapse pruning, with microglia numbers increasing in the first postnatal week to reach twice as much of those in adult retinas by P7 (Santos et al., 2008). Once the synapses are fully refined, microglia steadily reduce in number until the third postnatal week (Nikodemova et al., 2015) and maintain a unique pattern within the IPL and OPL. A fine balance of proliferation and apoptosis-driven microglia refinement is paramount to achieving region-specific cell densities within the retina.

1.5.2 The role of microglia in retinal vascularization

The entry of microglia into the retina precedes the formation of the vascular network and blood-retina barrier. In mice, unlike in humans, the retinal vasculature develops postnatally beginning postnatal day 1 (P1) when the hyaloid vessels sprout from the optic nerve, through the primitive vitreous to reach the anterior segment. The hyaloid vessels regress by regulated apoptosis to allow the formation of intraretinal vasculature preceded by an astrocyte network (Fruttiger, 2002). The apoptosis of endothelial cells of the hyaloid vessels is coordinated by microglia via the WNT signalling in the murine retina (Lobov et al., 2005). Although microglia are immune sentinels of the retina, during development, they participate in non-immune functions including the modulation of angiogenesis within the CNS (Checchin et al., 2006; Hattori, 2023). In the developing retina, microglia associate with endothelial tip cells and are thought to act as cellular chaperones for blood vessels in the tissue (Checchin et al., 2006; S. Chen et al., 2017; Fantin et al., 2010). The role of microglia in modulating angiogenesis has been highlighted in studies that have shown that either genetic or pharmacological depletion of microglia during postnatal life negatively impacted retinal vascular area and vascular density, a phenomenon rescued with the introduction of exogenous microglia into the vitreous (Checchin et al., 2006; Kubota et al., 2009).

1.6 Microglia in health and disease

In the healthy retina, microglia inhabit the retinal plexiform layers (IPL and OPL) from where they continually scan the retinal microenvironment with their long ramified extensions (Karlstetter et al., 2015). Microglia express an array of cell surface receptors including Toll-like receptor (TLR), Fc receptors (FcR), Dectin-1, complement receptors, Fractalkine receptor (CX3CR1), triggering receptor expressed on myeloid cells 2 (TREM2), mer tyrosine kinase (MerTK) and scavenger receptors that can bind specific ligands to exert desired effects (Fan et al., 2022; Rathnasamy et al., 2019). Microglia respond to tissue insults with a morphological and functional transformation into reactive phagocytes. This immunological change is termed microglia reactivity. In response to retina tissue injury, stress or disease-associated molecular patterns (DAMPs), microglia retract their protrusions, enlarge their cell bodies and migrate to the site of injury or danger. This mild activation is termed parainflammation, it is aimed at maintaining homeostasis and tissue function, and it is tightly regulated.

There exist several immune checkpoints to prevent mild inflammation from progressing to overt activation of microglia. For instance, microglia express the CD200R, CX3CR1 and transcription factors Mef2C and MeCP2 which activate a cellular signalling process aimed at modulating their reactivity (Deczkowska et al., 2018; Lauro et al., 2019; Wolf et al., 2013). However, under pathological conditions, immune checkpoint signalling becomes

counterproductive and microglia cells become overtly activated and lose their potential to resolve inflammation. Microglia seem to sense the prevailing disturbance as a new homeostatic state, accordingly readjust their phenotype, and increase their immune surveillance. In these chronic conditions, microglia assume the phenotype observed in aging. In the retina, activated microglia can traverse the INL and ONL and occupy the subretinal space (SRS) and retinal pigment epithelium (RPE) thereby phagocytosing healthy photoreceptors. The conversion of microglia phenotype from the homeostatic state (physiological) to the activated state (pathological) has resulted in a shift in their nomenclature. While homeostatic and activated microglia have traditionally been classified as M1 and M2, respectively, this naming has been challenged recently owing to the spatiotemporal transcriptional changes of microglia during development, adulthood and aging (Paolicelli et al., 2022).

During the onset and progression of retinal diseases such as wet and dry age-related macula degeneration (AMD) dysregulated innate immunity involving the complement system, inflammasome activation and activated microglia become key components of disease pathology. Indeed, sustained tissue stress owing to retinal vascular and degenerative diseases correlates with chronic inflammation of microglia with concomitant secretion of pro-inflammatory cytokines and mediators of inflammation (Kinuthia et al., 2020; Rashid et al., 2019). Additionally, drusen which accumulates in AMD patients' eyes is a trigger of inflammasome activation in macrophages and myeloid cells, corroborating the link between mononuclear cell activation in AMD (Doyle et al., 2012). Furthermore, drusen deposits in the RPE in AMD trigger chronic inflammation within the SRS and serve as a chemoattractant of microglia cells into the SRS and activation of the complement system. Indeed, activated microglia cells have been detected next to drusen in dry and wet AMD patients (Garcia-Garcia et al., 2022; Gupta et al., 2003).

1.6.1 Microglia in retinopathies

Ocular vasculopathies including DR, retinopathy of prematurity (ROP) and neovascular AMD are major causes of irreversible blindness. Although these diseases differ in their etiology, they share a common feature: immune cell activation. Previous studies in animal models and humans have shown that the inflammatory component and neurodegeneration in DR precede clinically detectable microvascular changes of the disease (Sohn et al., 2016). In human patients of ROP, activated mononuclear phagocytes were detected in the vitreous alongside complement factors (Rathi et al., 2017). ROP in infants has also been associated with inflammation characterized by elevated levels of IL-6 and TNF-α during postnatal (Hellgren et al., 2018).

In ischemic regions of oxygen-induced retinopathy (OIR), a model of ROP, microglia cells secrete IL-1β which triggers a cycle of microglia activation causing microvascular damage through secretion of semaphoring 3A by retinal ganglion cells (Rivera et al., 2013). Further studies in the OIR model have shown that a receptor-interacting protein-3 ($Rip3^{+}$) subpopulation of microglia advances retinopathy through the release of fibroblast growth factor 2 (FGF2) under hypoxia (He et al., 2021). Indeed, necroptosis in retinal microglia has been demonstrated to promote inflammation and neurodegeneration in retinopathy (Z. Huang et al., 2018, 2023). More recently, lactylation of the Yin-Yang-1 (YY1) transcription factor in retinal microglia has been shown to promote angiogenesis via the upregulation of FGF2 (X. Wang et al., 2023).

The hyperglycemic microenvironment in DR is implicated in the activation of retinal microglia. Indeed, activated microglia in the outer retina and SRS were observed in retinal sections from human donor samples of DR patients (Zeng et al., 2008). Hyperglycemia is known to activate nuclear translocation of hypoxia-inducible factor-1 (HIF-1) and the activation of the ERK1/2-NF-kB pathway in microglia (Z. Yu et al., 2016; Zhang et al., 2019). The activation of microglia in DR is associated with the secretion of pro-inflammatory factors (IL-6, IL-1β, TNF-α, CCL-2) and pro-angiogenic factors (VEGF, PGF) that contribute towards loss of the BRB function and proliferative pathology in the retina (Kinuthia et al., 2020) as illustrated in Figure. 2.

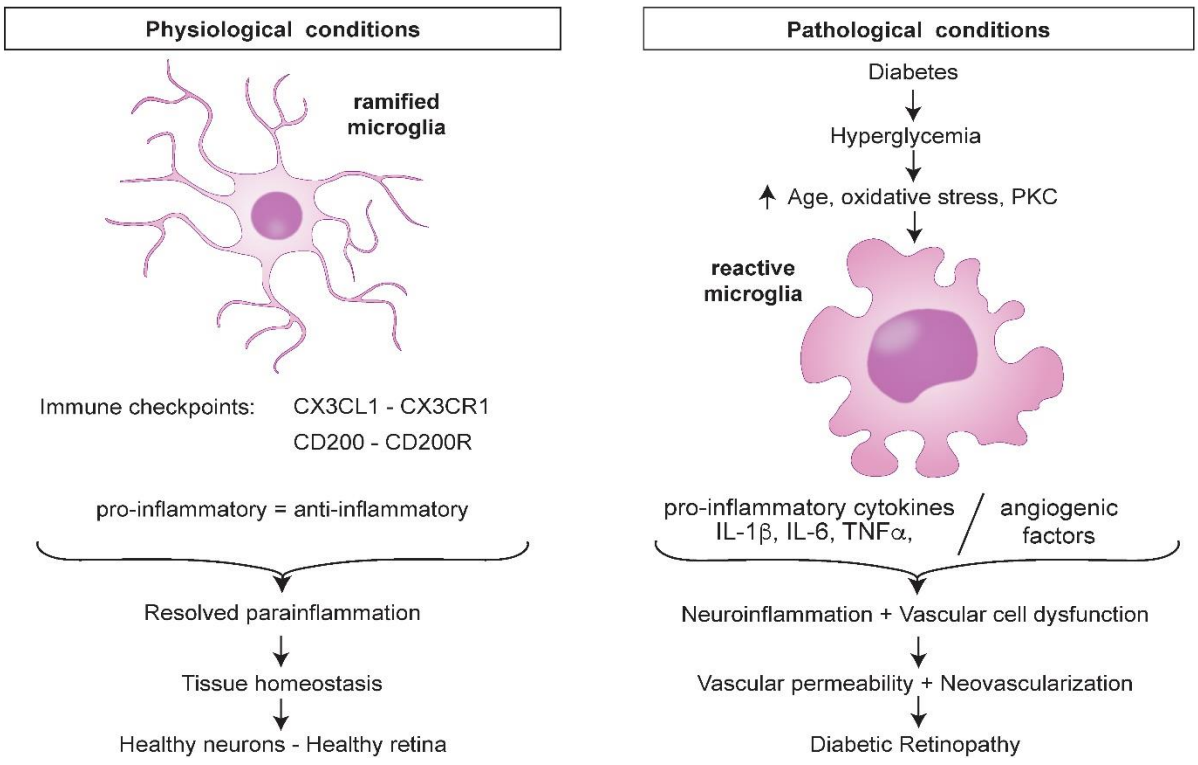

Figure 2: Schematic representation of the pathophysiology of diabetic retinopathy. Under physiological conditions, microglia exist in the ramified state with immune checkpoints controlling inflammation states. However, under sustained tissue stress, reactive amoeboid

shaped-microglia drive chronic inflammation and immune checkpoint breakdown in DR. Source: (Kinuthia et al., 2020)

Recent in vivo studies have identified elevated levels of factors associated with activated microglia including soluble CD-14, inflammatory cytokines (IL-1β, MCP-2, IFN-γ, and IFN-γ-induced protein 10) in the aqueous humor of DR patients (Lee et al., 2018; Vujosevic et al., 2016). In a more recent single-cell transcriptomic analysis of fibrovascular membranes (FVM) from PDR patients, microglia subpopulations with profibrotic and fibrogenic properties were identified as the main cell types within the FVMs (Hu et al., 2022). Further analysis showed that the profibrotic subpopulation of microglia was distinctively differentiated from bona-fide retinal microglia (Hu et al., 2022). Markers of microglia activation (F4/80, CD11b) and mediators of inflammation (VEGF, MM9, IL-1β) were also found in epiretinal membranes of diabetic patients (Vishwakarma et al., 2020). However, despite the progress in establishing the contribution of microglia in retinal vascular pathologies, there exist gaps in the cellular and molecular contributions of microglia toward disease progression. This necessitates the use of animal mouse models in preclinical studies owing to their first reproductive cycles and response to drugs.

1.7 Animal models of diabetic retinopathy

Chemical induction or genetic tools have been used to develop animal models to study the etiology and pathogenesis of DR. The induction methods entail treatment with streptozotocin (STZ), alloxan, surgical removal of the pancreas, laser damage to the eye, or a high-galactose diet whereas genetic induction involves gene editing or selective breeding. Although various animal species including cats, dogs, pigs and non-human primates have been used as models of DR, mice and rats are the most utilized species owing to their fast breeding, short life span and small size.

1.7.1 Chemical models of diabetic retinopathy

Alloxan, a derivative of uric acid with a structure similar to that of glucose transporter 2 (GLUT2) was the first drug discovered to induce diabetes by damaging the β cells of the pancreas (Dixon et al., 1960; McLetchie, 2002). Mechanistically, alloxan causes necrosis of islets of Langerhans in the pancreas, leading to the death of β cells, the release of stored insulin and the onset of hypoglycemia followed by the development of hyperglycemia within 24 hours. A single dose of alloxan administered to mice aged 8-10 weeks leads to the onset of hyperglycemia and diabetes (Weerasekera et al., 2015). In the FOT-FB mouse strain, the onset of diabetes is associated with pericyte ghosts and loss of retinal ganglion and microaneurysms within 7 and 21 days post-treatment respectively, as well as microglia activation (Gaucher et al., 2007; Weerasekera et al., 2015). In addition to the phenotype

observed in mice, rats developed neovascularization, capillary basement thickening and BRB breakdown up to 15 months post-induction as reviewed elsewhere (Olivares et al., 2017).

Streptozotocin is an antibiotic derivative of the bacteria *Streptomyces achromogenes* previously used for cancer chemotherapy. STZ is structurally similar to glucose and *N*-acetyl glucosamine and destroys the β cells of the pancreas by its DNA alkylating activity exhibited by a methylnitrosourea moiety (Eleazu et al., 2013; Lenzen, 2008). Unlike alloxan-induced diabetes, STZ is only effective in male mice, as female mice were found to be resistant to this treatment (Le May et al., 2006). In mice, hyperglycemia develops within two weeks after STZ treatment, a clinical condition that can be maintained for almost 22 months. The notable phenotypes of STZ-induced DR include gliosis, RGC loss, INL and ONL thinning, neovascularization alongside acellular capillaries and ghost pericytes (Feit-Leichman et al., 2005; Martin et al., 2004; Su et al., 2012).

Also, hyperglycemia has been induced in mice following a high galactose or high-fat diet (Chang et al., 2015; Joussen et al., 2009). Among the phenotypes observed in a high galactose diet in mice include capillary basement membrane thickening, acellular capillaries and pericyte ghosts (Joussen et al., 2009). In high-fat diet-induced diabetes mice, functional deficits such as electroretinographic defects preceded histopathological features such as capillary atrophy and permeability (Chang et al., 2015; Rajagopal et al., 2016). In a recent interesting study, rhesus nonhuman primates on a high-fat Western diet for > 5 years developed DR characterized by venous enlargement and tortuosity, microaneurysms, macular exudates, hemorrhages, microglia activation and increased fundus autofluorescence (Chan-Ling et al., 2023). This model of Western diet-induced DR has the limitation of the duration of time (5 years) required to induce DR.

1.7.2 Genetic models of diabetic retinopathy

Five models of genetically induced diabetes have been used to study the etiology and progression of DR. The models include non-obese diabetic (NOD), db/db (*Lepr*^{db}), *Ins2*^{Akita}, Kimba and Akimba mice that vary in the mode of disease development and progression (Olivares et al., 2017). The NOD mouse is a type 1 diabetes (T1D) model that mimics human autoimmune-insulin-dependent DM through $CD4^+$ and $CD8^+$ T-cell mediated damage of β cells of the pancreas (Serreze et al., 1997). The common phenotypes of DR in these mice include loss of pericytes, endothelial cells, and RGCs but there exists gender variability in the onset of hyperglycemia which occurs at 12 and 20 weeks in female and male mice, respectively (C. R. Li & Sun, 2010). The db/db (*Lepr*^{db}) mice carry a mutation in the leptin receptor and were developed to study type 2 diabetes (T2D) (H. Chen et al., 1996; Hummel et al., 1966). At a late stage of disease, db/db mice manifest signs of progressive disease such as neural-retinal

apoptosis, pericyte dropout, gliosis and BRB breakdown (Cheung et al., 2005). The *Ins2*^{Akita} mouse model of DR harbors a missense mutation in the *Insulin 2* gene that causes a misfolding of the proinsulin protein, and its subsequent accumulation in the pancreatic β cells, ultimately causing the death of the β cells (Arunagiri et al., 2018; Izumi et al., 2003). Disease pathogenesis entails loss of RGCs, acellular capillaries and leukocyte extravasation due to inflammation (Barber et al., 2005; Han et al., 2013).

The Akimba mouse model was developed by crossing the transgenic Kimba non-obese model of retinopathy with the *Ins2*^{Akita}. The transgenic Kimba mouse overexpresses VEGF under the control of a rhodopsin promoter and shows a significant thinning of INL and ONL by P7 and VEGF production peaks at P10 and declines by 6 weeks of age (Okamoto et al., 1997; Tee et al., 2008; van Eeden et al., 2006). At an early stage of the disease the Akimba mouse manifests pericyte and endothelial cell loss, neovascularization and vascular hyperpermeability whereas photoreceptor loss, thinning of nuclear layers and increased edema characterize the late stage of the disease (McLenachan et al., 2015; Rakoczy et al., 2010; Wisniewska-Kruk et al., 2014).

Although these mouse models of DR have expanded our understanding of the etiology and pathogenesis of DR, they fail to recapitulate key molecular and cellular features of human disease, necessitating the need for better animal models.

Recently, an innovative protocol for developing a mouse model of DR that mimicked phenotype of human disease including vascular hyperpermeability, increased retinal thickness (due to intra and sub-retinal fluid accumulation), hypoperfusion, mononuclear phagocyte activation, BRB breakdown and neoangiogenesis was established using an anti-PDGFRβ monoclonal antibody (mAb) (Ogura et al., 2017; Shiraya et al., 2020). Administration of a single i.p injection of anti-PDGFRβ mAb at postnatal day 1 to transiently pericyte recruitment to the developing retinal vessels and was sufficient to reproduce multiple vascular hallmarks of DR in adult mice. Similarly, tamoxifen-inducible depletion of PDGF-B in retinal ECs under control of the Ve-cadherin promoter produced characteristic features of human disease (Park et al., 2017). These experimental models provide a new means to investigate components of DR pathogenesis and provide new systems for the drug discovery process.

1.8 Microglia as therapeutic targets in diabetic retinopathy

Mounting evidence suggests that neuroinflammation precedes microvasculopathy in retinal vascular diseases. In the retina, microglia primarily orchestrate inflammation and are thus ideal molecular targets at the onset and progression of retinal diseases (Karlstetter et al., 2015). The contribution of microglial inflammatory responses to the pathogenesis of DR is supported by the therapeutic effect portrayed by microglia modulators in retinal neuroinflammation.

Several phytochemicals including galangin, curcumin, quercetin and epigallocatechin-3-gallate display improved outcomes in modulating microglia reactivity (Y. Chen et al., 2022; Cheng et al., 2021; Kim et al., 2019; Y. Yu et al., 2018). Additionally, tetracycline-derivatives such as minocycline protect against microglia reactivity and photoreceptor loss in the mouse model of light-induced degeneration (Scholz et al., 2015). Therefore, immune-modulating compounds that are safe and clinically tested proof to be beneficial in the regulation of microglia responses during inflammation in mouse models of DR.

1.8.1 Immunomodulatory role of minocycline on microglia

Tetracyclines are bacteriostatic compounds that inhibit growth of both Gram-positive and Gram-negative bacteria. In bacteria, they bind to the 30S ribosomal subunit of bacteria and block the transfer of aminoacycl-tRNA to the ribosome thereby preventing addition of amino acids to the growing polypetide chain (Chopra & Roberts, 2001). The early evidence for non-antibiotic properties of tetracycline and tetracycline derivatives; minocycline and doxycycline was reported in rheumatoid arthritis (Greenwald et al., 1992; Kloppenburg et al., 1996). Among the tetracycline antibiotics, minocycline has the longest serum half-life of about 11 – 18 hours (Chopra & Roberts, 2001) and it is the most lipid-soluble tetracycline with a high degree of CNS penetration.

Minocycline (7-dimethylamino-6-dimethyl-6-deoxytetracycline) is a second-generation tetracycline derivative. It possesses anti-inflammatory, anti-apoptotic and anti-angiogenic effects within the CNS and in the tumor microenvironment (Garrido-Mesa et al., 2013). Together with doxycycline, they are known to dampen microglia-mediated inflammatory responses in the retina and brain. In mice, minocycline has been reported to limit the expression of pro-inflammatory cytokines, microglia activation and microvascular damage (Eid et al., 2021; Krady et al., 2005). Additionally, clinical trials with minocycline and doxycycline reported reduced vascular leakage and central macular edema with concomitant improvements in visual function (Cukras et al., 2012; Scott et al., 2014). Tetracyclines, particularly doxycycline, prevents neuronal death and accumulation of inflammatory proteins and promote survival of mitochondrial disease models (Perry et al., 2021) thereby expanding knowledge on the non-antibiotic therapeutic effect of tetracyclines.

Previously, minocycline has been shown to limit photoreceptor loss and microglia activation in the mouse model of light-induced retinal degeneration (Scholz et al., 2015). Although minocycline is not a microglia-specific inhibitor, it was recently reported to suppress the inflammatory gene signature of microglia in a model of retinal photoreceptor loss (Ozaki et al., 2022). Despite the overwhelming evidence for anti-inflammatory effect of minocycline in the CNS, its cellular and molecular targets during the pathogenesis of DR remain elusive.

1.9 Study aim and objectives

Given the involvement of microglia in retinal inflammation and pathological angiogenesis, this study sought to understand the cellular and molecular changes associated with immunomodulation of microglia in the development and progression non-hyperglycemic experimental mouse models that mimic key features of the human diabetic retinopathy as this remains uncharacterized. To achieve this aim, the following specific objectives were set:

i. To determine the cellular and molecular changes associated with activated microglia in the onset and progression of the disease
ii. To investigate the immunomodulatory effects of minocycline and PLX3397 on retinal microglia and microvasculature in disease

The study is supported by the following hypotheses:

i. Postnatal attenuation of the PDGFB/PDGFRB signalling in the retina perturbs tissue homeostasis and leads to overt microglia activation and cytotoxic phenotype
ii. Immunomodulation of retinal microglia dampens their immunoreactivity and restores tissue homeostasis

2. MATERIALS AND METHODS

2.1 Mouse husbandry

Mice were housed under specific pathogen-free (SPF) conditions in individually ventilated cages (GM 500, Tecniplast® Greenline) with a maximum number of five adult mice in each cage. Room lighting was adjusted to a 12 h/12 h light/dark cycle with the light on at 6 a.m. and off at 6 p.m. The temperature and relative humidity were regulated to 22 ± 2 °C and 45-65%, respectively. Mice were fed an irradiated phytoestrogen-free standard diet for rodents (Altromin 1314; 59% carbohydrates, 27% protein, 14% fat) and had access to food and water *ad libitum*. All the animal husbandry and experimental procedures were carried out following the German law on animal protection and the ARVO statement for the use of animals in Ophthalmic and vision research. The governmental body responsible for animal welfare in the state of Nordrhein-Westfalen (Landesamt für Natur, Umwelt und Verbraucherschutz Nordrhein-Westfalen, Germany) reviewed and approved the experimental protocols in the present study. The animal experiment approval was issued under license no. 84-02.04.2020.A010.

2.2 Experimental animals and experimental design

Specific pathogen-free C57BL/6J mice were reared and bred at the Eye Clinic mouse container at the University Hospital of Cologne, University of Cologne. The B6.129P2-Pdgfb^{tm2Cbet}/J strain commonly referred to as *Pdgfb*^{flox} Jackson stock 017622 (Enge et al., 2002) mice were purchased from the Jackson Laboratory. In the *Pdgfb* ^{flox} mutant mice, exon 4 of the *pdgfb* gene is flanked by loxP. Through homologous recombination, exon 4 was floxed by the insertion of a loxP-flanked PGKneo cassette into intron 3 and the insertion of another loxP site into intron 4. The *VE-Cadherin-Cre*-ER^{T2} (Sörensen et al., 2009) males on the C57BL/6J background were a kind donation by Prof. Dr. Ralf Adams of the Max Plank Institute for Molecular Biomedicine, University of Muenster to our mouse facility and bred with the *Pdgfb*$^{flox/flox}$ mice. The Cre-ER^{T2} (estrogen receptor) mice were developed when a Ve-Cadherin-CreER^{T2} transgene vector carrying a genomic fragment of the Ve-Cadherin promoter was fused to a CreERT2 cDNA and injected into fertilized embryos of (C57BL/6 or FVB/N mice). The founder lines were backcrossed to establish mice heterozygous for the Ve-Cadherin-CreERT2 transgene. Both male and female mice were used in the experiments. The experiments of the present study were illustrated in the experimental plan in Figure 3 below.

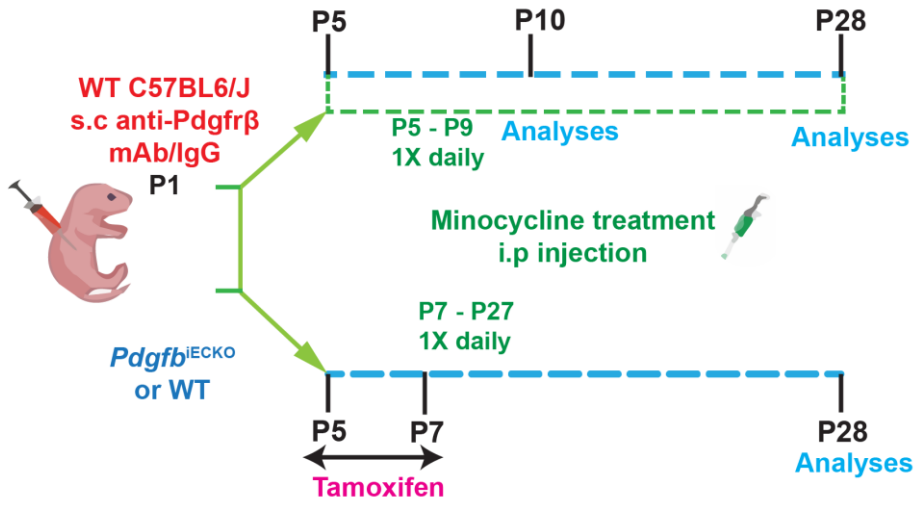

Figure 3: Experimental design for the blockade of PDGFRβ and conditional knock out of PDGFB. C57BL6/J WT mice received a single subcutaneous injection of 30µg of a rat-anti-mouse Pdgfrβ mAb (clone APB5) or IgG isotype control at P1 to block recruitment of Pdgfrβ-expressing pericytes onto the ECs. Control and APB5 WT mice were treated with minocycline (45mg/kg) from P5 to P9 or until P27 and analyses conducted at P10 or P28 according to the experimental plan. The PdgfbiECKO mice or age-matched WT controls received tamoxifen (100µg) from P5 - P7 then were treated with minocycline (45mg/kg) from P7 – P27 and analyses were conducted at P28.

2.2.1 Tamoxifen injections

TAM powder (T5648, Sigma-Aldrich) was partially dissolved in 100% ethanol and vortexed for 5 min. Heat-sterilized corn oil (C8267, Sigma-Aldrich) was added to a 9:1 oil: ethanol mixture ratio to a final concentration of 20 mg/ml TAM and incubated at 37 °C until full dissolution. The corn oil was heat sterilized in an oven at 160℃ and allowed to cool to room temperature before preparing aliquots under a sterile hood. The prepared tamoxifen working solution was stored at −20 °C protected from light and only diluted further in sterile corn oil to a concentration of 5mg/ml. To induce Cre recombinase activity and generate endothelial-specific *Pdgfb* knock-out, *Pdgfb*^{iECKO} mice and littermates expressing the CreERT2 but lacking respective loxP-flanked alleles were injected on 3 consecutive days, from P5 to P7, subcutaneously with 20µl TAM at a concentration of 5mg/ml in corn oil.

2.2.2 Pharmacological inhibition of pericyte recruitment

For the C57BL/6J mice, we aimed at blocking the recruitment of pericytes to growing endothelial cells since the retinal vasculature develops during postnatal life in mice. To achieve this, 30µg of a rat anti-mouse PDGFRβ monoclonal antibody (mAb) (Uemura et al., 2002) dissolved in PBS was injected subcutaneously once at P1. The control group received the same amount of a functional grade rat IgG isotype dissolved in PBS. Both the PDGFRβ and rat IgG isotype control, cat. 16-1402-82 and 16-4321-82, respectively, were sourced from Thermo Scientific™. The proteins were concentrated to 30µg using a 50k molecular weight

cut-off (MWCO) protein concentrator (Thermo Scientific™ cat.88540) and protein concentration was determined with BCA assay (Thermo Scientific™ 23227).

2.2.3 Minocycline treatment

Minocycline Hydrochloride (Sigma M9511) was dissolved in PBS at a final concentration of 22mg/ml. Solutions were prepared fresh for intraperitoneal injections and a dose of 45mg/kg bw. For the C57BL/6J mice, minocycline was administered once daily starting at P5 to P9 or until P27 for analyses at P10 and P28, respectively. In the *Pdgfb*^{iECKO} mice and wild-type controls, tamoxifen was administered once daily starting from P7 until P27 and analyses were conducted at P28.

2.3 Visual acuity testing

Visual testing relies on the principle that all animals have reflexes that help to stabilize an image in their eyes in a moving environment. The so-called optokinetic reflex causes these compensatory eye movements. Visual testing was performed with the OptoDrum device (StriaTech). Adult mice (4 weeks old) were placed on an elevated platform surrounded by computer monitors and a camera to observe animal behavior from above. The optomotor reflex was triggered with a black-and-white stripe pattern that rotated around the animal from the monitors. The stripe pattern is enhanced from wide stripes to much finer stripes, eventually reaching the threshold of the animal's vision and the reflex is not triggered anymore. At this point, the Optodrum software registers the visual acuity of the animal automatically. The control mice were used to establish the baseline threshold for the visual acuity.

2.4 Fluorescein angiography and spectral domain-optical coherence tomography

Four-weeks old mice were anesthetized with a mixture of ketamine (100 mg/kg bw, Ketavet; Pfizer Animal Health) and xylazine (2% Rompun; Bayer, 5 mg/kg bw) diluted in 0.9% sodium chloride by intraperitoneal (i.p.) injection. Topical application of a drop of 2.5% phenylephrine and 0.5% topicamide was used to dilate pupils. Following anesthesia and pupil dilation, mice received i.p injections of 100 µl of 2.5% fluorescein (Alcon®) diluted in 0.9% sodium chloride. Early phase angiograms were recorded within 1 min of fluorescein injection using Spectralis™ HRA/OCT (Heidelberg Engineering). Spectral-domain Optical Coherence tomography (SD-OCT) was used to measure retinal thickness and the Heidelberg Eye Explorer (HEYEX) software was used to construct retinal thickness heat maps within diameters of 3 and 6 mm from the optic nerve. The average of the four sectors surrounding the optic nerve within the 3 or 6mm diameter accounted for one value of thickness.

2.5 Molecular Biology

2.5.1 Genotyping

Mouse genomic DNA was obtained from the ear and tail biopsy using the Hotshot technique (Truett et al., 2000). Briefly, tissue biopsy was digested in alkaline lysis buffer at 95 ℃ for 15 min, then cooled at -20℃ for 10 min before neutralization with an equal volume of neutralization buffer. The quality of DNA was assessed using a NanoDrop 2000 Spectrophotometer (Thermo Fischer Scientific). A 260/280 ratio of approximately 1.8 was accepted as an indication of pure DNA. Genotyping for the Pdgfb^{flox} was performed with the recommendations of the Jackson Laboratory for mouse stock 01766. The genotyping for the Ve-Cadherin CreERT2 was performed according to the procedure of the originating laboratory. Custom-made primers were purchased from IDT and were used in combination with the Tag-S PCR kit (Genaxxon Bioscience). Each reaction mix contained 1× reaction buffer S, 1mM MgCl2, 0.2 µM of each primer, 0.2 µM of dNTPs, 1.25 U/µl of Taq S polymerase and 50 ng of DNA in a total volume of 25µl. Consequently, amplified DNA was mixed with loading dye and ethidium bromide and run on a 1% agarose gel at 140V for 40 min. GeneRuler 100 bp Plus DNA Ladder was used as a loading control (Thermo Scientific™ SM0322). The resulting amplicons were visualized under UV light ((Gel iX20 Imager, Intras). The Primer sets and PCR programs for genotyping are listed below in Tables 1 and 2, respectively.

Table 1: Primer sets used for genotyping

Gene	Primer	Sequence (5' - 3')	Amplicon size (bp)
Ve-Cadherin-CreERT2	Forward Reverse mutant Reverse common	tgtaaaatgagagtcacgatt ttgcgaacctcatcactcgtt ggatgatatggtagcaggtg	WT: 311 Mutant: 650 Heterozygous: 311 & 650
Pdgfb^{flox}	Forward Reverse	gggtgggactttggtgtagagaag ggaacggattttggaggtagtgtc	WT: 265 Mutant: 350 Heterozygous: 265 & 350

Table 2: PCR Programs used for genotyping

Gene	Step	Temperature (℃)	Time	Cycles
Ve-Cadherin-CreERT2	Initial denaturation	94	2 min	
	Denaturation	94	45 s	
	Annealing	55	25 s	34×

	Elongation Final elongation	72 72	25 s 5 min	
Pdgfb^{flox}	Initial denaturation Denaturation Annealing Elongation Denaturation Annealing Elongation Final elongation	94 94 65 68 94 60 72 72	2 min 20 s 15 s 10 s 15 s 15 s 10 s 2 min	1× -0.5℃ per cycle (10×) 28×

2.5.2 Immunohistochemistry

Enucleated eyeballs from P10 and P28 mice were fixed in 4% PFA at room temperature for 1.15 hours and 2 hours, respectively. For whole-mount staining, retinae and RPE were dissected carefully and permeabilized before blocking unspecific binding sites with Perm/Block buffer overnight at 4 ℃. Next, whole mounts were incubated with selected primary antibodies diluted in Perm/Block buffer in the following dilutions: 1:500 Iba1, CD31; and 1:200 NG2 overnight. After washing the tissues 3x with PBST-X (0.3% Triton X-100 in 1x PBS), tissues were further incubated with secondary antibodies (1:1000 diluted in PBST-X) for 1 h at room temperature protected from light. In addition, the retinal flat mounts were stained with TRITC-conjugated isolectin B4 from *Bandeiraea simplicifolia* (1:100 diluted in Perm/Block, L5264, Sigma-Aldrich) for 1 h at room temperature. After several washing steps in PBST-X, the retina and RPE flat mounts were prepared in DAKO mounting medium and allowed to dry at room temperature before microscopy. To prepare cryosections of the retina tissue, fixed eyes were placed in increasing concentration gradient of sucrose (10% - 20%) for P10 eyes and (10% - 20% - 30%) for eyes from 4-week-old mice for dehydration. Next, eyes were embedded in a cryomold filled with an optical cutting temperature medium (O.C.T^{TM}) and subsequently placed on dry ice. Retinal vertical sections of 10µm thickness were cut using a cryostat (Leica, CM3050S) and used immediately for *in situ hybridization* RNAScope experiments or preserved at -20 ℃ until staining. For processing of retinal sections, slides were allowed to thaw at room temperature for 10 min before hydration in 1× PBS. Furthermore, unspecific antigens were blocked with BLOTTO buffer for 30 min at RT followed by incubation with primary antibodies (diluted in antibody solution 1:500) at 4 ℃ overnight. After washing steps, the sections were incubated with secondary antibodies (1:1000 diluted

in 1× PBS) at room temperature for 1 h and protected from light. The antibodies used in the study are listed below in Table 3.

Table 3: Antibodies and conjugated labels used in the study

Antibodies	Species/clonality	Dilution	Manufacture, Cat. No
Anti-CD31	Rat monoclonal	1:500	BD Pharmingen, 550274
Anti-NG2	Rabbit polyclonal	1:200	Merck Millipore, AB5320
Anti-Iba1	Rabbit polyclonal	1:500	FUJIFILM Wako, 019-19741
Anti-GFAP	Rabbit polyclonal	1:500	Sigma Aldrich, G9269
Anti-GS	Mouse monoclonal	1:500	Merck Millipore, MAB302
Anti-cleaved Caspase 3	Rabbit	1:250	Cell Signalling, 9661S
Anti-FGF2	Mouse monoclonal	1:200	Santa Cruz Biotechnology. Sc 74412
Alexa Flour 488	Donkey anti-rabbit polyclonal	1:1000	Thermo Fisher Scientific, A21206
Alexa flour 488	Goat anti-mouse	1:800	Thermo Fisher Scientific, A11001
Alexa Flour 594	Goat anti-rat polyclonal	1:1000	Thermo Fisher Scientific, A-11007
Alexa Flour 647	Donkey anti-rabbit	1:1000	Invitrogen, A-31573
TRITC-conjugated isolectin B4	*Bandeiraea simplicifolia*	1:100	Sigma-Aldrich, L5264,

2.5.3 RNAScope in situ hybridization

RNAScope® ISH (ACD, RNAscope® Multiplex Fluorescent Reagent Kit v2) procedure was carried out with some modifications following the manufacturer's instructions. Briefly, fresh frozen sections were pre-treated with protease plus for 30 min at 40 ℃ in a hybridization oven (HybEZ^{TM}) followed by thorough washing with distilled water at RT. All the hybridization, amplification, and HRP blocking and signal detection steps were performed following the protocol provided by ACD. The following probes were used in this study: Mm-*Aif1*-C3, ACD 319141; Mm-*Vegf*-ver2-C1, ACD 412261, Mm-*Pgf*-C1, ACD 405921 and Mm-*Fgf2*-C1, ACD 316851. The C1 probes were labeled with TSA® Plus Fluorophore Cyanine 5 while the C3 probes were labelled with TSA® Plus Fluorophore Cyanine 3. Additionally, immunofluorescence staining was performed after in situ hybridization (ISH).

2.5.4 RNA isolation, cDNA synthesis and quantitative PCR

RNA was isolated from retinal tissue using the RNeasy Micro Kit (Qiagen) according to the manufacturer's instructions. Retinal samples for RNA sequencing were dissected and immediately stored in RNAlater solution (Thermo Fisher) overnight at 4 then frozen at -80 and shipped on dry ice to the sequencing facility. In brief, after thawing and centrifuging for 5 minutes at 5,000 x g, the RNAlater was removed and the sample was disrupted and homogenized in 350 µl RLT buffer containing 1% beta-mercaptoethanol with Precellys CK14 ceramic beads (1 cycle of 15 seconds at 5500 rpm) using a Precellys 24 Homogenisator (Bertin Corp., Rockville, MD, USA). Subsequently, the sample was centrifuged for 2 min at full speed and 350 µl of the cleared supernatant was transferred to a new tube. One volume of 70 % ethanol was added and the sample was applied to an RNeasy MinElute spin column followed by an on-column DNase digestion and several wash steps. Finally, total RNA was eluted in 14 µl of nuclease-free water. The purity and integrity of the RNA were assessed on the Agilent 2100 Bioanalyzer with the RNA 6000 Nano LabChip reagent set (Agilent, Palo Alto, CA, USA).

The first-strand complementary DNA (cDNA) was synthesized from the total mRNA using the RevertAid™ H Minus First-strand cDNA Synthesis Kit (Thermo Scientific) on a thermal cycler. Each reaction mix comprised 11µl RNA, 0.2µg/ml random hexamer primer,1× reaction buffer, 1U/ml Ribolock RNAse inhibitor, 1mM dNTP mix and 0.1U/µl RevertAid RNA transcriptase. Synthesized cDNA was diluted with ddH_2O to a working concentration of 20ng/µl and 10ng/µl for P10 and P28 retinas respectively. The transcript levels of the genes listed in Table 4 below were analyzed by quantitative real-time PCR performed in LightCycler® 480 II (Roche) with SYBR® Green (Takyon No Rox SYBR Master Mix dTTP blue, Eurogentec) technique using the program in Table 5. ATP synthase, H+-transporting, mitochondrial F1 complex, β polypeptide (Atp5b) was used as the housekeeping gene. Measurements were done in technical duplicates and the expression of indicated genes was normalized to expression of *Atp5b* using the ΔΔCT method.

Table 4: List of SYBR® Green primers used in the study

Mouse Gene	Forward Primer (5' – 3')	Reverse Primer (5' – 3')	NM accession number
Acta2	gacaccacccacccagagt	acatagctggagcagcgtct	NM_007392.3
Actg2	ttcaggctgtgctctcactc	atggggacattgtgggtgac	NM_009610.2
Aif1	ggatttgcagggaggaaaag	tgggatcatcgaggaattg	NM_019467.3
Ang2	ccaccagtggcatctacaca	acccacgtccatgtcacag	NM_007426.4
Atp5b	ggcacaatgcaggaaagg	tcagcaggcacatagatagcc	NM_016774.3
C1qa	ggagcatccagtttgatcg	catccctgagaggtctccat	NM_007572.2
C4b	ggggatgctgtgtctaagattc	tgccaggaatctccaaagtc	NM_009780.2
Casp1	gctcaagttgacctcagagaaat	cacctctttcaccatctccag	NM_009807.2
Ccl2	catccacgtgttggctca	gatcatcttgctggtgaatgagt	NM_011333
Clec7a	agagtgaagggccatggtt	ggaactgtatttctgacttgaaacg	NM_001309637.2
Edn2	ctgccaaagcgttgtgagtg	cagcttcaggccagtgtctt	NM_007902.3
Fgf2	gcgacccacacgtcaaacta	ccgtccatcttccttcatagc	NM_008006.2
Glycam1	agctggtatgagccagggaag	ccactgtctggcttgacttg	NM_001289587.1
Icam1	cccacgctacctctgctc	gatggatacctgagcatcacc	NM_010493.3
Il-1b	agttgacggaccccaaaag	agctggatgctctcatcagg	NM_008361.4
Inos	ctttgccacggacgagac	tcattgtactctgagggctga	NM_001313922.1
Lgals3	gtgaaacccaacgcaaaca	ctcattgaagcgggggtta	NM_001145953.1
Lyz2	gaatggaatggctggctact	cgtgctgagctaaacacacc	NM_017372.3
Pgf	ctgggttggctgtgcatt	ggcaccacttccacttctgt	NM_001271705.1, NM_008827.3
Sema3g	gccagagccaaaacaaagcag	agtgtagtttcctgcgtcatgg	NM_001025379.1
Spp1	atttgcttttgcctgttttgg	cagaatcagtcactttcaccg	NM_001204201.1
Stat3	ctgtgtgacaccaacgacct	caatgaatctaaagtgcggggg	NM_213659.3
Tnf-α	ctgtagcccacgtcgtagc	ttgagatccatgccgttg	NM_013693.3
Tspo	actgtattcagccatggggta	accatagcgtcctctgtgaaa	NM_009775.4
Tyrobp	tctttctgcggccatgtcta	tgtgacgtccaaccaagtgaa	NM_011662.3
Vcam1	tcttacctgtgcgctgtgac	actggatcttcagggaatgagt	NM_011693.3
Vegfa	aaaaacgaaagcgcaagaaa	tttctccgctctgaacaagg	NM_001025250, NM_001317041
Vwf	cagagtctgagcagatccatcc	acctgaaagggttcatcttgcc	NM_011708.4

Table 5: Program used in the SYBR® Green RT-PCR assay

Target °C	Acquisition mode	Hold (h:mm:ss)	Ramp rate (°C/s)	Acquisition (per °C)
		Pre-incubation 1 cycles		
95	none	00:05:00	4.8	none
		Amplification 45 cycles		
95	none	00:00:10	4.8	none
60	none	00:00:10	2.5	none
72	single	00:00:10	4.8	none
		Melting curve 1 cycle		
95	none	00:00:05	4.8	none
65	none	00:01:00	2.5	none
97	continuous		0.57	1
		Cooling 1 cycle		
40	none	00:00:30	2.5	none

2.5.5 Total RNA extraction

Total RNA was extracted from mouse retina stabilized in RNAlater buffer according to the "Purification of total RNA from animal and human tissue" protocol of the RNeasy Micro Kit (QIAGEN, Hilden, Germany). In brief, the retina was stored in RNAlater and shipped on dry ice. After thawing and centrifuging for 5 minutes at 5,000 x g, the RNAlater was removed and the sample was disrupted and homogenized in 350 µl RLT buffer containing 1% beta-mercaptoethanol with Precellys CK14 ceramic beads (1 cycle of 15 seconds at 5500 rpm) using a Precellys 24 Homogenisator (Bertin Corp., Rockville, MD, USA). Next, the sample was centrifuged for 2 min at full speed and 350 µl of the cleared supernatant was transferred to a new tube. One volume of 70 % ethanol was added and the sample was applied to a RNeasy MinElute spin column followed by an on-column DNase digestion and several wash steps. Finally, total RNA was eluted in 14 µl of nuclease-free water. The purity and integrity of the RNA were assessed on the Agilent 2100 Bioanalyzer with the RNA 6000 Nano LabChip reagent set (Agilent, Palo Alto, CA, USA).

2.6 RNA sequencing

Library preparation and RNAseq were carried out as described in the Illumina "Stranded mRNA Prep Ligation" Reference Guide, the Illumina NextSeq 2000 Sequencing System Guide (Illumina, Inc., San Diego, CA, USA), and the KAPA Library Quantification Kit - Illumina/ABI Prism (Roche Sequencing Solutions, Inc., Pleasanton, CA, USA). In this procedure, 200 ng of

total RNA was used for purifying poly-A-containing mRNA molecules using oligo(dT) magnetic beads. The mRNA was fragmented into small pieces, with an average size of 200-400 bases, using divalent cations at an elevated temperature of 94°C for 8 minutes. These RNA fragments were reverse transcribed into first-strand complementary DNA (cDNA) using reverse transcriptase and random hexamer primers. The inclusion of Actinomycin D ensured RNA-dependent synthesis, which improved strand specificity and prevented spurious DNA-dependent synthesis. Subsequently, the second strand cDNA was synthesized using DNA Polymerase I, RNase H, and dUTP nucleotides. dUTP was incorporated instead of dTTP to prevent further amplification during PCR. The resulting cDNA fragments were adenylated at the 3' ends and the pre-index anchors were ligated. Finally, DNA libraries were created using a 15 cycles PCR to selectively amplify the anchor-ligated DNA fragments and to add the unique dual indexing (i7 and I5) adapters. The libraries were bead purified twice and quantified using the KAPA Library Quantification Kit. Equimolar amounts of each library were sequenced on an Illumina NextSeq 2000 instrument controlled by the NextSeq 2000 Control Software (NCS) v1.4.1.39716, using two 50 cycles P3 Flow Cells with the dual index, single-read (SR) run parameters. The Real-Time Analysis Software (RTA) v3.9.25 was used for image analysis and base calling, and the resulting .cbcl files were converted into .fastq files with the bcl2fastq v2.20 software. RNA extraction, library preparation and RNAseq were performed at the Genomics Core Facility “KFB - Center of Excellence for Fluorescent Bioanalytics” (University of Regensburg, Regensburg, Germany; www.kfb-regensburg.de).

2.7 FASTQ file processing: Alignment and differential expression analysis

The Illumina BaseSpace Sequence Hub was utilized to process the Fastq files obtained from Illumina sequencing. The mouse mm39 reference genome (.fasta file) and corresponding reference annotation file (.gtf file) were acquired from NCBI and uploaded onto BaseSpace Hub to build a custom genome using the Reference Builder application (Illumina®). The DRAGEN RNA Pipeline (Illumina®) on BaseSpace Hub was used to align all the .fastq files against the custom genome and generate BAM files. The DRAGEN differential expression tool was used to analyze the BAM files and identify differentially expressed genes and gene counts, with significance at $P \leq 0.05$ and a Log2 fold change of ±1. The identified DEGs were further processed on DAVID bioinformatics resource (D. W. Huang et al., 2009; Sherman et al., 2022). Venn diagrams were created at http://www.interactivenn.net/ (Heberle et al., 2015) and modified on Adobe Illustrator (Adobe) and volcano plots were generated on GraphPad Prism.

2.8 Chemicals, buffers, kits, devices, software and program

The chemicals, reagents and buffers used in this study are listed below in Table 6 and 7, respectively. The list of kits, electronic devices, software and programs are listed in Table 8, 9 and 10, respectively.

Table 6: List of chemicals and reagents

Name	Manufacturer, Cat. No.
Agarose	Biozym; 84004
Artelac® Splash	Bausch & Lomb; PZN 07706996
Bovine serum albumin (BSA)	Sigma-Aldrich; A9418
Bromophenol blue	Sigma-Aldrich; B-6131
Dako Fluorescence Mounting Medium	Dako_301514EFG_03
Ethanol absolute	AppliChem; A3678
Ethanol, 70 %	Carl Roth; T868.1
Ethidium bromide	Sigma-Aldrich; 46067
Ethylenediaminetetraacetic acid (EDTA)	Sigma-Aldrich; E9884
Fluoromount-G with DAPI	Invitrogen; 00-4959-52
GeneRuler 100 bp plus	Thermo Scientific; SM0332
Ketaset 100 mg/ml	Zoetis; PZN 12467832
Milk powder (low fat)	Roth; T145.3
Minocycline Hydrochloride	Sigma; M9511
Normal donkey serum (NDS)	Linaris; ADI-NDKS-10
Pexidartinib 3397 hydrochloride	MedChemExpress; HY-16749A
Phalloidin-TRITC	Sigma-Aldrich; P1951-.1MG
Phenylephrine 2.5 % / Tropicamide 0.5 %	University Hospital Cologne; Pharmacy
Phosphate buffered saline	AppliChem; A9177
RNA Later ™ Stabilizing Solution	Invitrogen™; AM7020
Rompun 2 % (Xylazine)	Bayer; PZN 1320422
Roti Histofix 4 %	Roth; P087.4
Sodium Chloride (NaCl) 0.9 %	Fresenius Kabi; PZN 06605514
Sodium hydroxide (NaOH)	Merck; 1.06462
Sucrose	Roth; 4621.1
Tissue-Tek® optimal cutting temperature (O.C.T.™) compound	Sakura Finetek; 4583
TRIS	Carl Roth; 4855.3
Tri-Sodium citrate dihydrate	Roth; 3580

Triton X-100	Sigma-Aldrich; X100
Vectashield® HardSet™ Mounting Medium	Vectashield®; H1400

Table 7: List of buffers and solutions

Buffer / Solution	Chemical composition / Manufacturer, Cat. No.
Alkaline lysis buffer	25 mM NaOH
	200 mM EDTA pH 12 in ddH_2O
Antibody solution	2 % BSA
	0.3 % Triton X-100 in 1x PBS
Blotto	1 % milk powder
	0.3 % Triton X-100 in 1x PBS
DNA loading dye (6x)	30 % Glycerol
	0.25 % bromophenol blue in ddH_2O
DNase I dilution buffer	50 mM TRIS-HCL
	1 mg/ml BSA
	10 nM $MgCl_2$
Neutralization buffer	40 mM TRIS-HCl pH 5 in ddH_2O
PBST-X	0.3 % Triton X-100 in PBS
Perm / Block buffer	5 % NDS
	0.2 % BSA
	0.3 % Triton X-100 in 1x PBS
Permeabilization Solution	0.1 % Sodium Citrate
	0.1 % Triton X-100
Phosphate buffered saline (DPBS)	Gibco; 14190-094
TBE buffer (10x)	1 M Boric acid
	1 M Tris pH 7.5
	20 mM EDTA ph 8.0 in ddH_2O

Table 8: List of Commercial Kits

Kit	Manufacturer, Cat. No
In situ Cell Death Detection Kit, TMR red	Roche; 12156792910
RNAscope® Multiplex Fluorescent Detection Kit v2	Advanced Cell Diagnostics
RevertAid RT Kit	Thermo Scientific; K1691

RNeasy® Micro Kit	Qiagen; 74004
RNeasy® Micro Plus Kit	Qiagen; 74136
Takyon™ No ROX Probe MasterMix blue dTTP	Eurogentec; UF-NPMT-B0701
Taq-S PCR Kit	Genaxxon Bioscience; M3313

Table 9: List of instruments and devices

Device	Manufacturer
Adventurer Pro Balance	Ohaus®
BlueMarine™ 200 Electrophoresis Unit	SERVA Electrophoresis GmbH
Centrifuge 5415 R	Eppendorf
Centrifuge Mini Star	VWR International
Compass™ balance	Ohaus®
Cryostat CM3050 S	Leica Biosystems
Digital Incubator	INCU-Line® IL 10 VWR
Explorer R Ex 124 Balance	Ohaus®
Hybridization oven	HybEZ™ ACD
Intas Gel iX20 Imager	Intas
LightCycler® 480 Instrument II	Roche Applied Science
Magnetic stirrer	Unistirrer LLG LABWARE
MatrixTM Multichannel Pipette	Thermo Scientific
Microwave	MWG 729 CLATRONIC®
MSC-Advantage Hood	Thermo Scientific
NanoDrop 2000 Spectrophotometer	Thermo Scientific
Optodrum	Striatech GmbH
PeqSTAR 2x Cycler	Peqlab
See-saw rocker SSL4	Stuart®
Spectralis™ HRA+OCT	Heidelberg Engineering
Thermomixer Compact	Eppendorf
Vibracell 75115 Sonicator	Fisher Bioblock Scientific
Vortex-Genie™	Scientific Industries
Zeiss Imager M.2 with ApoTome.2	Zeiss

Table 10: List of software and applications used in this study

Software	Manufacturer
Adobe Illustrator (v27.3.1)	Adobe Systems
AngioTool (v0.6a)	National Cancer Institute
DAVID 2021	Laboratory of Human Retrovirology and Immunoinformatics (LHRI)
DRAGEN differential Expression (v4.0.3)	BaseSpace Labs
DRAGEN RNA Pipeline (v3.7.5)	Edico genome Inc
GraphPad Prisim 9 (v9.5.1)	GraphPad Software; Inc.
Heidelberg Eye Explorer (HEYEX)	Heidelberg Engineering
FIJI (v1.53v)	Wayne Rasband; NIH
Intras Gel Documentation Software	Intras Science Imaging
Light Cycler® 480 Software (v1.5.1)	Roche Applied Science
Mendeley	Mendeley Limited
Microsoft Office 2016	Microsoft Corporation
NanoDrop 2000 Software	Thermo Scientific
Optodrum software (v1.3)	Striatech GmbH
Reference Builder (v 1.1.0)	Illumina, Inc.
Zen Blue Edition (v3.1)	Zeiss

2.9 Image analysis

Morphometric analyses of the retinal microglia were performed on 2-D images on MotiQ, an ImageJ (Fiji) plugin. Retinal vascular density was measured and expressed as the percent of $CD31^+$ or $IB4^+$ area divided by the total measured area using the AngioTool software version 0.6a (Zudaire et al., 2011). Pericyte coverage was calculated as $NG2^+$ area divided by total $CD31^+$ area of the capillary plexus. Vessel diameter was measured with the scale bar applied as a global measurement feature on ImageJ. The particle analyzer and pointer tools of ImageJ were used to count caspase 3^+ cells and Iba^+ cells on retina whole mounts and vertical sections.

2.10 Statistical analysis

Alignment of RNAseq fastq files was performed on Illumina BaseSpace Hub using a custom mouse genome and the DRAGEN RNA pipeline application. Further processing and differential expression analyses were performed using the DRAGEN differential analysis application on Illumina BaseSpace Hub.

All data were analyzed using GraphPad Prism (version 9). One-way analysis of variance (ANOVA) followed by Šídák's multiple comparisons test was used to calculate the difference between treatment groups. Data are presented as mean ± standard deviation (SD). *$P < 0.05$, **$P < 0.01$, ***$P \leq 0.001$, ****$P \leq 0.0001$.

3. RESULTS

3.1 Minocycline attenuates dysregulated remodeling of retinal vasculature after inhibition of the PDGFB/PDGFRβ pathway

Retinal physiological angiogenesis in mice proceeds postnatal starting at P1 and continues until P10. By P7 and P8, the vascular plexus grows deeply into the plexiform layers. To study the effects of impaired angiogenesis, 30µg of a rat anti-mouse Pdgfrβ mAb (clone APB5) was injected subcutaneously into P1 C57BL6/J mice while the control mice received an isotype control IgG. In retinas treated with 30µg of APB5, pericyte coverage was reduced by almost one-third compared to control IgG-injected mice by P10 (Figure 4A-D). Next, we sought to investigate the apoptotic loss of ECs, which is associated with inadequate retinal pericyte coverage. We detected increased number of ECs that expressed cleaved caspase 3 in the APB5 retinas as compared to the IgG or minocycline treated retinas at P10 (Figure 4E-H). In the deep vascular plexus, a considerable proportion of cell bodies of $Iba1^+$ cells co-localized with $CD31^+$ ECs in the APB5 group. Here, we observed that only the cell bodies of microglia were aligned with the ECs whereas the microglia processes extended without wrapping around the vasculature. A similar observation was observed in the IgG group treated with minocycline (Figure 4I-L). Quantification of the pericyte coverage, cleaved caspase 3 and capillary associated microglia (CAM) showed that minocycline did not rescue impaired pericyte coverage but significantly reduced the number of apoptotic ECs as well as CAM (Figure 4M-O).

Furthermore, minocycline reduced the APB5-triggered vascular anastomoses of retinal vessels (Figure 5A-D), including enlarged arteries, veins and capillaries (Figure 5E-G). Quantification of vascular attributes showed that APB5 did not alter superficial vascular lacunarity but increased superficial vascular density while the deep vascular density decreased significantly, a phenomenon that was rescued with minocycline treatment (Figure 5H-J). Further analyses showed an increase in vascular branching index and artery-vein crossing in APB5 retinas when compared to controls (Figure 5K&L). Timely treatment with minocycline rescued the APB5-induced retinal vascular abnormalities thereby restoring the normal retinal patterning. Taken together, these findings suggested that minocycline promoted physiological retinal vascular remodeling in pericyte free ECs.

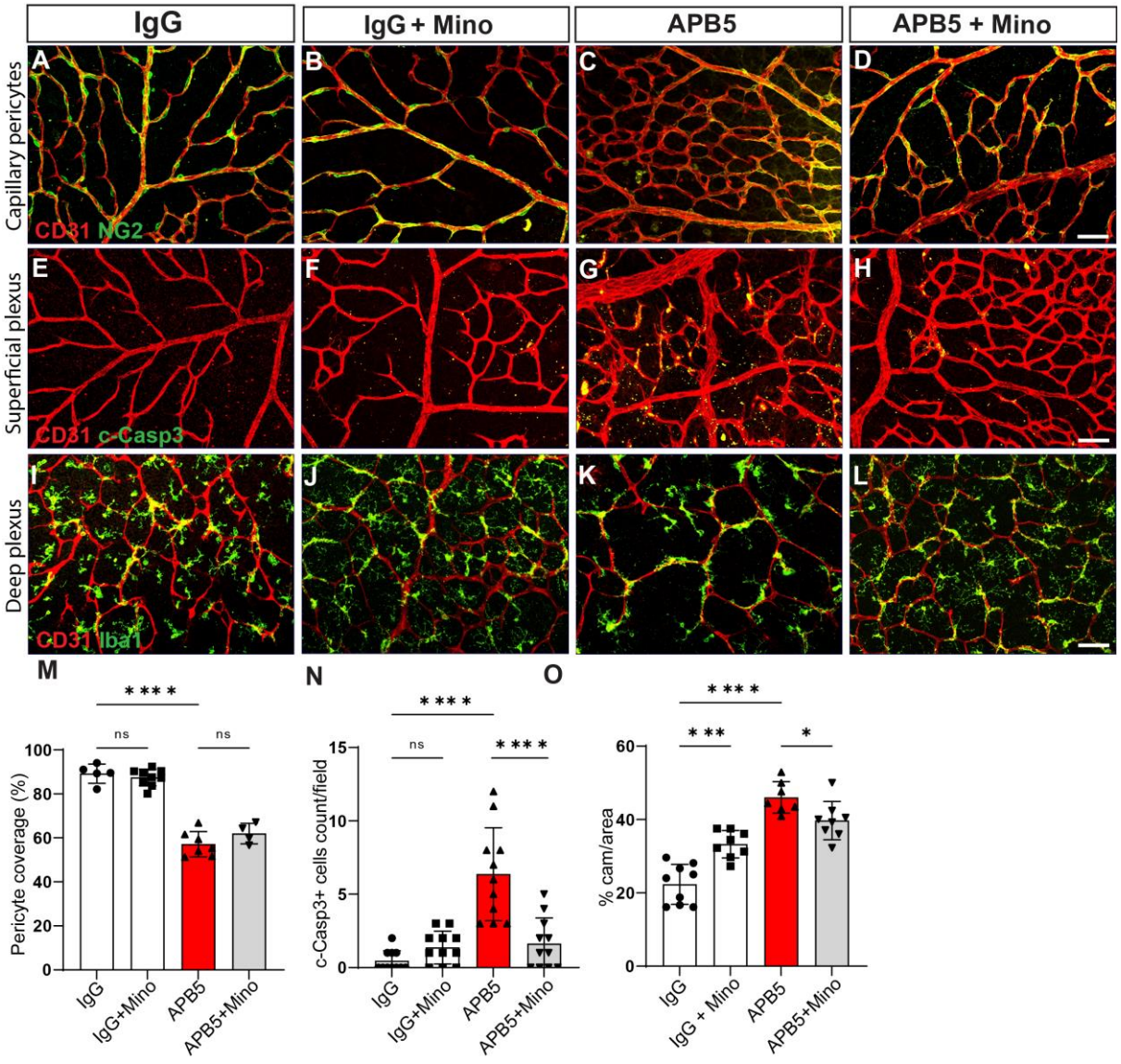

Figure 4: Changes in the retinal neurovascular unit upon inhibition of PDGFRβ in postnatal mice (P10). Representative merged IHC images of CD31$^+$ ECs and NG2$^+$ PCs on the capillary plexus (A-D). Representative merged IHC for CD31$^+$ ECs cleaved-caspase 3$^+$ ECs on superficial plexus (E-H). Merged images for IHC of CD31$^+$ and Iba1$^+$ cells in the deep vascular plexus (I-L). The graphs M, N & O show the percentage of pericyte coverage (n = 4-6), number of apoptotic ECs (n = 11) and relative capillary-associated microglia in the deep plexus (n = 8) per retina. The scale bar is 50 µm. *P < 0.05, ***P < 0.001, ****P < 0.0001, ns; not significant. Data presented as mean ± SD.

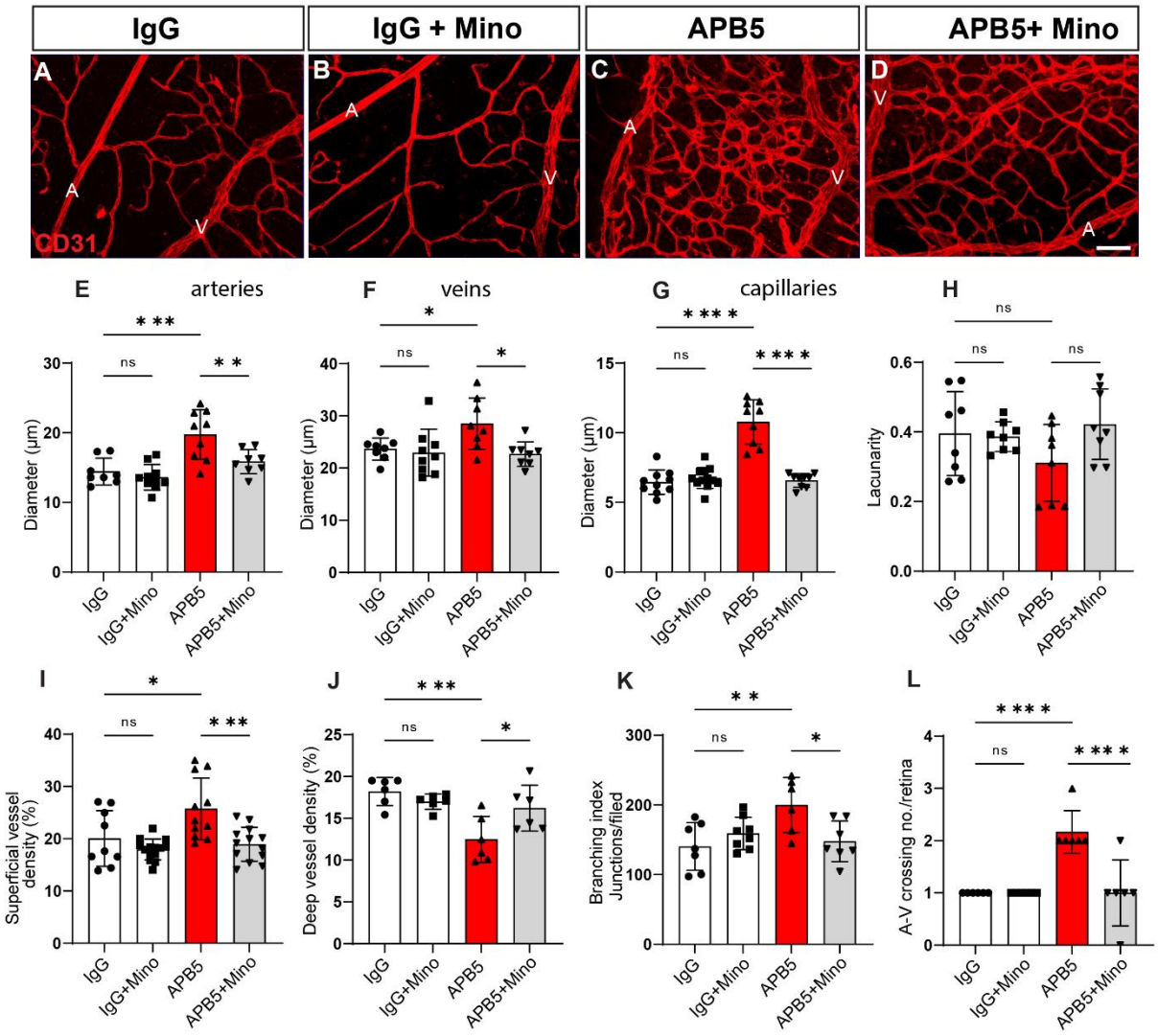

Figure 5: Minocycline stabilizes retinal vasculature after transient postnatal inhibition of Pdgfb/Pdgfrβ signalling. CD31+ ECs in the mid-retina region showing the superficial vasculature with marked arteries and veins (A-D), inside the images, A is artery and V is vein. Treatment with minocycline improves the diameters of arteries (E), veins (F) and capillaries (G) following APB5 challenge in retina. Quantification of vascular attributes; superficial vessel lacunarity (H), superficial vessel density (I), deep vascular density (J), superficial vascular branching index (K) and artery-vein crossings (L) with AngioTool. Analyses E-I; n = 8, J-L; n = 6. *P < 0.05, **P < 0.01, ***P < 0.001, **** P < 0.0001, ns; not significant. Data represent mean ± SD. Scale bar is 50µm

3.2 APB5 triggers retinal microglia activation at an early time point

The inhibition of PDGFB-PDGFRβ signalling at P1 triggered microglia activation within the plexiform layers of the retina as shown by immunohistochemistry for Iba1$^+$ (Figure 6A-H). APB5 induced an increase in the number of microglia within the IPL and OPL as shown by the number of Iba1$^+$ cells (Figure 6I-J)). The increase in microglia numbers is an indication of immune cell recruitment and response to physiological stress. In addition, we performed morphometric analyses of microglia in the OPL at P10 using the MotiQ tool. Our findings showed that APB5 reduced the ramification index, area, number of branches, number of

junctions and total tree length of microglia in the retina (Figure 6L-P). However, treatment with minocycline restored microglia to their homeostatic phenotype except for the tree length (Figure 6P).

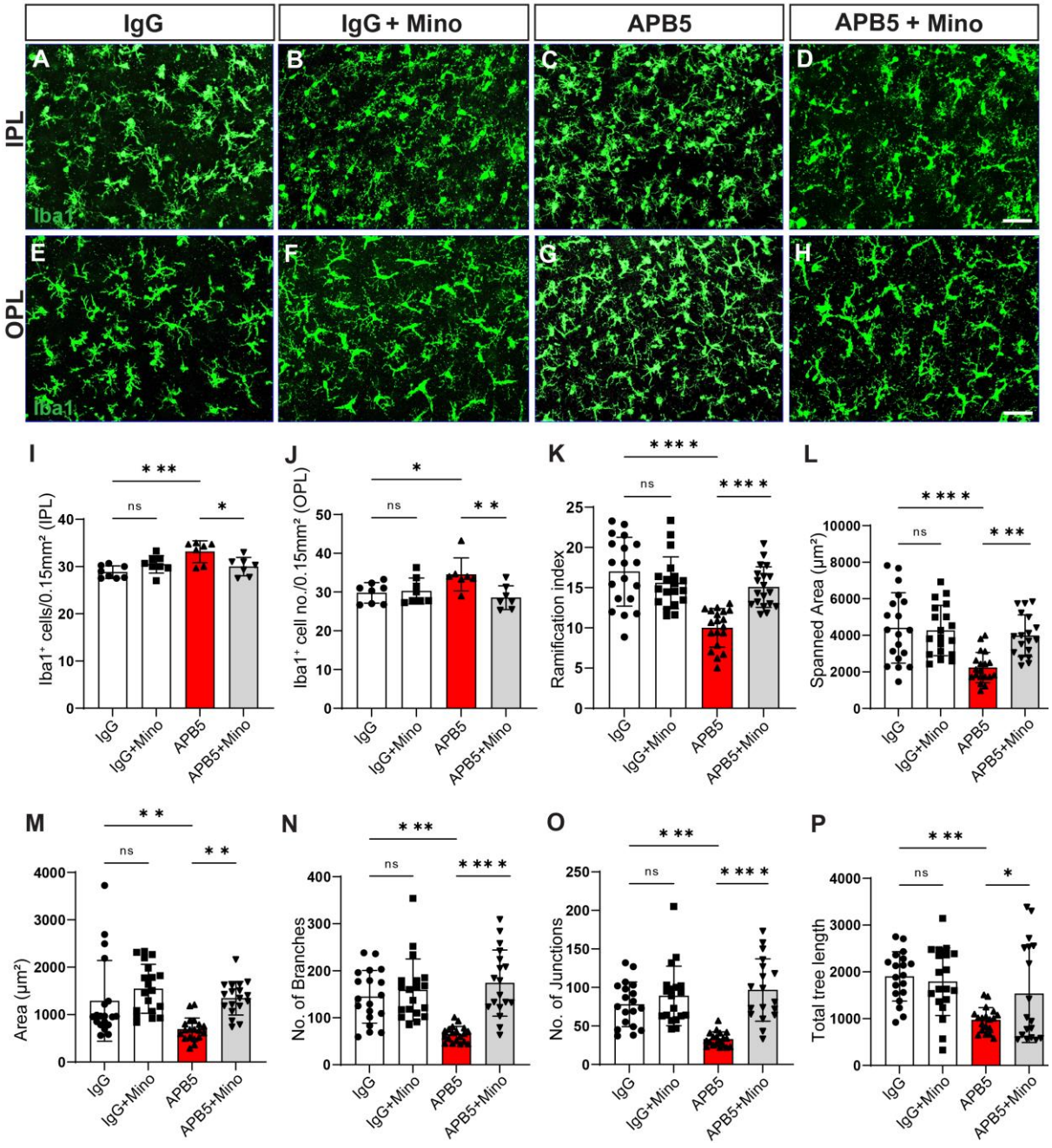

Figure 6: APB5 triggers early activation of microglia in the IPL and OPL. Representative images of Iba1$^+$ cells in the IPL (A-D) and OPL (E-H). Quantification of Iba1$^+$ cells shows that APB5 triggered their increase in the IPL and OPL but this was moderated by minocycline (I&J). Morphological analyses of retinal microglia showed that APB5 affected all analyzed parameters; ramification index, spanned area, area, number of branches, number of junctions and total tree length (K-P). Treatment of APB5 retinas with minocycline restored the homeostatic state in all analyzed morphometric attributes. For Iba$^+$ cell count in IPL & OPL n = 7-8 retinas analyzed. For microglia morphological analyses (K-P), n = 19 Iba1$^+$ cells per group. The scale bar is 50µm. *P < 0.05, ** P < 0.01, *** P < 0.001, ****P < 0.0001, ns; not significant. Data represent mean ± SD.

Preceding experiments on retina flat-mounts showed that minocycline inhibited overt microglia activation by restoring the homeostatic phenotype as evidenced by morphometric analyses at P10. A key feature of activated microglia is their migration across the nuclear layers of the retina whereby they phagocytose dying photoreceptors. In this experiment, we sought to investigate whether APB5 induced early degeneration and whether the immune-dampening effect of minocycline reduced microglia migration. Our findings show that APB5 did not induce loss of photoreceptors within the ONL across all treatment groups (Figure 7A-D). In addition, we observed that fewer microglia cells inhabited the plexiform layers of the IgG groups with or without minocycline (Figure 7E-F & I-J) compared to the APB5 groups that showed microglia increased numbers in the INL and OPL (Figure 7G-H & K-L). Further, we show that treatment with minocycline limits APB5-triggered activation and microglia migration within the inner retina at an early time point (Figure 7M).

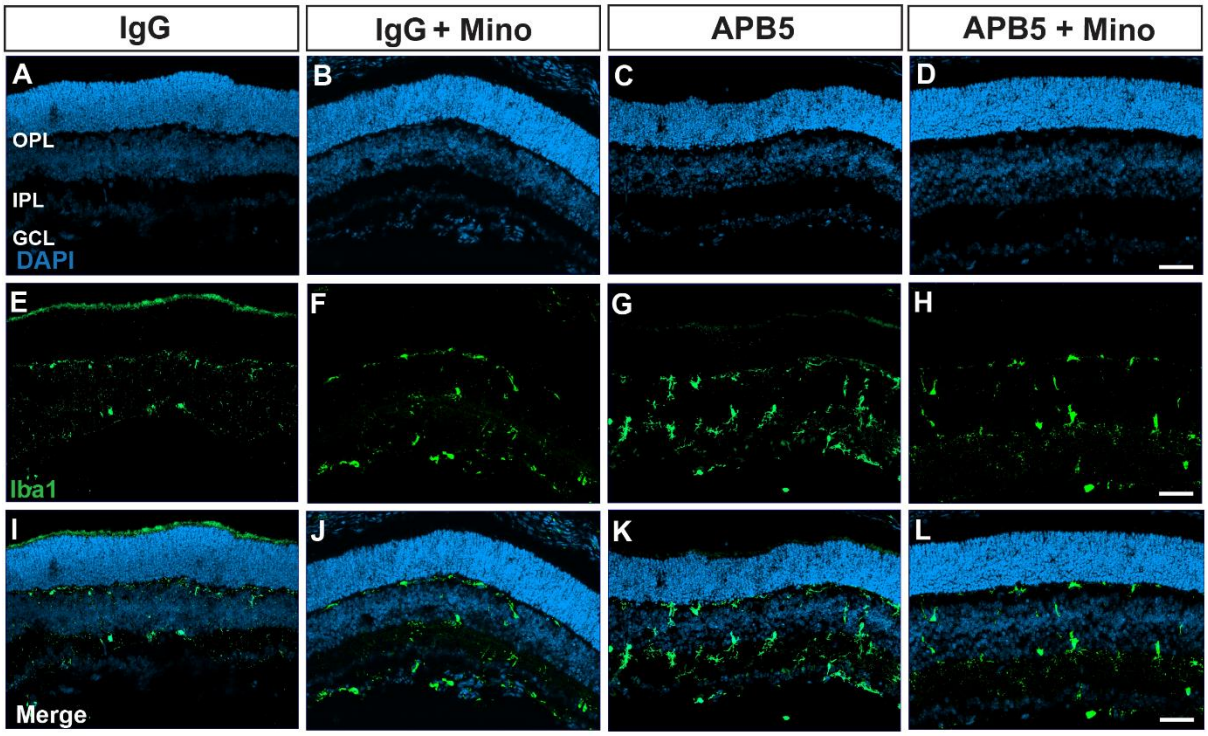

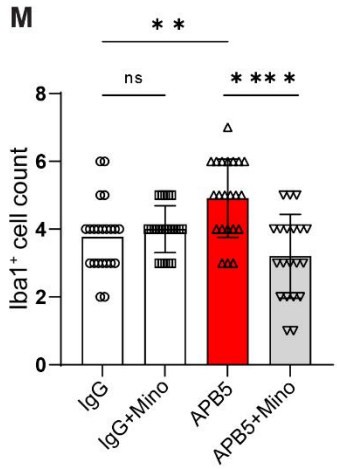

Figure legend is on the next page

Figure 7: Retina sections showing Iba1$^+$ cells location at P10. Representative single channel images of DAPI in IgG, IgG+Mino, APB5 and APB5+Mino (A-D). Representative single channel images of Iba1$^+$ cells (E-H) and merged channel images (I-L). Quantitative analyses of migratory Iba1$^+$ cells in the whole retina (M). For all groups n=19. The scale bar is 50µm. ***P* < 0.01, *****P* < 0.0001, ns; not significant. Data represent mean ± SD

3.2 Minocycline ameliorates APB5-induced astrocytic and Müller gliosis in P10 retinas

Astrocytic stress and reactive gliosis are common hallmarks of neurodegenerative diseases. Although reactive gliosis may not be a common feature in retinal vascular diseases, we hypothesized that attenuated EC-PC signalling triggers the activation of astrocytes through increased glial fibrillary acidic protein (GFAP) expression. To test this hypothesis, we stained the retinal section with an anti-GFAP antibody to observe the location and intensity of the GFAP$^+$ glial cells. Our results demonstrated that APB5 induced mild activation of astrocytes within the GCL, which was not observed in the control mice (Figure 8A-D) and corresponding increase in Müller cell activation (Figure 8E-H). Further, we could observed the ingrowth of GFAP stress fibres into the APB5 retina but this was not present in minocycline treated-retinas (Figure 8I-L).

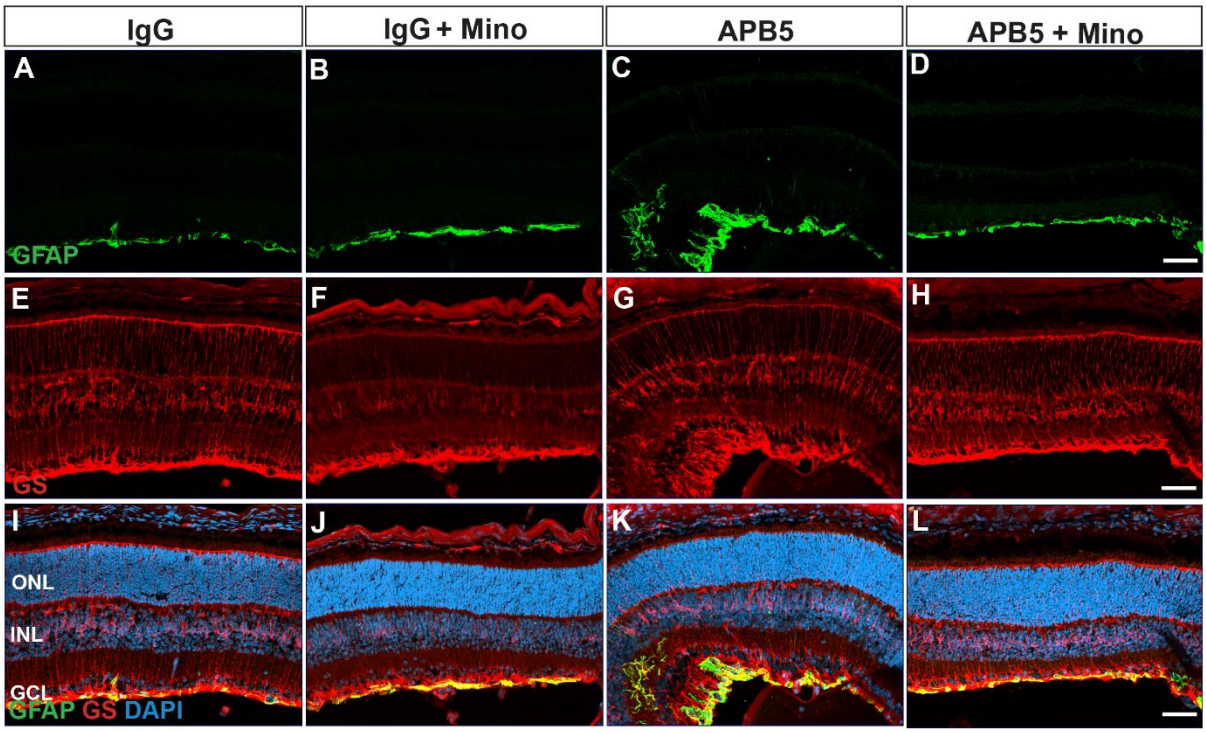

Figure 8: Immunofluorescence of GS and GFAP on P10 retinas. Vertical retinal sections from IgG control, IgG + Mino, APB5 and APB5 + Mino. Immunostaining with GFAP (green) and GS (red) shows astrocyte and Müller cell gliosis in APB5 retinas (G&K) which was reversed by treatment with minocycline (H&L). Nuclei were stained with DAPI. ONL, outer nuclear layer; INL, inner nuclear layer; GCL, ganglion cell layer. GFAP: Glial fibrillary protein, GS: Glutamine synthetase. Scale bar is 50 µm.

3.3 Minocycline attenuates pro-inflammatory and pro-angiogenic factors in the postnatal retina

Inflammation has been described as an indicator of PC loss in the APB5 retina (Ogura et al., 2017). In the present study, we indeed confirm that genes encoding pro-inflammatory factors; CCL2, INOS, IL-1β, and TNFα were highly upregulated PC-free retinas at P10 (Figure 9A-D). Consistently, increased levels of genes encoding angiogenic factors including VEGF, PGF, ICAM1 and SEMA3G were present in the APB5 retinas (Figure 9E-H). Surprisingly, the expression levels of ANGPT2 in APB5 retinas were not significantly different from that of control retinas (Figure 9I). These elevated levels of inflammatory and angiogenic factors indicate that inflammation and dysregulated angiogenesis contribute to the disease pathology upon attenuation of the PDGFB/PDGFBRβ signalling in postnatal retina. Further, we sought to determine whether retinal microglia were involved in the inflammatory response by quantifying the mRNA expression levels for genes encoding TSPO, IBA1 and Galectin-3, key biomarkers of activated microglia implicated in retinal diseases. Interestingly, APB5 retinas showed higher TSPO, AIF and LGALS3 transcripts than control retinas (Figure 9J-L). Notably, treatment with minocycline suppressed the expression of CCL2, INOS, ICAM1, VEGFA, PGF, TSPO and LGALS3. These findings confirm the anti-inflammatory effect of minocycline and suggest that minocycline confers beneficial effects on the diseased vasculature by limiting expression of angiogenic factors.

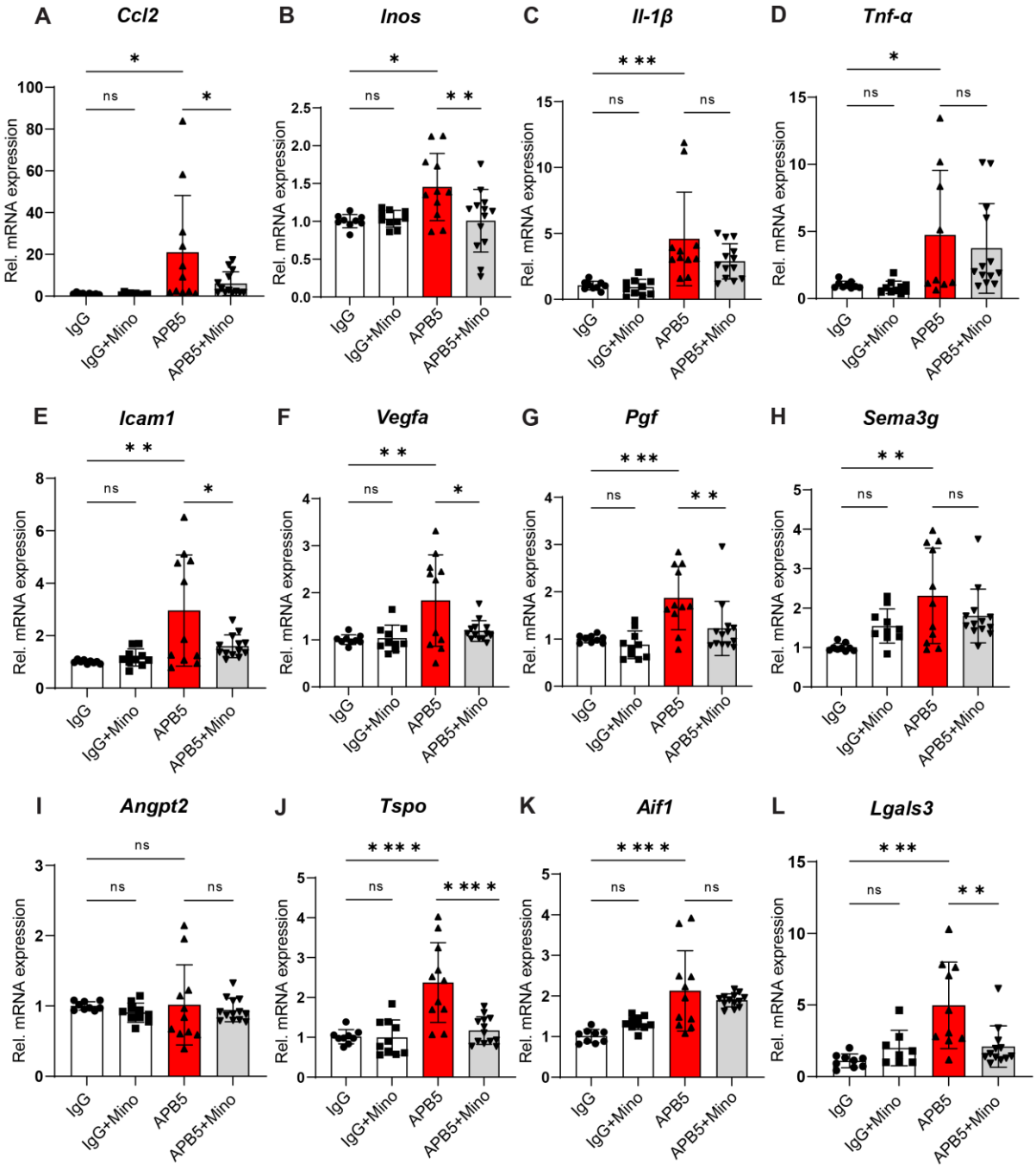

Figure 9: qRT-PCR analyses of inflammatory and pro-angiogenic factors in P10 retinas. APB5 induced the expression of pro-inflammatory genes; *Ccl2, Inos, Il-1β, Tnf-α* but minocycline suppressed the mRNA expression levels of Ccl2 and Inos but not Il-1β or Tnf-α (A-D). Pro-angiogenic genes; *Icam1, Vegfa, Pgf* and *Sema3g* were elevated in APB5 retinas (E-H) but the mRNA levels of *Angpt2* were not significantly different from control groups (I). mRNA levels for markers of activated microglia; *Tspo, Aif* and *Lgals3* were significantly upregulated in APB5 retinas and downregulated by minocycline with the exception of Aif1 (J-L). IgG; n=9, IgG+Mino; n=10, APB5; n=11 & APB5+Mino; n=13. **P* < 0.05, ***P* < 0.01, ****P* < 0.001, *****P* < 0.0001, ns; not significant.

3.4 Expression of PGF and VEGF in the APB5 retina

VEGF and PGF are known to aggravate disease outcome during the progression of retinal vascular pathologies. We have previously shown that retinal mononuclear phagocytes drive disease pathology through increased secretion of VEGF and PGF in the CNV model of wet AMD (Balser et al., 2019). Here, we hypothesized that retinal microglia secrete VEGF and PGF that contributed to disease pathology at the early stage. To test our hypothesis, we performed RNAscope in situ hybridization (ISH) on retinal sections to investigate the presence and location of *Vegf* and *Pgf* mRNAs together with *Aif1* mRNA. We detected *Aif1* mRNA within the GCL, INL and OPL indicating presence of microglia in these regions (Supplementary Figure 1A-D). Notably, the signal intensity of the *Vegf* mRNA within the INL was higher in the APB5-treated retinas when compared controls and APB5 retinas treated with minocycline (Supplementary Figure 1E-H). This observation implies that VEGF is secreted by cells within the INL and actively migrating microglia transitioning the INL to populate the OPL. Previously, Müller glia which inhabit the INL have been identified as key producers of VEGF in the murine retina under hypoxic conditions (Pierce et al., 1995). The Müller glia-derived VEGF is a major contributor to retinal neovascularization and BRB breakdown in models of OIR and STZ-induced diabetes (Bai et al., 2009; J. Wang et al., 2010).

Next, we sought to investigate the presence of *Pgf* and *Aif1* mRNA by RNAscope in situ hybridization of retinal sections. Our results showed that *Aif* mRNA was retained in the plexiform layers (Supplementary Figure 2A-D) but *Pgf* mRNA was distributed within the INL and GCL (supplementary Figure 2E-H). Here we did not observe the co-localization of *Pgf* with *Aif-1* mRNA in all experimental groups (Supplementary Figure 2I-L). Although the expression of *Pgf* mRNA was minimal in the control mice it was high in the APB5 retinas (Supplementary Figure 2G). Notably, treatment with minocycline reduced the expression of *Pgf*.

3.5 APB5 induced retinal transcriptomic changes at P10

Next, we sought to determine how inhibition of the PDGFB/PDGFBRβ signalling with APB5 affected the retinal transcriptome. For this aim, we conducted comparisons between gene expression profiles of control and APB5 retinas at P10. Overall, there were 4,131 differentially expressed genes (DEGs) in the APB5 retina relative to the control retina at P10. At a Log2 Fold change of ±1 and *P* adjusted value (FDR) < 0.05, we identified 255 DEGs out of which 248 were upregulated whereas 7 were downregulated. The DEGs are illustrated with volcano plot (Figure 10A). A complimentary heat map is presented to show selected genes involved in retinal pathologies (Figure 10B). The top 20 upregulated genes encode proteins involved with extracellular matrix (ECM) reorganization and integrin binding (e.g. *Optc, Serpine1, Fmod,*

Fbln1), cell motility (*Actg2* and *Acta2*), immune cell function (*Mfap4, Ltbp2, Spp1, Lyz2, Glycam1, Lilrb4*) and angiogenesis (*Serpine1, Adm*) (Table 11). In addition, we identified other DEGs involved in vascular destabilization (*Angptl2, Sema3g, Pdgfb, Edn1, Igfbp5 and Adm*), genes linked to an activated microglia (*Clec7a, Tspo, Lyz2, Spp1, Tyrobp and Cd68*) and the complement system (*C1qa, C1qb, C1qc and C4b*) (Table 11 and Figure 10B).

Table 11: Top 20 upregulated DEGs (APB5 relative to IgG)

Gene ID	Log2 FC	P adj.	function
Optc	3.623	1.27E-139	extracellular matrix structural constituent
Slc13a4	3.528	1.61E-69	transmembrane transporter
Actg2	3.068	3.98E-25	cell motility
Otx1	2.896	5.96E-32	transcription factor
Best2	2.625	8.47E-20	forms calcium-sensitive chloride channels
Serpine1	2.602	4.66E-37	regulation of angiogenesis
Acta2	2.569	1.69E-91	cell motility, structure and integrity
Mfap4	2.565	7.14E-86	complement activation, lectin pathway
Ltbp2	2.548	1.14E-22	regulates elastic fiber activity
Spp1	2.531	7.72E-60	immune cell specificity
Fmod	2.499	6.14E-92	Extracellular matrix organization
Lyz2	2.496	3.30E-43	lysosome activity
Gfap	2.494	2.80E-86	cell-specific marker, astrocytes
Glycam1	2.444	4.90E-16	cell and sulfate binding activity
Adm	2.425	6.81E-35	regulation of vasculogenesis
Fbln1	2.347	1.85E-50	extracellular matrix organization
Cd84	2.243	1.71E-16	regulation of signal transduction
Lilrb4	2.232	1.13E-11	integrin binding activity
Gpnmb	2.230	1.60E-40	heparin and integrin binding activity
Ndufa4l2	2.140	1.03E-86	mitochondrial respiratory chain complex IV
Ltbp2	2.548	1.14E-22	regulates elastic fiber activity

To unravel the biological functions moderated by the 248 differentially upregulated genes, we conducted GO enrichment analyses using the DAVID tool https://david.ncifcrf.gov/. In the GO domain: biological processes, identified several terms linked to inflammation and immune response (e.g. positive regulation of macrophage cytokine production, microglial cell activation, neutrophil chemotaxis, positive regulation of chemotaxis) (Figure 10C). The GO molecular function domain identified terms associated with extracellular matrix, protein tyrosine kinase and integrin binding, cytokine and signalling receptor activity (Figure 10D). To complement the GO term enrichment analyses, we conducted KEGG pathway enrichment analyses focusing on all the differentially upregulated genes induced by APB5 relative to control and identified the top 10 significantly enriched pathways (Figure 10E). Four pathways were linked to immune responses including complement and coagulation cascade, phagosome, cytokine-cytokine receptor interaction, and neutrophil extracellular trap (NET) formation (Figure 10E). These immune responses-related pathways indicate an inflammatory microenvironment reminiscent of retinal pathologies. Indeed, NETs are drivers of diabetic complications (L. Wang et al., 2018). Other enriched pathways were associated with hypoxia (HIF-1 signalling), and diabetes (AGE-RAGE signalling pathway in diabetic complications) including five pathways for cellular signalling linked to immune activation and one pathway associated with leukocyte-endothelial cell motility (Figure 10E).

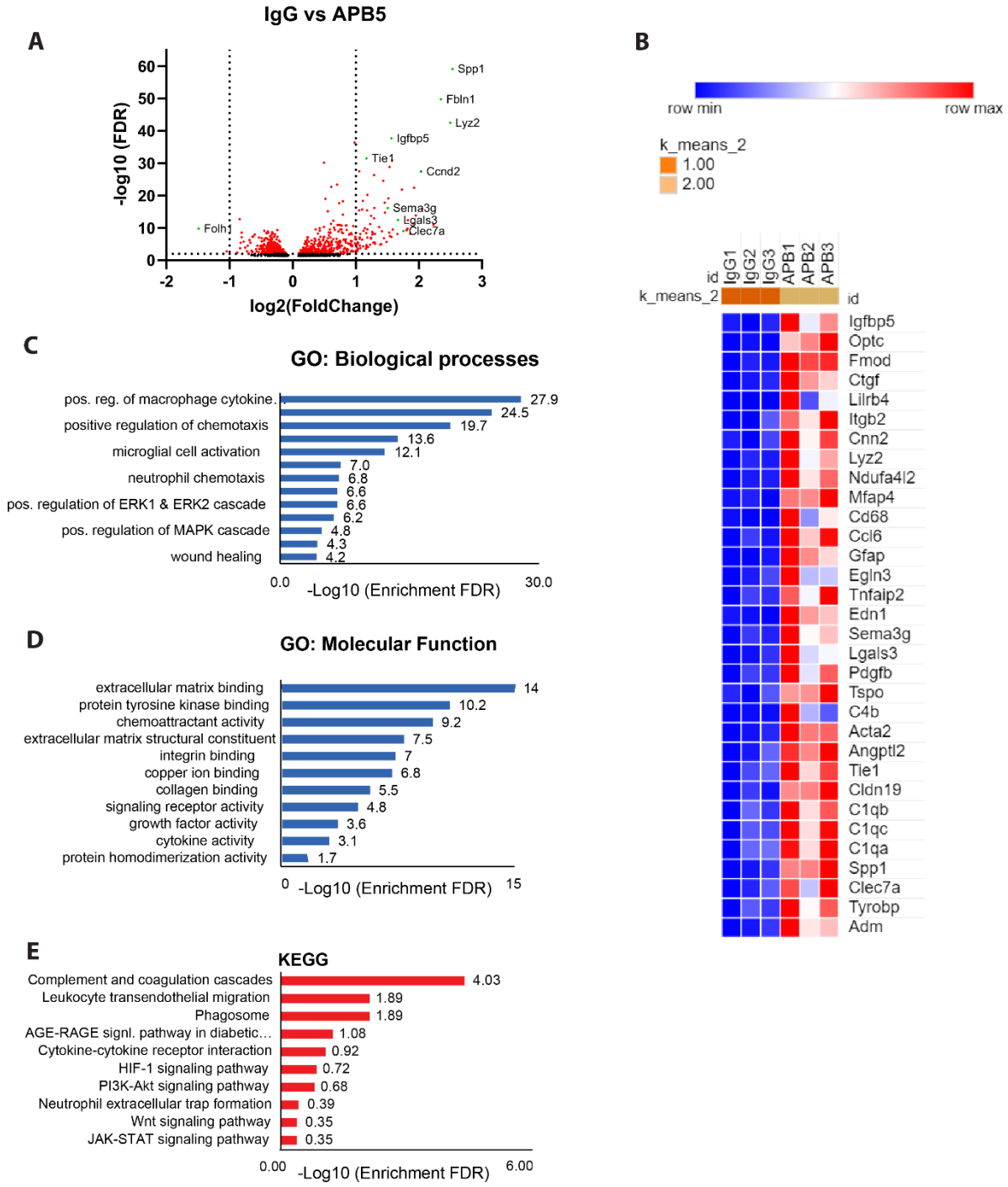

Figure 10: RNA-seq transcriptome analyses of APB5 retinas relative to IgG retinas at P10.Volcano plot showing comparison of DEGs from control IgG and APB5 retinas at P10 (A). Heat map showing selected genes involved in retinal pathologies (B). GO domain biological processes showing key processes activated by APB5 (C). GO molecular function domain showing the key functions affected by APB5 (D). KEGG Pathway analysis shows the most significantly enriched pathways in diseased retinas (E). The green dots on the volcano plots represent the most significantly regulated genes. The set cut-off for the DEGs shown on the volcano plot was Log2 FC of ±1 and FDR of < 0.05. n = 3 mice in each group.

3.6 Verification of the RNAseq data

We used qRT-PCR to verify the RNAseq data and validated the upregulation of *Acta2, Actg2, Tyrobp, C4b, C1qa, Fgf2,* and *Spp1* (Figure 11A-G). Our findings showed that minocycline reduced the mRNA expression levels of these transcripts except *Spp1*. The high expression of genes encoding smooth muscle cell contractile factors, *Acta2* and *Actg2,* 10-20 fold of control correlates with motility of ECs in the APB5 retina indicating vascular remodeling. Therefore, the high expression of *Acta2* and *Actg2* mRNA levels coincides with the vascular remodeling in the APB5 mice. Treatment with minocycline reduced the mRNA levels of *Acta2* and *Actg2* thus suggesting its potential to regulate proliferation of ECs and change in vascular endothelium. Furthermore, minocycline regulated genes of the complement system, *C1qa* and *C4b,* which are associated with phagocytic microglia during retinal vasculopathy. SPP1 is secreted phosphoprotein 1/osteopontin and has been identified as a marker for disease-associated microglia (DAM) in Alzheimer's disease and the degenerating retina in CNV (Keren-Shaul et al., 2017; O'Koren et al., 2019; Schlecht et al., 2020). Conversely, overexpression of SPP1 in astrocytes is confers protection and improves visual function in mice (S. Li & Jakobs, 2022). In yet another separate study, upregulation of perivascular *Spp1* promoted a phagocytic phenotype of microglia with concomitant expression of *C1qa*, *Ctsb* and *Grn* genes in Alzheimer's brains (De Schepper et al., 2023). These contrasting findings open up new research gaps on the spatial and temporal functions of SPP1 in the onset and progression of neuroinflammatory diseases and vasculopathy.

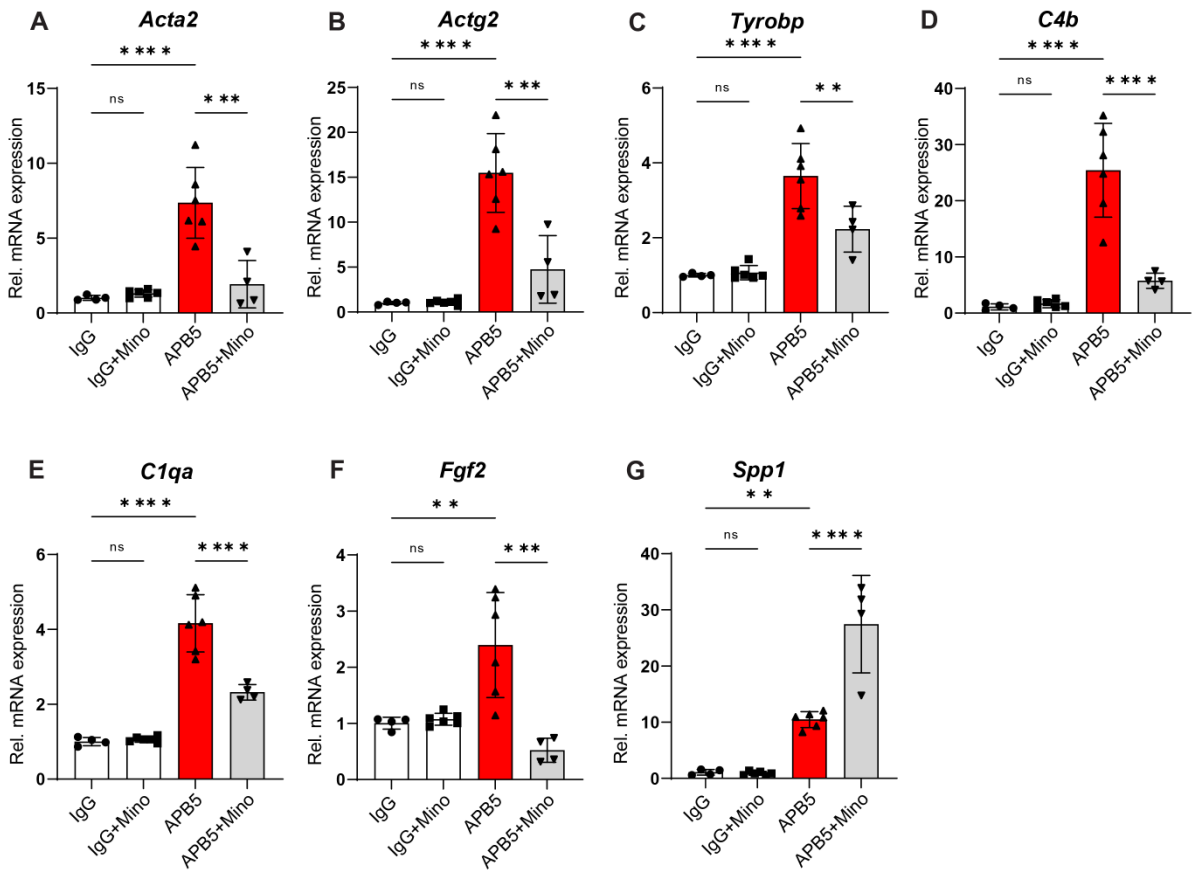

Figure 11: Verification of selected DEGs at P10. Relative gene expression analysis by qRT-PCR confirmed that minocycline suppressed the expression levels of *Acta2*, *Actg2*, *Tyrobp*, *C4b*, *C1qa*, and *Fgf2* but increased the levels of *Spp1* mRNA transcripts. n = 4-6 individual mice, mino is minocycline. *$P < 0.05$, **$P < 0.01$, ***$P < 0.001$, ****$P < 0.0001$. Data represent mean ± SD

3.7 Pericyte depletion-retinopathy affects visual outcomes in adult mice

Upon attainment of the weaning age, mice were reared until postnatal day 28 when visual acuity/function was tested. For this purpose, mice were placed on an elevated platform in the optodrum with fixed rotation. At 4 weeks of age, the control mice showed normal visual acuity (mean of 0.41 cycles/degree) whereas the APB5-treated group showed a decrease in visual function (0.32 cycles/degree) (Figure 12O). Treatment with minocycline improved the visual phenotype observed in the APB5 group with a mean score of 0.38 cycles/degree, but this was not significantly different. Considering the improvement of vision upon treatment with minocycline as recorded on the optodrum, we sought to determine whether there were changes in the retinal neural and vascular structure in the APB5 mice. For this purpose, adult (P28) IgG control and APB5 mice with or without treatment with minocycline were anesthetized and the retinal thickness and vessel perfusion were examined with the SD-OCT and fluorescein angiography. SD-OCT scans showed that IgG groups had a normal retinal structure but retinal thinning was observed in the APB5 mice, which was rescued with

minocycline (Figure 12A-D). The corresponding heat maps indicate the color changes associated with normal retinal thickness (green hue) and thin retina (blue) (Figure 12E-H). Fluorescein angiography revealed that APB5 induced leakage within retinal capillaries, which accounts for the cloudiness in the APB retina, which was diminished with minocycline (Figure 21-L). It is worth noting that APB5 had varied effects on the retinal structure. In several mice, the thinning of the ONL was accompanied by progressive thickening of the whole retina due to intraretinal fluid leakage. Quantification of retinal thickness within the central and peripheral regions of the mice retinas showed that APB5 triggered retinal thinning in both regions but minocycline rescued thinning at the peripheral region but not the central region (Figure 12M-N). Testing of visual acuity using the optodrum showed that APB5 reduced the mean visual acuity of mice, which was not significantly improved with minocycline (Figure 12O).

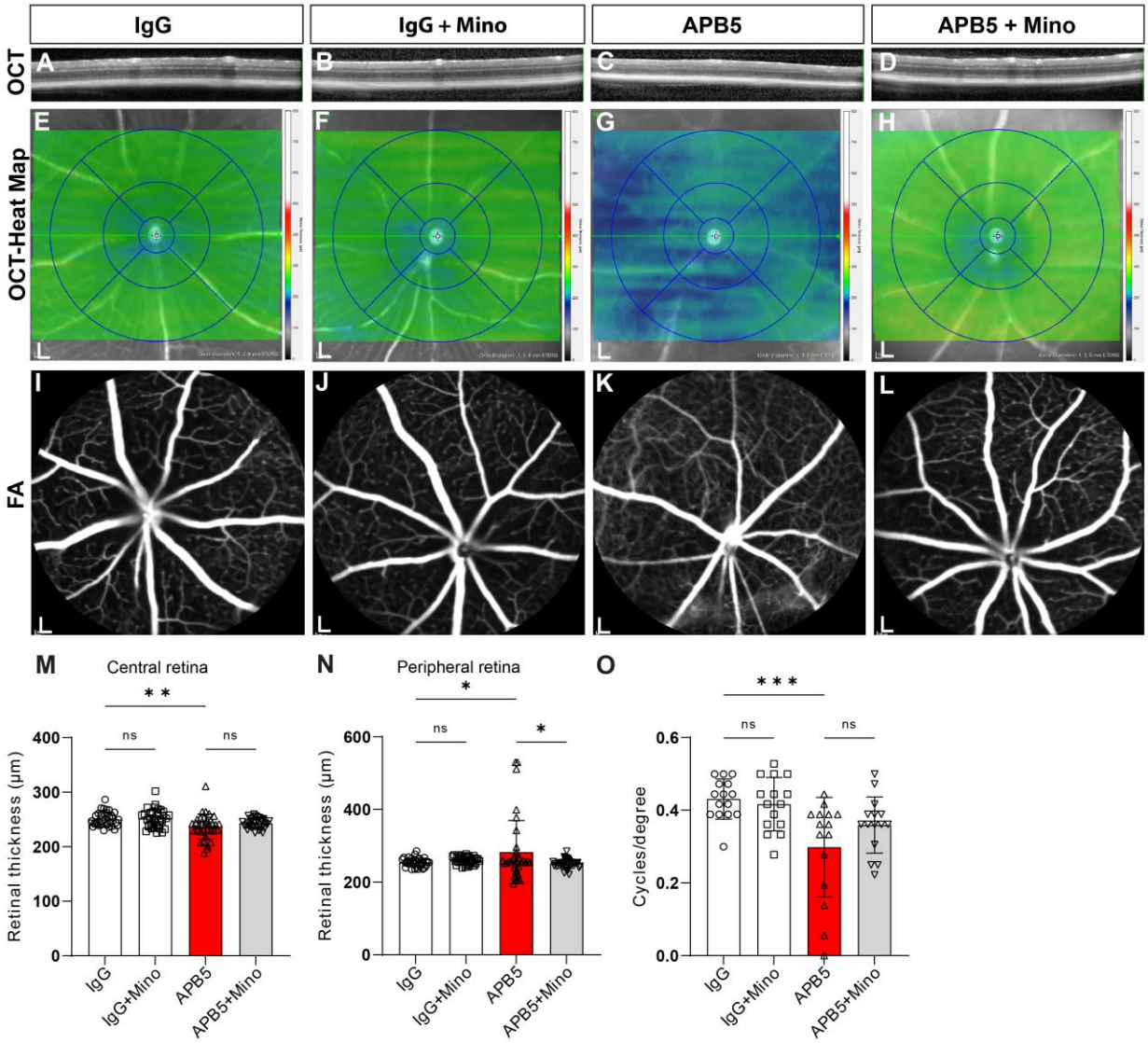

Figure 12: Analyses of retinal structural integrity and leakage in IgG and APB5 mice at P28. SD-OCT scans of IgG, IgG+Mino, APB5 and APB5+Mino (A-D). SD-OCT heat maps (green indicates normal retinal thickness while blue indicates retinal thinning) showing the

difference in retinal thickness in IgG, IgG+Mino, APB5 and APB5+Mino (E-H). Fluorescein angiography showing retinal vessel structure and capillary leakage (I-L). Quantification of retinal thickness within a diameter of 3mm (central) and 6 mm (peripheral) from the optic nerve (M&N). Analyses of contrast sensitivity (cycles per degree) as a test of visual acuity (O). For SD-OCT; IgG n=34 eyes; IgG+Mino n=36 eyes; APB5 n=39 eyes and APB5+Mino n=39 eyes. *$P < 0.05$, **$P < 0.01$, ***$P < 0.001$, ****$P < 0.0001$. Data represent mean ± SD. SD-OCT; spectral domain optical coherence tomography, FA; fluorescein angiography. The scale bar for FA is 200µm.

3.8 Minocycline rescues APB5-induced retinal degeneration in the mature murine retina

The attenuation of the PDGFB/PDGFBRβ signalling in postnatal retinal has been associated with sustained inflammation in adult mice (Ogura et al., 2017). To elucidate the involvement of retinal immune sentinels, and microglia, we stained retinal sections for ionized calcium adaptor molecule 1 (Iba1) to detect microglia localization in both control IgG and APB5 mice with or without minocycline. In the IgG control groups, microglia were restricted within the plexiform layers (IPL and OPL) and hardly any microglia were present in the ONL and SRS (Figure13A-B and Figure 13E-F). However, postnatal inhibition of the PDGFB/PDGFBRβ signalling at P1 induced and sustained the activation of microglia in adult mice (Figure 13C,G). Prolonged treatment with minocycline modulated microglia, thereby limiting the migration of these immune cells into the ONL and SRS (Figure 13D, H & J).

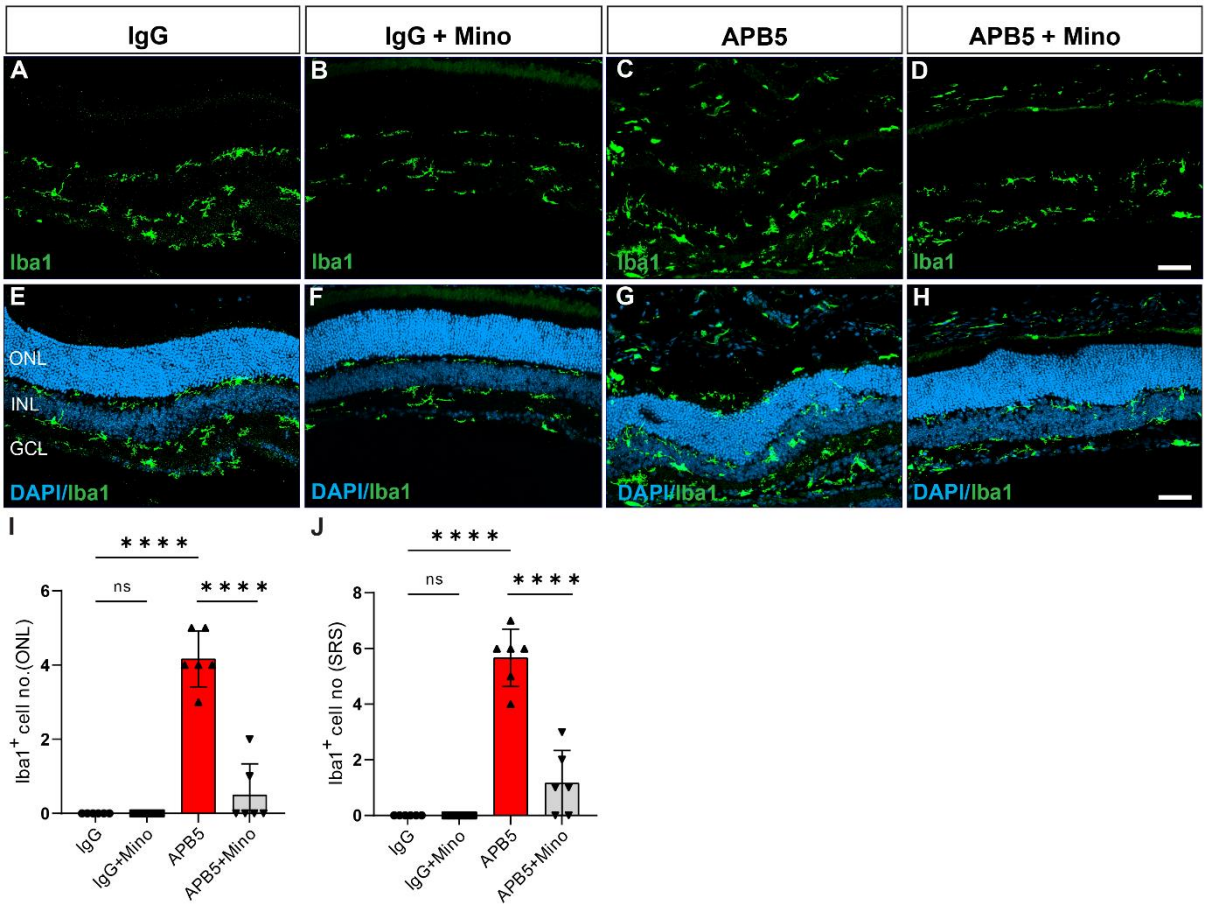

Figure 13: Minocycline limits microglia reactivation and migration in the mature retina. Representative single-channel images of Iba1$^+$ cells in the retina of IgG, IgG+Mino, APB5 and APB5+Mino at P28 (A-D). Representative merged images of retinal sections showing Iba1$^+$ cells and retinal layers in IgG+Mino, APB5 and APB5+Mino at P28 (E-H). Quantification of Iba1$^+$ cells in the ONL and SRS layers (I&J). n = 6 retinas per group. **P* < 0.05, ***P* < 0.01, ****P* < 0.001, *P* < 0.0001. Data represent mean ± SD. The scale bar is 50µm.

3.9 Minocycline limits astrocyte and Müller gliosis in APB5 mature retinas

Reactive gliosis in the retina involves not only microglia cells but also astrocytes. Indeed, it is known that astrocytic stress, as marked by activated glial fibrillary acidic protein (GFAP), is a result of chronic stress within the CNS (Vecino et al., 2016). In the normal healthy retina, GFAP is expressed by astrocytes. However, under tissue stress, Müller glia express GFAP. To visualize the expression of GFAP by astrocytes and Müller glia, we stained the retinal sections with antibodies against GFAP and GS. GS is expressed by Müller cells that traverse the retinal vertically. Therefore, the expression of GFAP by Müller glia would show whether APB5 induced Müller cell gliosis in adult retinas. In the IgG groups, we detected minimal GFAP expression in the GCL (Figure 14A&B) but an increase in its expression was observed in the APB5 groups, with GFAP stress fibers extending vertically into the retinal layers (Figure 14 C&D). The GS staining was minimal in the IgG groups (Figure14 E&F) but increased within the APB5 groups (Figure 14G&H). Across the treatment groups, APB5 had the most intense staining for GFAP and GS, which was reduced by minocycline. It is worth noting that Müller gliosis was present in the APB5 retina even in the absence of photoreceptor loss. Quantification of the mRNA levels of *Gfap* in retinas from the mature mice at P28 revealed that minocycline significantly reduced the expression levels of *Gfap* in APB5 retinas (Figure 14M).

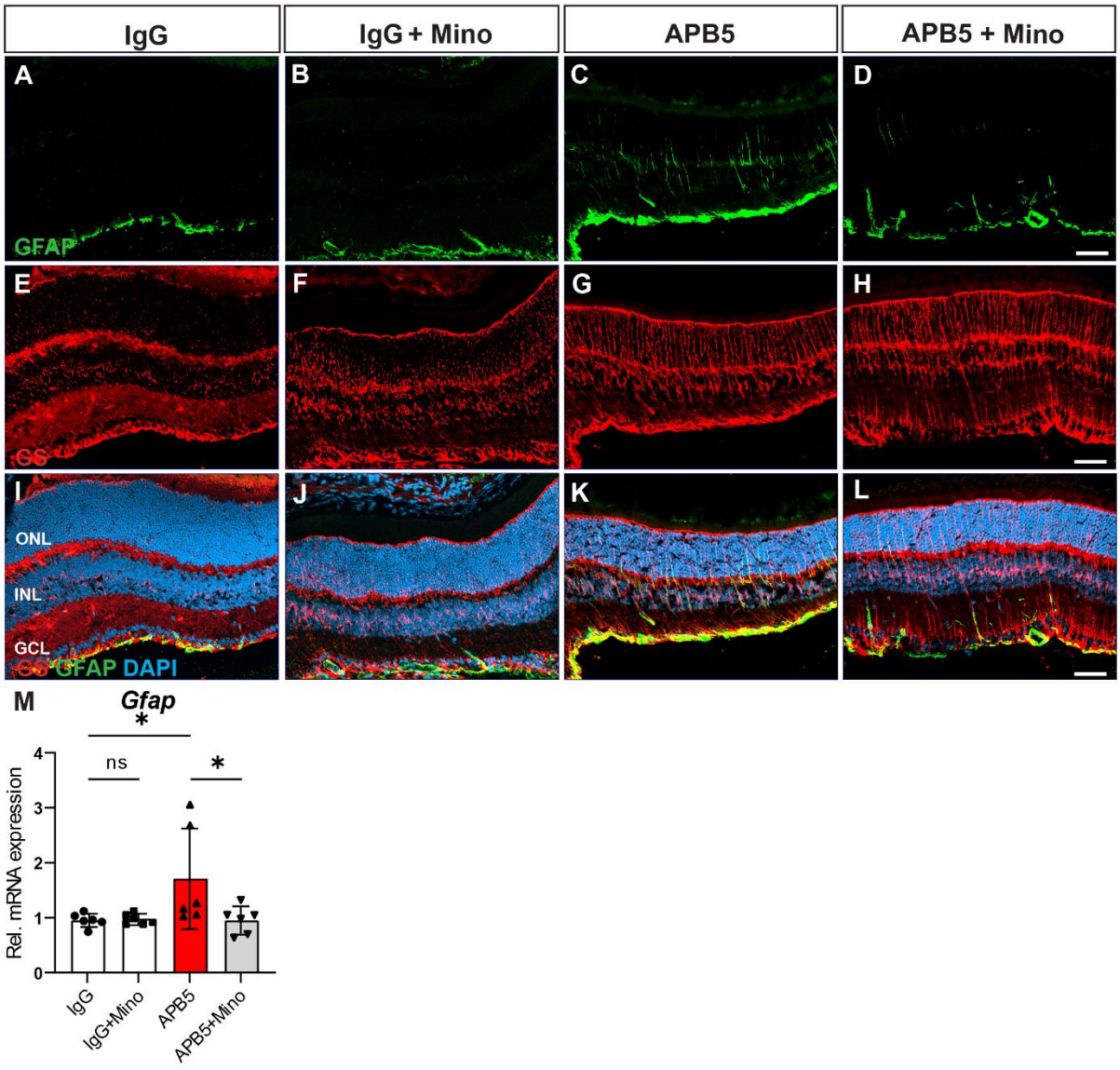

Figure 14: Astrocyte and Müller cell gliosis in the adult retinas. Representative single-channel images for GFAP staining in the IgG, IgG+Mino, APB5, APB5+Mino groups (A-D). Single channel images of GS staining (E-H) and merged images showing the localization of both GFAP and GS in the retinas of IgG, IgG+Mino, APB5 and APB5+Mino (I-L). qRT-PCR quantification of *Gfap* mRNA levels in retinas (M), n = 6 retinae per group. GFAP; glial fibrillary acidic protein; GS; Glutamine synthetase.. *$P < 0.05$, ns, not significant. Data represent mean ± SD. The scale bar is 50µm

3.10 Minocycline limits APB5-induced microgliosis in the mature retina

Following the observation of microglia migration in the ONL and SRS on retinal sections, we sought to analyze comprehensively the morphology and population of microglia within the retina plexiform layers. Quiescent microglia are characterized by a ramified morphology whereas activated microglia are less ramified with an amoeboid phenotype. In the degenerating retina, microglia acquire the amoeboid morphology and migrate across the

retinal layers phagocytosing photoreceptor debris. In the APB5 retina, the phenotype of activated microglia remains to be revealed. Therefore, we sought to study the morphology of microglia and the sequential conversion from a ramified form to an activated form. In addition, we were interested in determining whether immunomodulation by minocycline had effects on microglia morphology during disease progression. Our findings revealed that in the IgG groups, microglia in the IPL retained the classical ramified phenotype (Figure 15A&B) whereas microglia in the IPL of APB5 retinas were less ramified when compared to APB5 retinas treated with minocycline (Figure 15C&D). Within the OPL, microglia in the IgG retinas retained their homeostatic ramified morphology (Figure 15E&F) but were more populated in the APB5 retinas, with visibly reduced branching which was reversed by immunomodulation with minocycline (Figure 15G&H). In healthy retinas the SRS is devoid of microglia cells as was the case in the IgG retinas (Figure 15I-J) but activated and phagocytic microglia cross the ONL and reside in the SRS upon the breakdown of the BRB in APB5 retinas (Figure 15K&L). Further analyses showed that the number of $Iba1^+$ cells in the IPL and OPL was increased significantly in the APB5 retinas but was reduced upon treatment with minocycline (Figure 15M-N). Next, we analyzed key morphological attributes of microglia in the OPL as an indicator of microglia activation. We chose to analyze $Iba1^+$ cells in the ONL because we recorded a high degree of visible microglia activation in this region. Microglia in APB5 retinas showed a significantly reduced ramification index, spanned area, number of branches, number of junctions and tree length (Figure 15O-P) when compared to the IgG retinas. Although treatment with minocycline significantly increased the spanned area and tree length of microglia in APB5 retinas, its effect on the ramification index, number of branches or number of junctions (Figure 15O-T) was not significant to restore the morphology as observed in the IgG retinas.

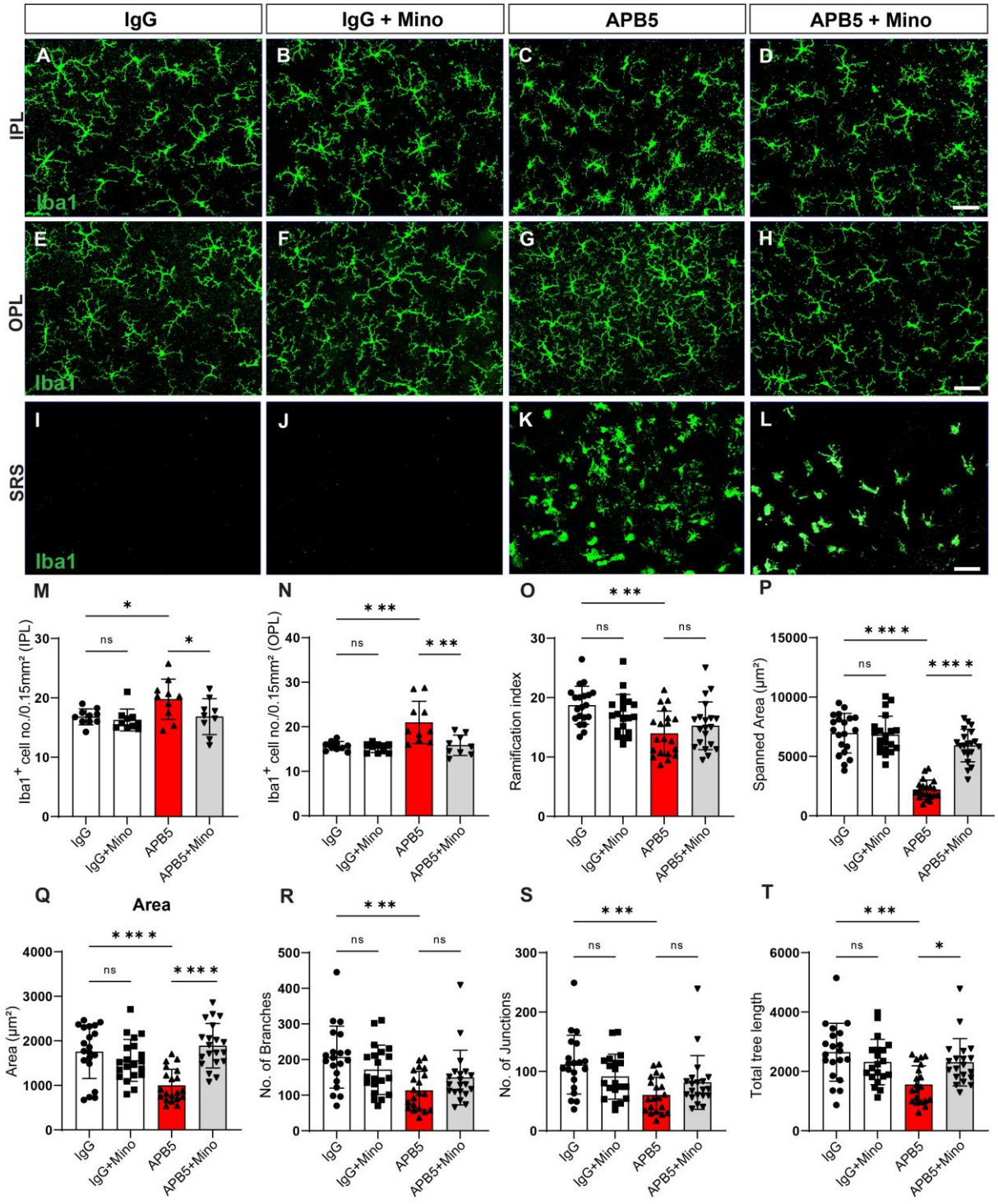

Figure 15: APB5 triggered microglia activation in the adult retina (P28). Representative images of Iba1$^+$ cells in the IPL (A-D), OPL (E-H) and SRS (I-L). Quantification of Iba1$^+$ cells in the plexiform layers and microglia morphometric analyses. Quantification of Iba1$^+$ cells in the IPL (M) and OPL (N) of IgG, IgG+Mino, APB5 and APB5+Mino groups (n = 9 retinas). Morphometric analyses of microglia attributes in the OPL: ramification index (O), spanned area (P), Total area (Q) number of branches (R), number of junctions (S) and total tree length (T) (n = 20 Iba1$^+$ cells across all groups). IPL; inner plexiform layer, OPL; outer plexiform layer; SRS; subretinal space. The scale bar is 50µm. *P < 0.05, ***P < 0.001, ***P < 0.001, ns; not significant. Data represent mean ± SD.

3.11 Variation in the extent of abnormalities in adult vasculature in APB5 and minocycline-treated retinas

Cognizant of the role of PDGFB/PDGFRβ signalling in the postnatal retina, we sought to investigate the extent of vascular abnormalities in the adult retina by immunohistochemistry. Immunohistochemistry for CD31, the endothelial cell marker, on retina whole mounts showed normal capillary organization in the IgG treated retinas (Figure16 A&B) but enlarged capillaries in the APB5 retina (Figure 16C) an observation that was abrogated in the minocycline treated APB5 retinas (Figure 16D). Additionally, we observed no adverse morphological patterning of the retinal veins in the IgG retinas (Figure 16E&F) as well as in APB5 retinas. Furthermore, we quantified various morphological attributes of the retinal vasculature and observed no significant variations in vessel density, number of junctions and lacunarity among the treatment groups (Figure 16I-K). Although these variations were present in the postnatal retina at P10, their absence in the adult vasculature may suggest the involvement of compensatory pericyte coverage of adult vasculature. Nonetheless, APB5 treated retinas had high occurrence of artery-vein crossings and increased capillary size when compared to IgG treated retinas (Figure 16L&M).

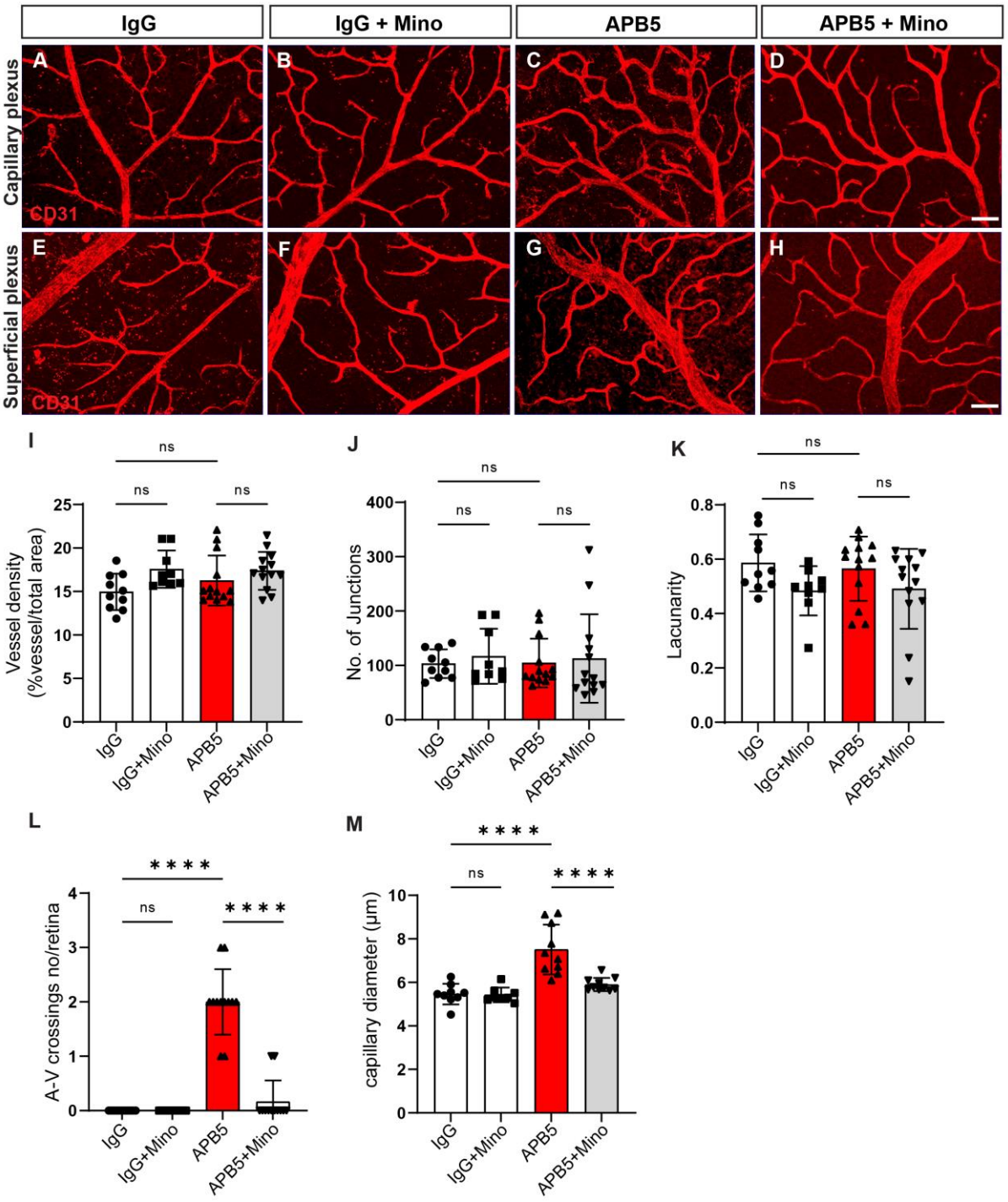

Figure 16: Immunohistochemistry for CD31+ endothelial cells in mature retina. Representative images of CD31⁺ endothelial cells in the capillary plexus (A-D) and superficial plexus showing main veins and linked capillaries (E-H). The scale bar is 50µm. Quantification of the vascular density (I), vessel branching/junctions (J) lacunarity (K), artery-vein crossings (L) and capillary diameter (M) in adult vessels in the superficial plexus (arteries, veins and capillaries). Quantification of vessel density, number of junctions and lacunarity, IgG, n = 10; IgG+Mino, n= 9; APB5, n = 13 and APB5+Mino, n = 13. The scale bar is 50µm. Quantification of artery-vein crossings; n = 10 for all groups. Quantification of capillary diameter: IgG, n = 9; IgG+Mino, n = 8; APB5, n = 10; APB5+Mino, n = 10.. ****$P \leq 0.0001$, ns; not significant. Data represent mean ± SD.

3.12 Minocycline exerts global transcriptomic changes in the APB5-treated retinas

Following the immunohistochemical analyses on retinal flat mounts and cryosections, it was evident that inflammation played a key role in pericyte depletion retinopathy. Next, we sought to investigate the transcriptomic changes in the APB5 retina and the immunomodulatory role of minocycline during disease progression. Firstly, we compared the gene expression profile between the APB5 and IgG retinas at P28. We identified 116 DEGs out of which 102 were upregulated (supplementary table 1) whereas five were downregulated at a cut-off set to Log2 fold change ± 1 and $p \leq 0.05$. Surprisingly, these were the only DEGs genes in when comparing APB5 retinas to IgG retinas. The few genes may be partly attributed to the fact that treatment was done in P1 retinas and analyses done at P28. Among the top expressed genes were the highly conserved male chromosome Y-associated genes including *Ddx3y, Eif2s3y* and *Uty*. In addition, we identified genes related to complement system such as *C4b, Cfi, C3*, and *C1qa* as well as inflammation-related genes including *Lyz2, Glycam1, Fgf2, Edn2*, and *Icam1*. Some of the upregulated genes are shown on the volcano plot (Figure 17A) and a heat map of the top 30 DEGs was generated using the DRAGEN software on Illumina Basespace sequence hub (Supplementary figure 3). Next, we performed gene set enrichment analyses (of all DEGs) using the Kyoto Encylopedia of Genes and Genomes (KEGG) and Gene Ontology (GO) databank and identified key pathways activated in the APB5 retina by P28 (Figure 17B-D). The top 10 KEGG pathways revealed enrichment of pathways involved in inflammation and diseases such as cancer, HIF-1 signalling, complement and coagulation cascades and cellular senescence that correspond with proliferative diabetic retinopathy (Figure 17B). Furthermore, the GO biological processes domain revealed inflammation, hypoxic and vascular remodeling processes among the top APB5-induced processes (Figure 17C). In the molecular function domain, we discovered protein binding, actin binding and integrin binding among the top APB5-induced functions (Figure 17D).

Surprisingly, *Vegf* was not among the differentially expressed genes in the APB5 retinas when compared to control retinas. This finding propelled us to analyse *Vegf* mRNA via RNAscope ISH on retinal sections. Our results from ISH showed no differences in the distribution of *Vegf* mRNA within the INL of the treatment groups. This observation by validated by quantification of gene counts of the RNAseq data (supplementary figure 4).

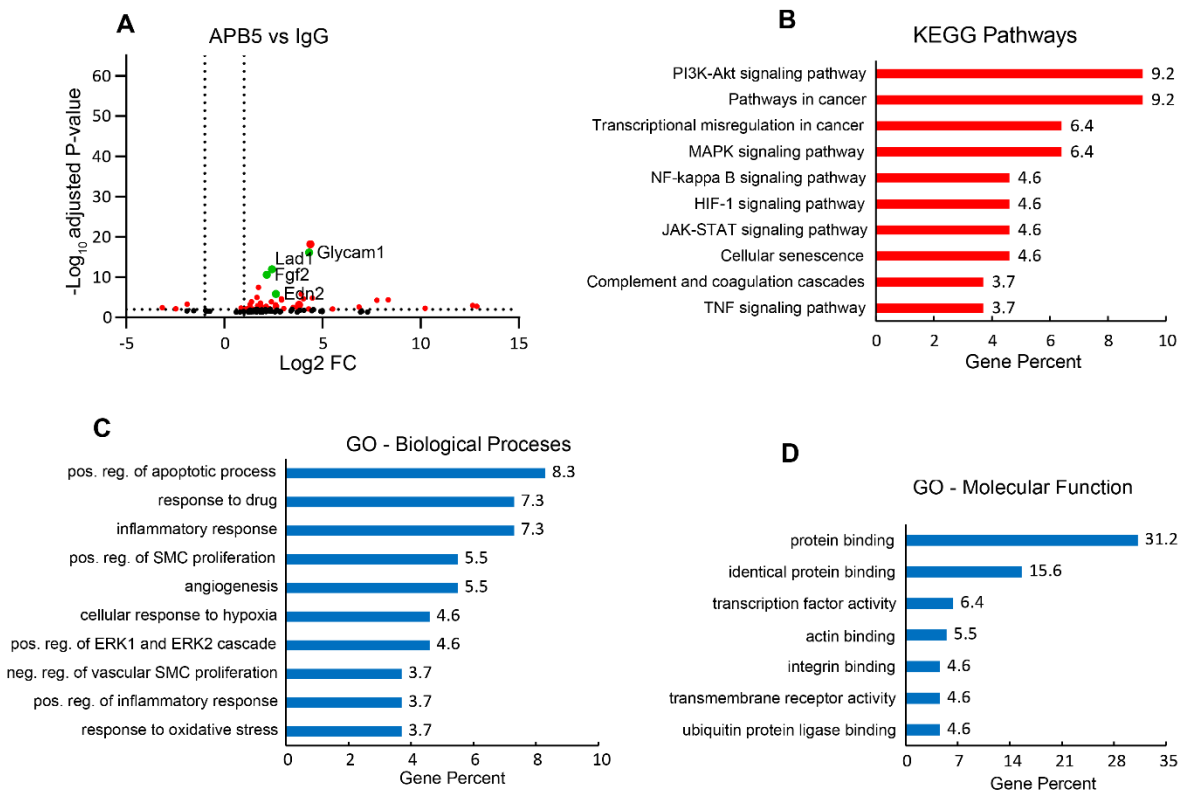

Figure 17: RNA-seq transcriptome analyses of APB5 vs IgG retinas mice at P28. Volcano plot showing comparison of DEGs from control IgG and APB5 retinas at P28 (A). KEGG Pathway analysis showing the top 10 enriched pathways (B). GO domain biological processes showing key processes activated by APB5 (C). GO molecular function domain showing the key functions affected by APB5 (D). The green dots on the volcano plots represent the most significantly upregulated genes. The set cut-off for the DEGs shown on the volcano plot was Log_2 FC of ±1 and FDR of < 0.05. n = 3 mice in each group.

Next, we sought to investigate the immunomodulatory effects of minocycline in the retinas of APB5 mice. Differential gene expression analyses using a false discovery rate-adjusted $P \leq 0.05$ and Log_2 fold change ±1 identified 981 downregulated and 304 upregulated genes. The top 103 differentially downregulated genes are presented in supplementary table 3. We noted that minocycline downregulated some genes that were previously upregulated by APB5 including *Fgf2, Glycam1, Ndufa4l2*, and *Edn2* as illustrated by a volcano plot (Figure 18A). By using a Venn diagram, we show that minocycline modulated the expression of 81 genes that were upregulated by APB5 in P28 retinae (Figure 18B) some of which are presented on the heat map of the top 30 DEGs was generated using the DRAGEN software on Illumina Basespace sequence hub (Supplementary figure 5). Furthermore, we performed gene set enrichment analysis using all the 1,285 DEGs (both up and down at the set cut-off) to identify pathway enrichment. The GO biological processes domain identified processes such as angiogenesis, response to hypoxia, regulation of genes expression and response to drug, as triggered by minocycline (Figure 18C). In the molecular function domain, protein binding, protein homodimerization, enzyme binding, actin binding and integrin binding were among the

top enriched functions (Figure 18D). From the KEGG analysis we identified inflammation associated pathways (P13k-Akt signalling, phagosome, cytokine-cytokine interaction, complement and coagulation cascades, c-type lectin receptor signalling), vascular remodelling pathways (cell-adhesion molecules, regulation of actin cytoskeleton, leukocyte transendothelial migration) and cell death and senescence pathways (apoptosis and cellular senescence) as key pathways regulated by minocycline (Figure 18E). Lastly, we used Morpheus to generate a heat map of top genes upregulated by APB5 and downregulated by minocycline (Figure 18F).

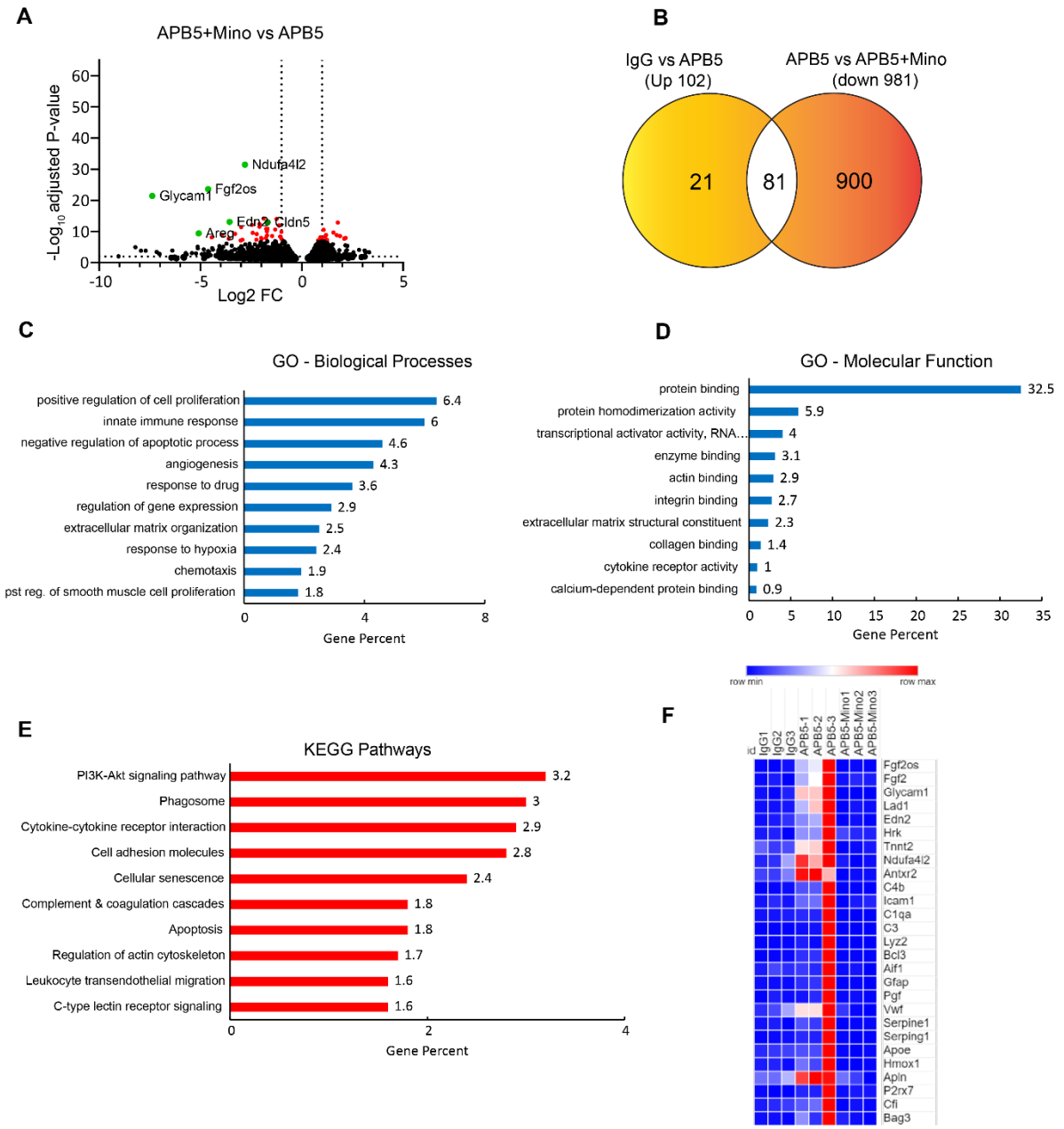

Figure 18: RNA-seq transcriptome analyses of APB5+mino vs APB5 retinas at P28. Volcano plot showing comparison of DEGs from APB5+mino and APB5 retinas at P28 (A). A Venn diagram of the DEGs upregulated by APB5 and downregulated by minocycline (B).

Eighty-one out of the 102 genes upregulated by APB5 were downregulated by minocycline (B). GO domain biological processes showing key processes enriched by minocycline in APB5 retinae (C). GO molecular function domain showing the key functions enriched by minocycline in the APB5 retinae (D). KEGG Pathway analysis shows the top 10 pathways enriched by minocycline (E). A heat map showing the DEGs in the IgG, APB5 and APB5+Mino groups (F). The green dots on the volcano plots represent the most significantly downregulated genes. The set cut-off for the DEGs shown on the volcano plot was Log_2 FC of ±1 and FDR of < 0.05. n = 3 mice in each group.

Next, we performed gene expression analyses by qRT-PCR to validate our RNA-seq transcriptome data with selected marker genes. We observed a high expression of mRNA levels of *Fgf2, Edn2, Aif-1, Casp-1, Lyz2, Tyrobp, Glycam1,* and *Actg2* in the APB5 treated retina, which were significantly reduced in minocycline-treated mice (Figure 19A-H). The strong expression of genes encoding angiogenic factors (*Fgf2 and Edn2*), mediators of inflammatory leukocyte trafficking (*Glycam-1*) and immune cell inflammatory factors (*Aif1, Casp-1, Lyz2 and Tyrobp*) in the disease model highlights the contribution of inflammatory pathways in disease outcome.

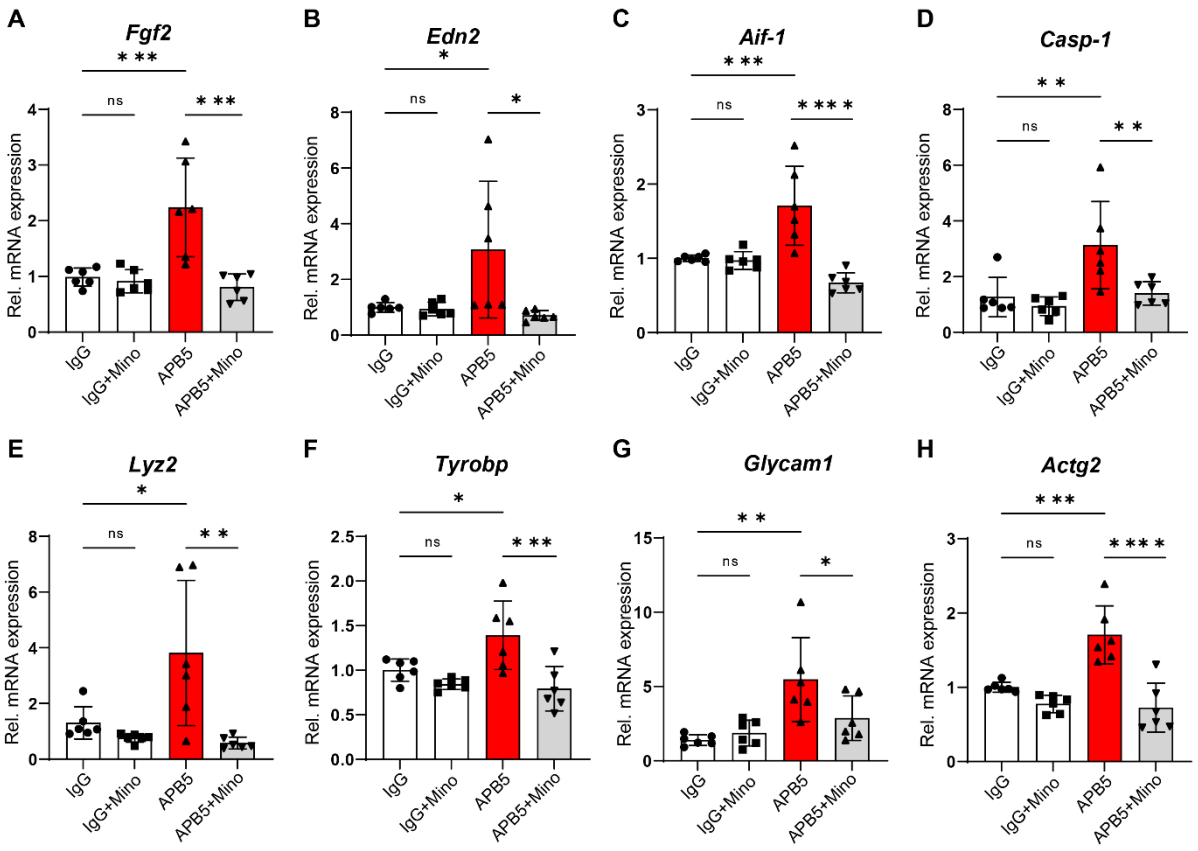

Figure 19: Validation of inflammatory factors and activated microglia signature genes. qRT-PCR analyses of relative mRNA transcript levels of selected genes in the retinas in four weeks old mice treated with IgG or APB5 with or without minocycline. n = 6 retinas. $^{*}P < 0.05$, $^{**}P < 0.01$, $^{***}P < 0.001$ $^{****}P < 0.0001$, ns = not significant. Data presented as mean ± SD.

In another gene expression profiling of the retinas, we observed a significant upregulation of *Icam-1* and *Ccl2* in APB5 retinas, which was significantly reduced with minocycline treatment. (supplementary Figure 6).

Next, we Fibroblast growth factor 2 (FGF2) was among the highly expressed genes downregulated by minocycline. Although FGF2 is an angiogenic factor, it has been found to be expressed by necroptotic microglia in retinopathy. Therefore, we sought to investigate whether AB5 triggered the expression of FGF2 by microglia. For this purpose, retinal cross-sections of mice from the four experimental groups were stained for both FGF2 and Iba1. As shown below, Iba1$^+$ cells within the IPL/OPL expressed FGF2 minimally in the IgG groups (Figure 20A-D) whereas a high expression was observed in the APB5 group (Figure 20E-H). Quantification of FGF2$^+$Iba1$^+$ cells established that the APB5 group had a high abundance of these cells, which was reduced in the APB5-minocycline-treated group (Figure 20M).

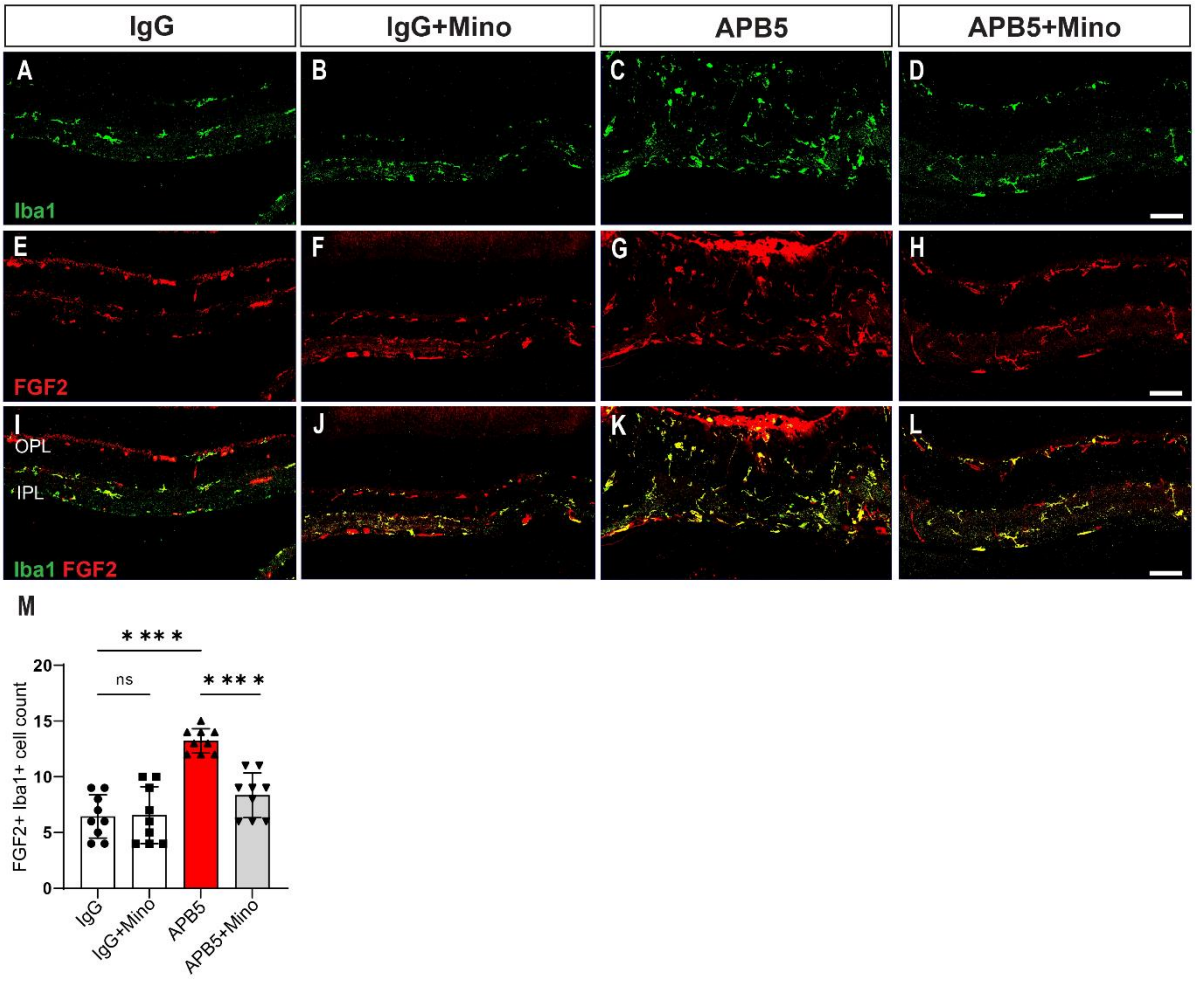

Figure 20: Expression of FGF2 and Iba1 on retinal sections. Representative single-channel images of Iba1$^+$ cells on retinal sections of IgG, IgG+Mino, APB5 & APB5+Mino groups (A-D). Single image channels of FGF2$^+$ cells on retinal sections (E-H). Representative merged images showing Iba1$^+$ FGF2$^+$ microglia cells on retinal sections (I-L). Note the FGF2$^+$Iba1$^+$ cells in the subretinal space of APB5 mice (K). Quantification of FGF2$^+$Iba1$^+$

cells/section in all retinal layers (M). n = 3 eyes; 4 sections/eye. ****P < 0.0001, ns = not significant. Data represent mean ± SD. The scale bar is 50µm.

3.13 Tamoxifen-inducible *Pdgfb* gene deletion efficiency in mature mice

Proper retention of PDGFB in the endothelium is necessary for adequate recruitment and investment of pericytes to ECs (Lindblom et al., 2003) and reduced pericyte density leads to a phenotype reminiscent of human DR (Enge et al., 2002). In order to gain deeper insight into the PDGFB/PDGFRβ signaling in the mature retina, we created an endothelium-specific tamoxifen-inducible PDGFB ablation mouse model by crossing the *Pdgfb*$^{flox/flox}$ (Enge et al., 2002) with the *Cdh5*-Cre-ER^{T2} (Okabe et al., 2014). This breeding strategy generated Cre-positive *Pdgfb*$^{flox/flox}$ litters, which were used as conditional EC PDGFB knock out; *Pdgfb*^{iECKO} mice (Figure 21A). The *Pdgfb*^{iECKO} and age-matched Cre-negative *Pdgfb*$^{flox/flox}$ pups were administered with tamoxifen (100µg in 20µl volume) from P5-P7 and treated with or without minocycline (45mg/kg bw) from P7-P27 once daily and sacrificed at P28. Quantitative PCR analyses of *Pdgfb* transcripts in whole retina lysates revealed that *Pdgfb* mRNA levels were reduced significantly, almost by 50%, in the *Pdgfb*^{iECKO} retinas compared to control mice (Figure 21B). Although the transcript levels of *Cdh5* seemed to be upregulated in the *Pdgfb*^{iECKO} retinas, this was not statistically significant (P < 0.0912) when compared to control retinas (Figure 21C). The transcript levels of the pericyte marker, *Pdgfrβ*, seemed to be lower in the *Pdgfb*^{iECKO} retinas than in control retinas, but this reduction was not significant (P < 0.0739) (Figure 21D). The transcripts were quantified from whole retina lysates and not specifically from endothelial fragments.

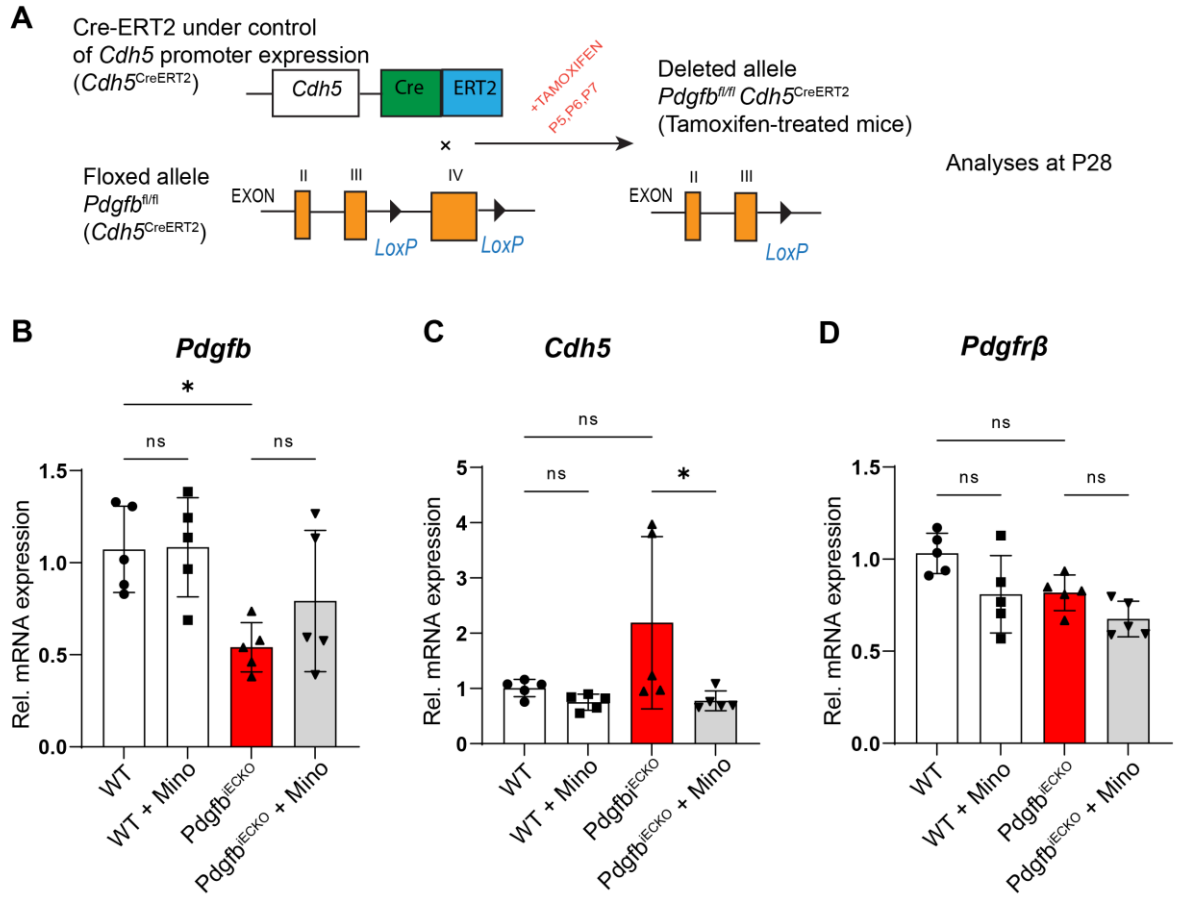

Figure 21: *Pdgfb* deletion in postnatal mouse and gene deletion efficiency in mature mouse retina (P28). Experimental scheme showing tamoxifen-inducible (P5, 6 &7) deletion of exon IV of Pdgfb gene in mouse endothelium under the Cdh5 promoter and analyses at P28 (**A**). Quantitative analyses of mRNA transcripts of Pdgfb (**B**), Cdh5 (**C**) and Pdgfrβ (**D**) in P28 retinas with or without treatment with minocycline (n = 5 retinas). *$P < 0.05$, ns = not significant. Data represent mean ± SD.

3.14 Endothelium-derived PDGFB is necessary for maintenance of BRB integrity

Next, we sought to investigate adult retinal pathology associated with PDGFB ablation during postnatal life. We performed fluorescein angiography *in vivo* to assess the retinal vascular integrity. We observed that the *Pdgfb*^{iECKO} retinas manifested enlarged main vessels and capillaries with fluorescein leakage. The vessels abnormalities in the *Pdgfb*^{iECKO} retinas were lessened upon treatment with minocycline (Figure 22A-D). Next, we analysed the thickness of the retinas by OCT and observed thinning in the central and peripheral regions of some of the *Pdgfb*^{iECKO} retinas when compared to the control mice (Figure 22E-H). In several mice we also observed vessel abnormalities but without concomitant retinal thinning (Figure 22I-L). Treatment of *Pdgfb*^{iECKO} mice with minocycline restored the normal thickness of the retina in the central retina but not the peripheral retina (Figure 22M&N).

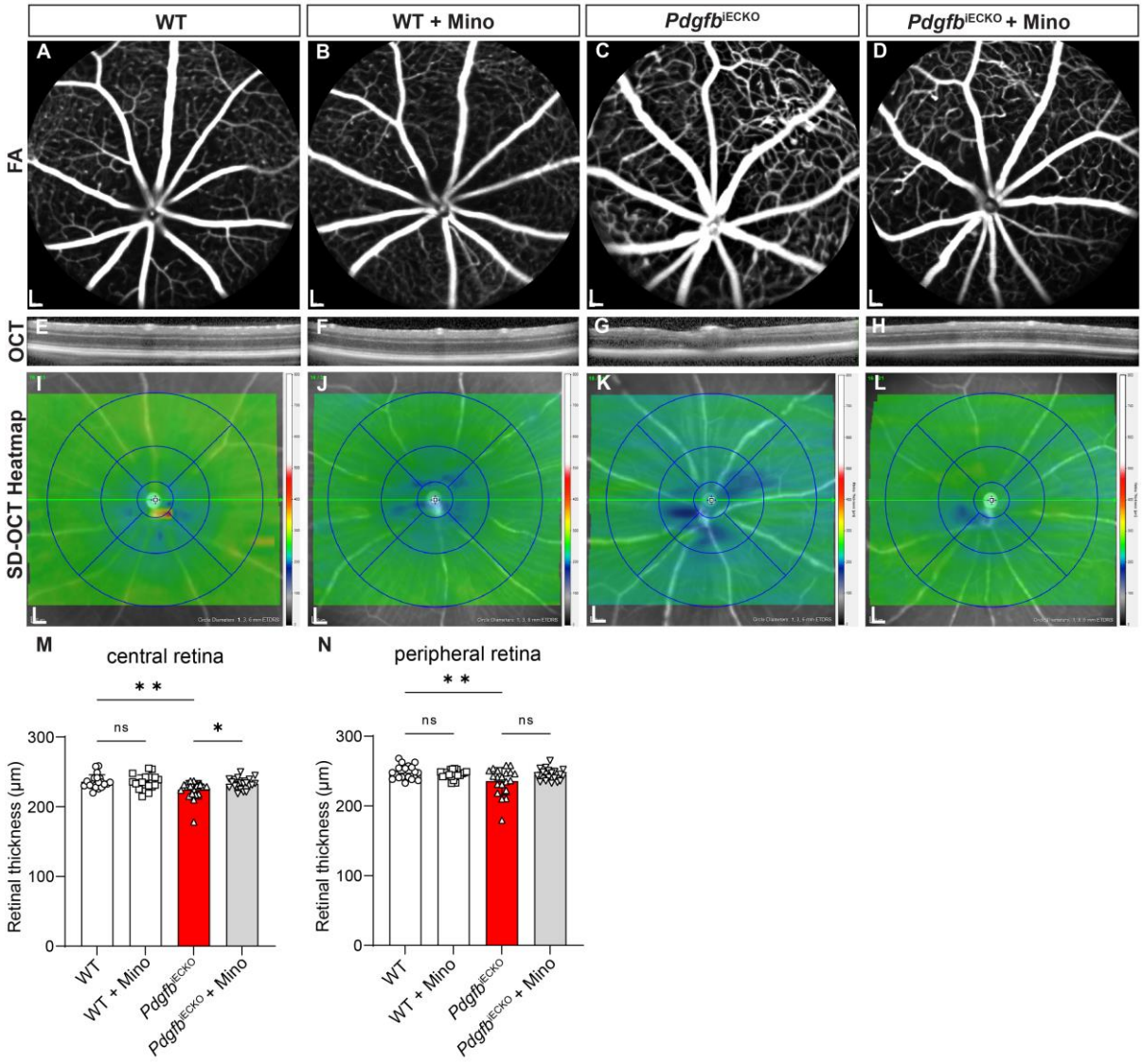

Figure 22: Figure 22: Assessment of retinal vascular integrity and thickness in *Pdgfb* ablation retinas. Fluorescein angiography (FA) images of control and Pdgfb-deficient retinas with or without treatment with minocycline (A-D), note the enlarged vessels and microaneurysm like feature in the Pdgfb^{iECKO} retinas (C). spectral domain-optical coherence tomography (SD-OCT) scan images showing the retinal layers in all groups (E-H). SD-OCT heatmaps showing the volume scans of the whole retina with main vessels visible (I-L) and quantification of retinal thickness across treatment groups (M&N). For retinal thickness, n = 20 eyes per group. *P < 0.05, **P < 0.01, ns = not significant. Data represent mean ± SD. Scale bar for FA and SD-OCT heat maps is 200µm.

The progression of vascular abnormalities in the *Pdgfb*^{iECKO} retinas mimicked some key features of the human disease. Although we used genetic inducible method to knock out *Pdgfb* in retinal endothelium, we observed intra-individual variation in the same mouse. For instance, we observed that the retinal vessels were enlarged in one eye but not the other in the same *Pdgfb*^{iECKO} mice (Figure 23A&B). Furthermore, our analyses of the FA of *Pdgfb*^{iECKO} mice revealed that the vascular abnormalities and leakage were more likely to occur in both eyes of males than in female mice (supplementary table 3). In addition, among the male mice, the

likelihood of the phenotype occurring in the left and right eye was 80% and 50%, respectively. In the female mice, the likelihood of the vascular phenotype occurring in the left and right eye was 50% and 50%, respectively. This suggests that male mice are more susceptible to tamoxifen inducible Pdgfb deletion in the retinal vascular endothelium than females, a phenomenon that deserved further investigation. Previously, Enge and colleagues reported this intra and inter-individual variation in disease phenotype in endothelium-restricted PDGFB loss in the CNS but with a focus on pericyte coverage (Enge et al., 2002). The intra-individual variation in disease progression has been correlated with the clinical progression of human DR, whereby microvasculopathy is manifested in one eye of a patient at early stages of the disease. Pharmacological intervention with minocycline ameliorated vessel tortuosity (Figure 23C&D).

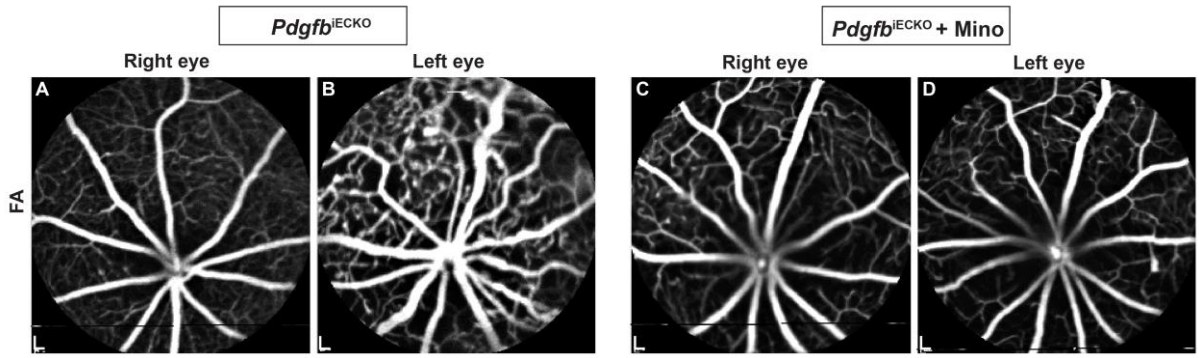

Figure 23: Fluorescein angiography (FA) shows intra-individual variation in vessel abnormalities in the *Pdgfb*^{iECKO} mice. Endothelium-specific loss of PDGFB in postnatal retina produced tortuous vessels in one eye of the adult mouse retina but not the other (A-B). Treatment with minocycline abrogated vessel tortuosity in all the eyes (C-D). The scale bar is 200µm.

Analyses of retina whole mounts stained with the endothelial cells marker, isolectin B4, revealed the extend of vascular malformations in the capillary plexus of *Pdfgb*^{iECKO} retinas when compared to WT mice (Figure 24A-D). Upon examining the superficial vascular network, we observed that only the capillaries linked to the veins in the *Pdfgb*^{iECKO} retinas were enlarged but not the veins (Figure 24E-H). Quantitative analyses of the vascular attributes showed no significant differences in vessel density, number of junctions and lacunarity across treatment groups (Figure 24I-K). However, we observed a significant increase in capillary diameter in the *Pdfgb*^{iECKO} retinas that was significantly reduced in minocycline treated mice (Figure 24L).

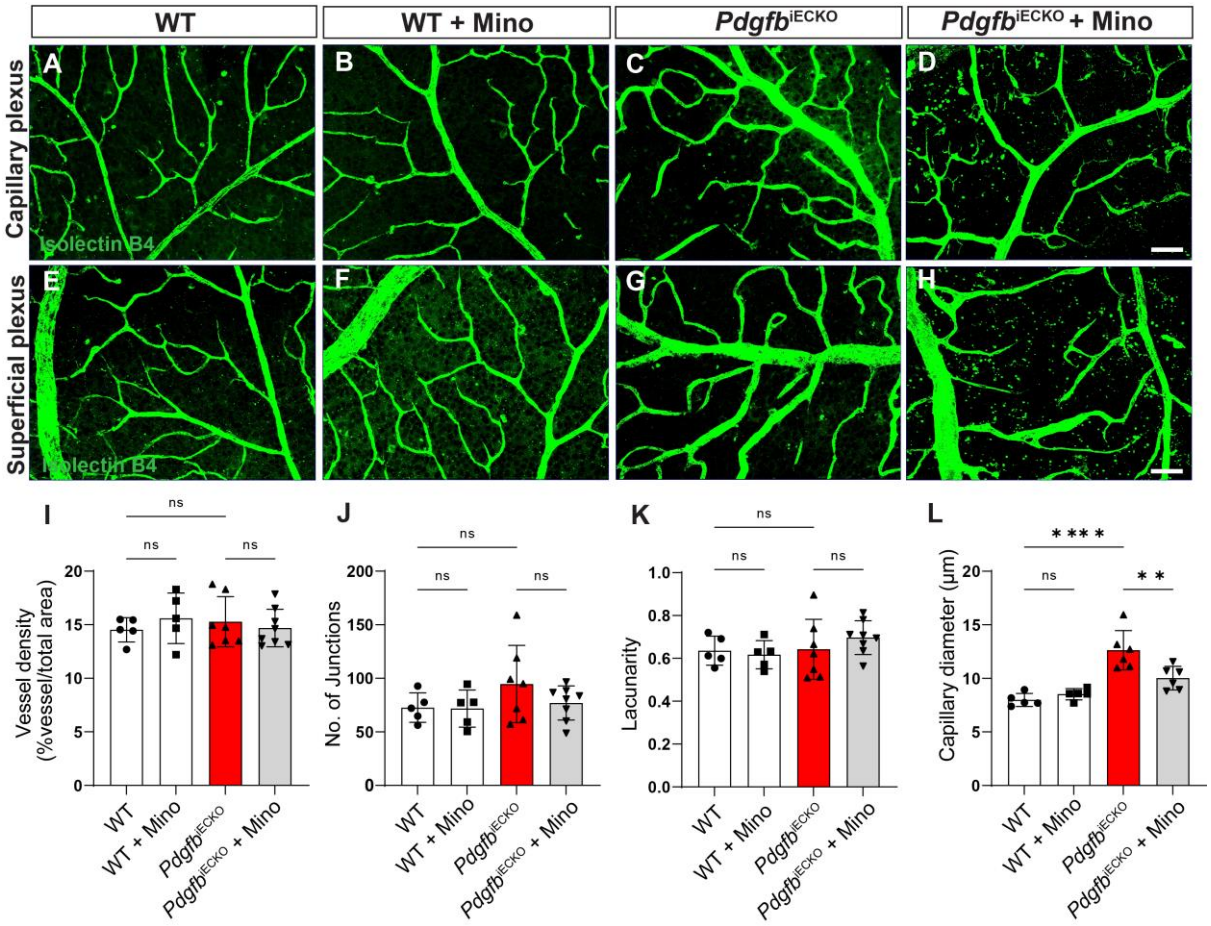

Figure 24: Immunohistochemistry for isolectin B4 and vascular analyses in P28 retinas. Representative images of Isolectin B4 labelled ECs in capillary plexus of WT and *Pdgfb*^{iECKO} retinas with or without minocycline (A-D) and superficial plexus showing main vessels linked to arterioles and capillaries (E-H). Quantification of Isolectin B4 stained area (I), number of vascular junctions (F), vessels lacunarity (K) and capillary diameter (L). I-K; n = 5, 5, 7 and 8 retinas for WT, WT+Mino, *Pdgfb*^{iECKO} and *Pdgfb*^{iECKO} + Mino. L; n = 5 retinas for WT and WT+Mino, n = 6 retinas for *Pdgfb*^{iECKO} and *Pdgfb*^{iECKO} + Mino retinas. ***P* < 0.01, *****P* < 0.0001, ns = not significant. Data present mean ± SD. The scale bar is 50µm.

3.15 Minocycline dampens microglia reactivity upon loss of PDGFB in retinal vasculature

Here, we sought to investigate whether microglia activation was present at the late stage of the disease (P28). Staining of retina whole mounts with Iba1 showed ramified Iba1$^+$ cells in the IPL of WT groups but smaller cells with retracted processes were detected in the *Pdgfb*^{iECKO} group (Figure 25A-C). A similar pattern in microglia morphology was observed in the OPL (Figure 25E-G) of *Pdgfb*^{iECKO} retinas when compared to the control groups. Treatment of *Pdgfb*^{iECKO} mice with minocycline restored the homeostatic morphology of microglia n the IPL and OPL (Figure 25D&H). Activated microglia possess an amoeboid shape and are migratory. This migratory phenotype was confirmed by the presence of many Iba1$^+$ cells in the SRS of *Pdgfb*^{iECKO} retinas (Figure 25I-L). Further, we analyzed the morphological attributes of Iba1$^+$ cells in the OPL to reveal the changes in activated microglia vis a vis homeostatic

microglia. Anatomically, the microglia inhabiting the OPL are positioned close to the SRS than those in the IPL and this positional advantage would make them likely to migrate into the SRS.

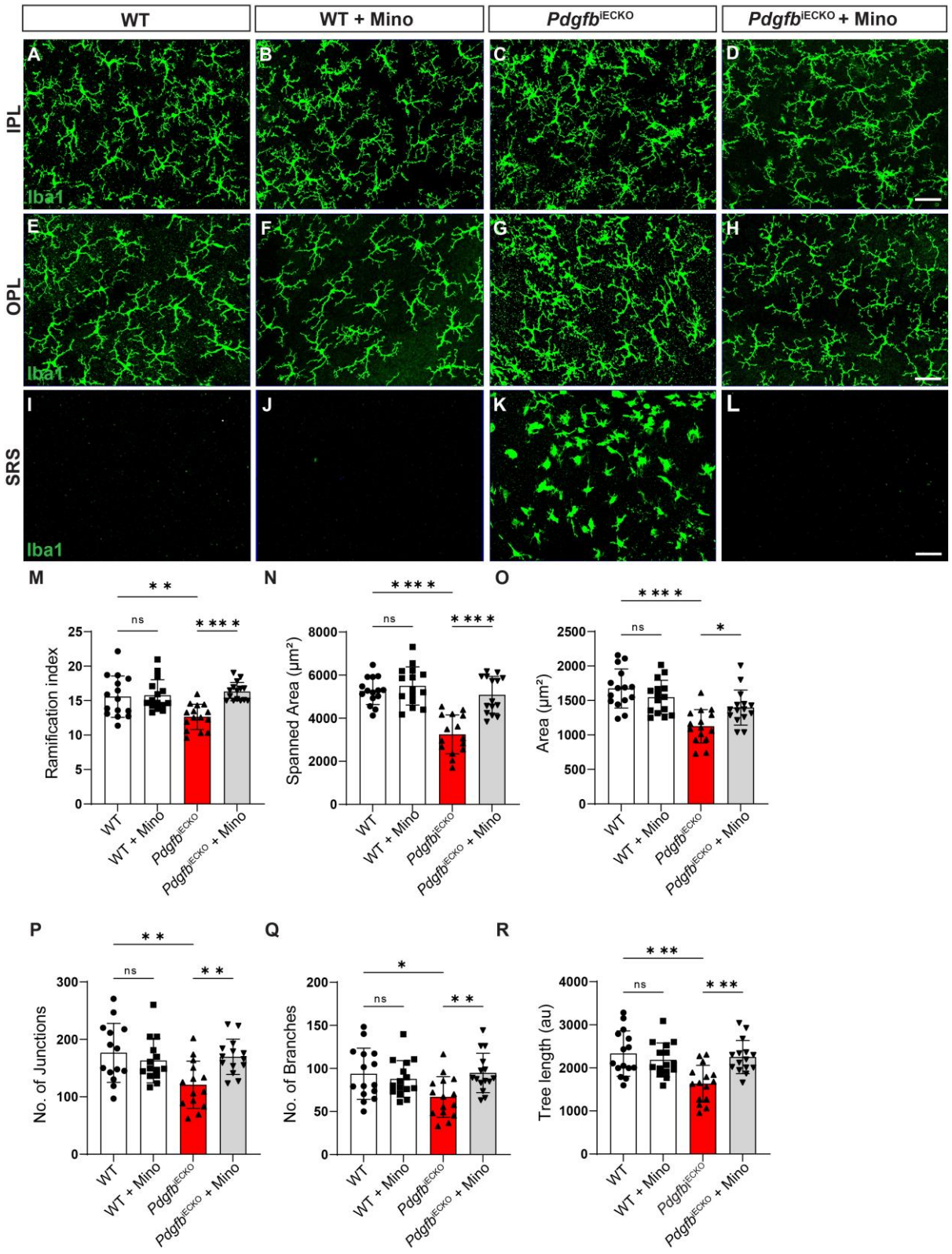

Figure 25: Minocycline limits microglia activation associated with loss of PDGFB in retinal endothelium. Immunohistochemistry of microglia cells in the IPL of WT and Pdgfb^{iECKO} retinas treated with or without minocycline (A-D). *Figure legend continued in page 64*

Note the irregularly shaped microglia in the IPL of *Pdgfb*^{iECKO} retinas (C). Microglia cells in the OPL of WT and Pdgfb^{iECKO} retinas treated with or without minocycline (E-H) with irregular distribution of microglia in the OPL of *Pdgfb*^{iECKO} retinas (G). Iba1+ cells in the SRS of WT and *Pdgf*b^{iECKO} retinas treated with or without minocycline (I-L) with high number of microglia in the SRS of *Pdgfb*^{iECKO} retinas (K). Morphometric analyses of microglia cells in the OPL (n = 20), ramification index (M), spanned area (N), total area (O), number of junctions (P), number of branches (Q) and total tree length (R). Treatment with minocycline restored microglia to their homeostatic morphology. *P < 0.05, **P < 0.01, ***P < 0.001, ****P < 0.0001, ns = not significant. Data represent mean ± SD. The scale bar is 50µm.

3.16 Minocycline exerts anti-inflammatory and anti-angiogenic effect in the *Pdgfb*^{iECKO} retina

Next, we analyzed the expression of the several markers of inflammation and angiogenesis by qRT-PCR. We detected a strong induction of the genes encoding microglia activation markers including *Aif-1, Tspo, Lgals3* and *Lyz2*, in *Pdgfb*^{iECKO} retinas, which was significantly reduced by treatment with minocycline (Figure 26A-D). In comparison to WT mice retinas, *Pdgfb*^{iECKO} retinas showed a significant upregulation of genes encoding potent angiogenic factors including *Edn2*, *Ffg2*, *Pgf* and *Vegfa*, which was significantly reduced by minocycline treatment (Figure 26 E-H). Since FGF2 is known to induce endothelial STAT3 activity to drive pathological neovascularization (Dong et al., 2019), we tested whether minocycline abrogated the mRNA expression of STAT3. Our findings demonstrated that minocycline not only limits the expression of STAT3, but also VWF (Figure 26I-J), key factors driving inflammation of retinal ECs and breakdown of tight junctions in retinal endothelium.

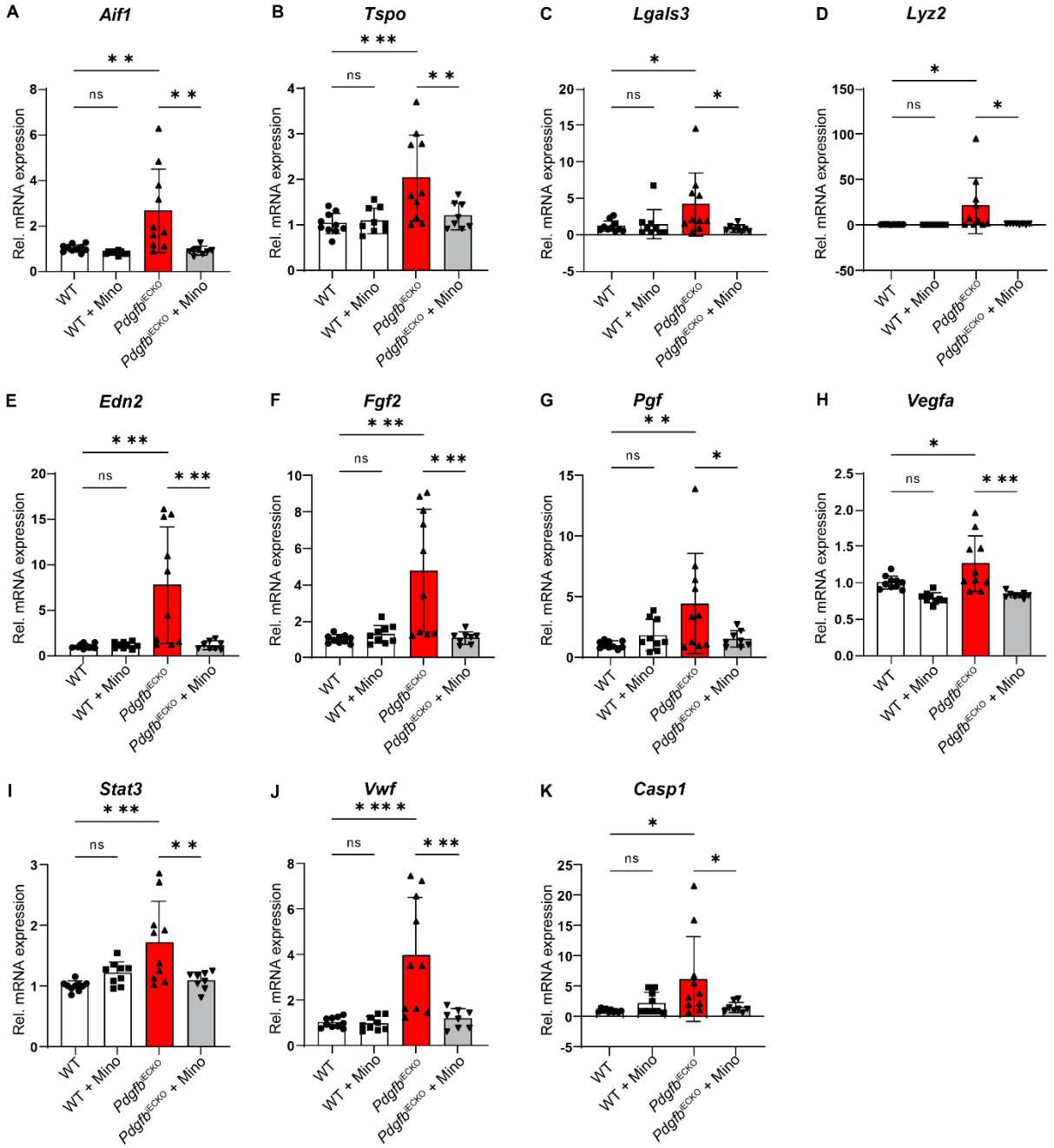

Figure 26: qRT-PCR analyses of pro-inflammatory and pro-angiogenic factors in mature retinas. mRNA transcript levels of *Aif1*, *Tspo*, *Lgals3*, *Lyz2* were significantly upregulated in *Pdgfb*^{iECKO} retinas compared to control WT retinas (A-D). This upregulation was abrogated in *Pdgfb*^{iECKO} retinas of mice treated with minocycline. Analyses of angiogenic factors, *Edn2*, *Fgf2*, *Pgf* and *Vegfa*, showed that they were also elevated in *Pdgfb*^{iECKO} retinas, but were significantly reduced in minocycline treated *Pdgfb*^{iECKO} retinas (E-H). Similarly, we noted a significant downregulation of the transcription factor *Stat3*, *Vwf* and inflammatory factor *Casp1* in *Pdgfb*^{iECKO} retinas treated with minocycline (I-K). WT; n = 10, WT + Mino; n = 9; *Pdgfb*^{iECKO}; n = 10 , *Pdgfb*^{iECKO} + Mino; n = 8. * $P < 0.05$, ** $P < 0.01$, *** $P < 0.001$, **** $P < 0.0001$, ns = not significant. Data represent mean ± SD.

Given that microglia reactivity entails their migration from plexiform layers into the nuclear layers, we stained retinal sections for the microglia marker using an anti-Iba1 antibody. We coupled the immunohistochemical staining of Iba1 with in situ hybridization of *Aif-1* and *Fgf2*

mRNAs. Interestingly, we show that *Fgf2* mRNA within the INL of WT mice translocated to the ONL of *Pdgfb*^{iECKO} mice (Figure 27A-D) but without co-localization with *Aif-1* mRNA which encodes for the microglia marker, Iba1 (Figure 27E-H). Additionally, the translocation of *Fgf2* mRNA to the ONL was reversed by minocycline. Our findings showed that microglia occupied the IPL and OPL layers in the WT groups with or without minocycline but migrated in to the nuclear layers in the *Pdgfb*^{iECKO} retinas (Figure 27I-L). Treatment of *Pdgfb*^{iECKO} mice with minocycline limited microglia migration into the nuclear layers.

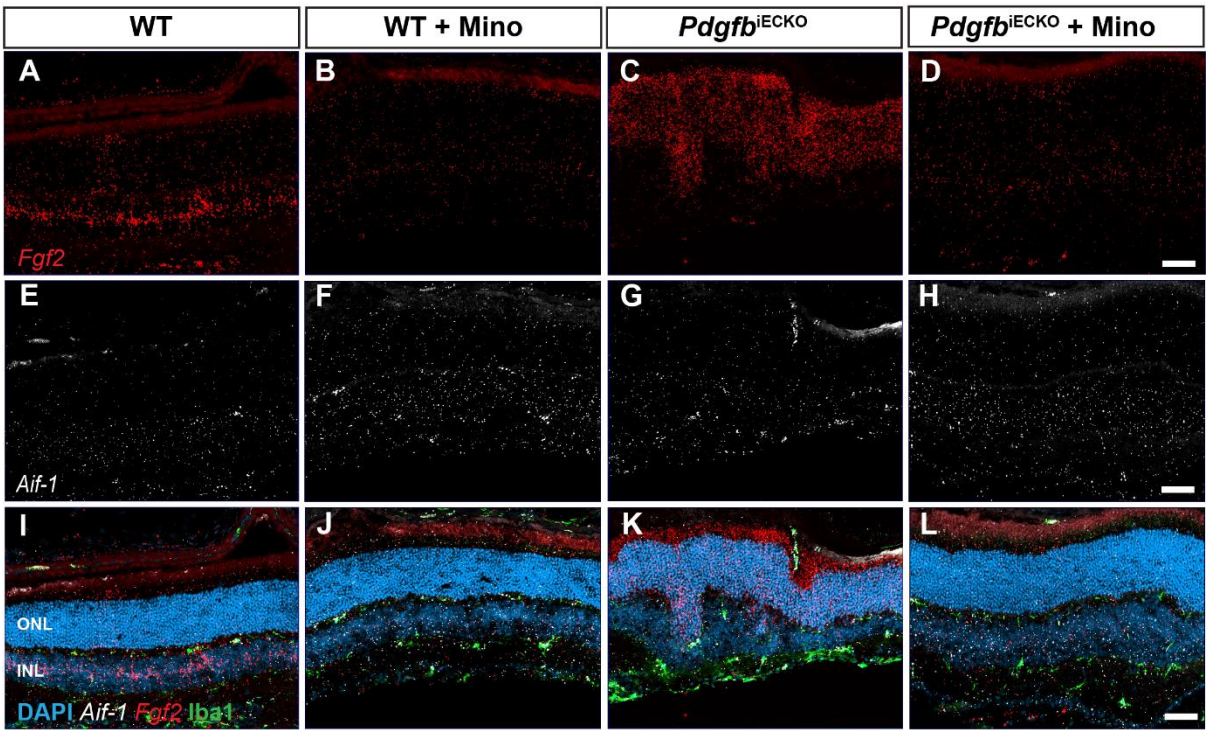

Figure 27: Dual RNAscope ISH of *Aif-1* and *Fgf2* and immunohistochemistry of Iba1 in mature retinas. Representative images showing Fgf2 mRNA expression within the INL of WT mice and its translocation to the ONL of *Pdgfb*^{iECKO} retina (A-D). Representative images of Aif-1 mRNA expression within the retina (E-H) and merged channel images showing the expression of *Fgf2*, *Aif-1* and Iba1^{+} cells (I-L). Note the Iba^{+} cells migrating into the SRS of *Pdgfb*^{iECKO} retina (K). Nuclei stained with DAPI. *Aif-1*; allograft inflammatory factor 1, *Fgf2*; fibroblast growth factor 2. Scale bar is 50µm.

3.17 Minocycline suppressed Müller cell gliosis in the *Pdgfb*^{iECKO} retina

Lastly, we investigated whether Müller cell gliosis was a key feature of retinal pathology associated with conditional loss of PDGFB in the mature retina and the effect of minocycline in astrocyte and Müller cell gliosis. In comparison with WT mice, *Pdgfb*-deficient retinas showed signs of astrocytic stress and Müller cell gliosis, marked by GFAP fibers growing vertically in the retina (Figure 28A-D). Also, we observed what we could classify as a collapse of Müller glia cell bodies *Pdgfb*-deficient retinas (Figure 28E-H). qRT-PCR quantification of

mRNA transcripts showed that mRNA levels of *Gfap* were significantly upregulated in the *Pdgfb*^{iECKO} retinas, an effect that was reversed by treatment with minocycline (Figure 28H).

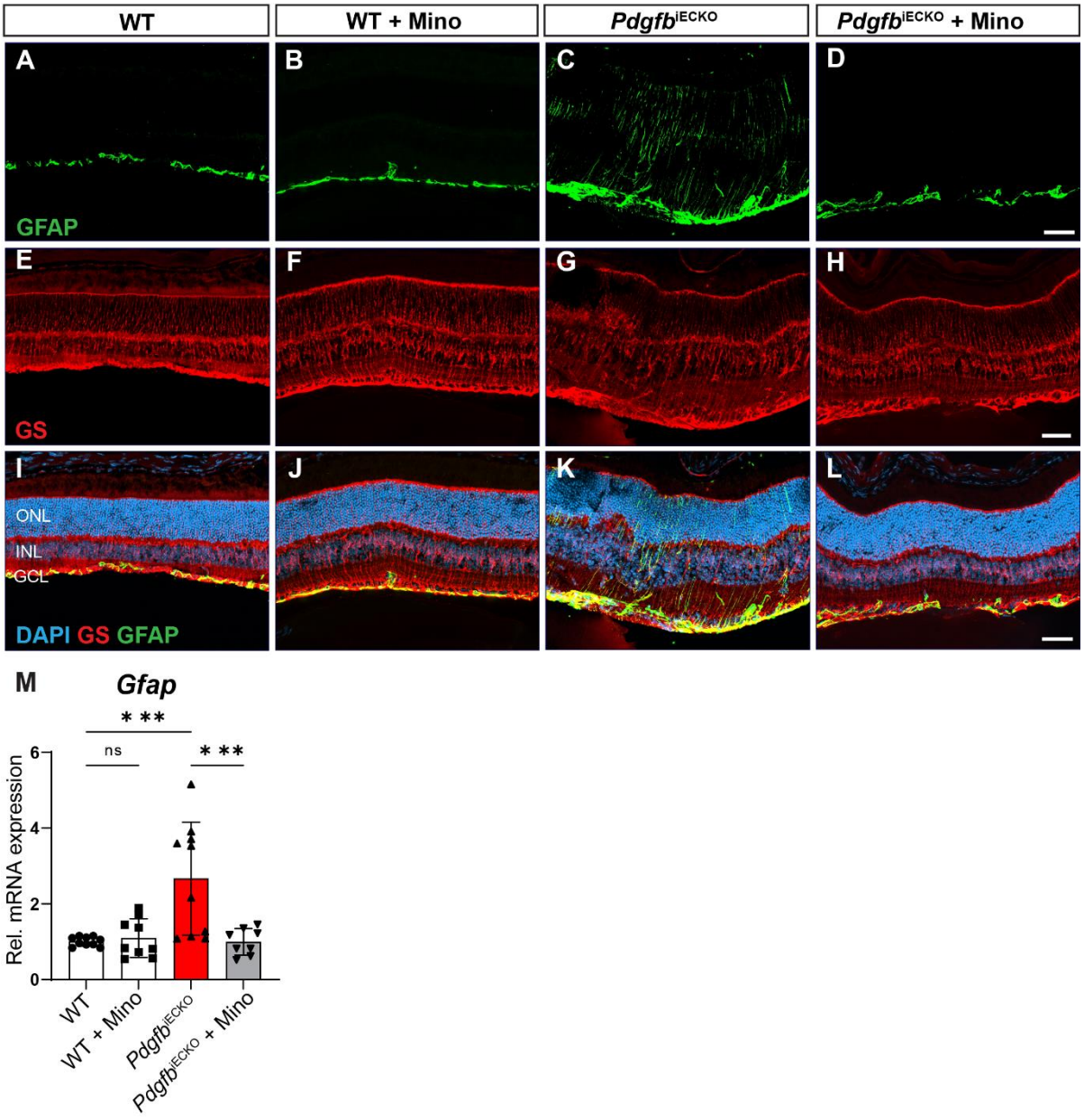

Figure 28: Astrocyte and Müller cell gliosis in the *Pdgfb*^{iECKO} retinas. Representative images of astrocyte labelling with GFAP (A-D). Note the GFAP fibers traversing the retina in Pdgfb^{iECKO} mice (C). Representative images showing of Müller cells labelled with glutamine synthetase (E-H) and merged channel images of both GFAP and GS with nuclei stained with DAPI (I-J). qRT-PCR analysis of *Gfap* mRNA levels in the retinas show their upregulation in *Pdgfb*^{iECKO} retinas with a significant reduction upon treatment with minocycline (M). For qRT-PCR: WT; n = 10, WT + Mino; n = 9; *Pdgfb*^{iECKO}; n = 10, *Pdgfb*^{iECKO} + Mino; n = 8 retinas. , ***P < 0.001, ns = not significant. Data represent mean ± SD. Scale bar is 50µm.

4. DISCUSSION

The PDGFB/PDGFRβ signalling is important for the development of retinal vasculature, maintenance of BRB integrity and retinal homeostasis. Injection of APB5 caused partial or complete dissociation of pericytes from the ECs, loss of tight junction proteins and leakage of blood derived proteins and cells into the retina (Ogura et al., 2017). Also, insufficient retention of PDGFB in retinal ECs led to incomplete pericyte coverage of ECs and loss of BRB integrity in mice (D. Y. Park et al., 2017). In the present study, we have used two models of pharmacological and genetic inhibition of PDGFB/PDGFRβ signalling in the mouse retina. These two models provide new insights in to the pathogenesis of DR by reproducing key features of the human disease unlike previous models of hyperglycemia, which fail to recapitulate the human vascular pathology.

Importantly, the present study has investigated the therapeutic effect of minocycline on retinal vasculature, angiogenic and inflammatory responses in APB5 injected and PDGFB-knock out retinas. In the postnatal mouse retina (P10) injected with APB5, we identified the effect of minocycline by immunohistochemical staining of retinal EC, pericytes, cleaved caspase 3 and microglia. In addition, we have analyzed the mRNA expression levels of key pro-angiogenic, pro-inflammatory and microglia activation markers in the P10 retinas. Our results have indicated that minocycline has no direct effect on retinal pericytes but reduced apoptotic death of ECs, reduced vessel diameters and limited microglia reactivation in the postnatal retina.

Although all types of retina vessels were enlarged with concomitant increase in superficial vascular density and reduced deep vascular network, minocycline restored the postnatal vascular patterning to almost that of control mice. This observation suggests that timely treatment with minocycline promoted the mitotic activity of pericyte-free ECs and their sprouting into the deep vascular layers. Furthermore, we postulate that minocycline protects the postnatal retina vasculature by downregulating the expression of key angiogenic factors including PGF, VEGF, ICAM-1 and Sema3G in APB5 retinas by P10. Dysregulated secretion of these angiogenic factors injures retinal vasculature causing loss of tight junctions, leakage of blood-derived proteins and cells, which trigger activation of retinal microglia. Indeed, previous studies in APB5-treated retinas detected infiltration of perivascular macrophages at P6 in and upregulation of ICAM-1 in whole retinas by P8 (Ogura et al., 2017). In addition, ICAM-1 promotes the infiltration and adhesion of leukocytes in retinal ECs during inflammation. As an inflammatory molecule, ICAM-1 not only upregulates VEGF but also increases vascular leakage and promotes BRB breakdown in the pathogenesis of diabetic macula edema (Jain et al., 2013; Y.-G. Park et al., 2019).

Moreover, we report that minocycline limited the expression Sema3G, an angiogenic factor that has been previously reported in the vitreous fluid of patients with PDR and during the regression phase of OIR in mice (D.-Y. Chen et al., 2021). Sema3G is derived from the endothelium and promotes the functional interaction of β-catenin and VE-cadherin through neuropilin 2 (NRP2) and as a guidance peptide coordinating orderly vascular patterning via Notch signalling (D.-Y. Chen et al., 2021; Hyun et al., 2022). However, its upregulation is associated with angiogenic responses that worsen disease pathology.

Transcriptome analyses of whole retinas revealed pathological pericyte activation in APB5 retinas, a phenotype manifested by the high induction and expression of smooth muscle genes (SMGs), *Acta2* and *Actg2* at P10. Both *Acta2* and *Actg2* encode for actin-beta, a component of the cytoskeleton of pericytes and their upregulation suggests cytoskeletal alterations and inflammation of mural cells. We postulate that PDGFRβ sequestration by APB5 led to not only reduced pericyte coverage of ECs but also increased synthesis of SMGs to remodel the actin cytoskeleton and compensate for migration of pericytes along the PDGFB gradient of the ECs. In addition, the high expression of SMGs at P10 could also be due to a compensatory mechanism to replace pericytes and repair tight junctions in the denuded ECs in APB retinas.

The Angiopoietin/Tie2 and VEGF/VEGFR2 pathways represent signalling systems that regulate vascular homeostasis and control angiogenic response (Saharinen et al., 2017). In the present study, we did not detect elevated mRNA levels of *Ang2* but we have reported *Tie1* among the significantly differentially upregulated genes in the APB5 retina at P10. The use of total retinal lysates for qRT-PCR quantification in our study could partly explain the lower levels of *Ang2* detected in the APB5 retinas since high levels have been reported in the angiogenic front of tip ECs as well as in pericyte-free tip ECs (del Toro et al., 2010; Felcht et al., 2012; D. Y. Park et al., 2017). Intriguingly, the loss of pericytes was associated with increased expression on Tie1 but not Tie2 in APB5 retinas. Although we did not further characterize the activation of Tie1 as opposed to Tie2, our observations support previous findings that reported increased levels of soluble Tie1 (cleaved ectodomain) in the vitreous fluid of EC-specific PDGFB knock-out mice (D. Y. Park et al., 2017).

Microglia activation was also an early feature of retinal inflammation in the APB5 mouse model of DR. This was confirmed by the increase in number of $Iba1^+$ cells and their morphological change in the OPL of APB5 retinas at P10 when compared to the control mice. Our study identified mRNA transcripts of genes encoding key markers of microglia activation including 18kDa *Tspo, Lgals3, Aif1* and *Ccl2* that were significantly upregulated in the APB5 retinas at P10. The upregulation of *Aif1* and *Ccl2* corroborates our histological finding of increased $Iba1^+$ cells in the OPL. At this early time point, our gene expression results showed that minocycline

reduced the expression of *Ccl2*, *Tspo* and *Lgals3* in APB5 retinas. Suppressed secretion of CCL2 leads to a reduction in macrophage recruitment, which explains the lower numbers of $Iba1^+$ cells in minocycline-treated retinas when compared to APB5 retinas. Previously, microglia reactivity in the postnatal APB5 retinas was evidenced by an increase of $F4/80^+$ macrophages in the retina (Shiraya et al., 2020).

Furthermore, transcriptomic analyses of APB5-treated retinas at P10 revealed an activated microglia signature (*Clec7a, Spp1, Itgax, Tyrobp and Lyz2*), previously classified as disease-associated microglia (DAM) in the 5X FAD model of Alzheimer's disease (Keren-Shaul et al., 2017). Although the DAM signature in the 5X FAD model was identified by scRNA sequencing in adult mouse brains, we identified it by bulk RNA sequencing in the diseased postnatal murine retina, suggesting that the DAM signature is expressed at different developmental stages in distinct CNS tissues, retina and brain. Therefore, we also postulate that postnatal attenuation of the PDGFB/PDGFBRβ signalling induced DAM-related gene expression that was not observed in age-matched controls. Deeper analyses with KEGG and GO identified pathways involved in innate immune response.

Although retinal inflammation is considered a secondary consequence of photoreceptor degeneration, we show that in the APB5 retina microglia cells are activated without any observable loss of photoreceptors in the ONL. Although the transcriptomic analyses of the retinas of minocycline-treated APB5 mouse pups is not shown here, we quantified mRNA transcripts of selected markers of inflammation by qRT-PCR. Our findings showed that minocycline reduced the expression of some of the DAM (*Tryobp, Lyz2, Clec7a*) as well as the complement system (*Cq1a* and *C4b*). This beneficial effect of minocycline on the DAM phenotype has been reported in the $Rho^{-/-}$ model of retinal photoreceptor degeneration (Ozaki et al., 2022). Taken together, our results suggest that the anti-inflammatory function of minocycline had suppressed DAM phenotype and complement factors.

Attenuation of PDGFB/PDGFBRβ signalling by either pharmacological inhibition with APB5 or conditional knockout of PDGFB manifests some differences in disease outcome in the 4-week old mouse retina. Whereas APB5 did not trigger upregulation of VEGF but FGF2 in the retinas of 4-week old mice, conditional knockout of PDGFB in ECs triggered upregulation of both VEGF. In PDGFB KO retinas, the expression of VEGF was upregulated under hypoxic conditions caused by capillary blockade and reduced blood flow whereas this led to upregulation of FGF2 in the APB5 retinas. Although the development of DR is mostly associated with VEGF for which treatment is designed, 40-60% of DR patients fail to respond to anti-VEGF therapy (Duh et al., 2017; Gurung et al., 2023) raising the need for more studies in the pathomechanism of DR. The identification of FGF2 in the APB5 retinas opens up a new

route in the search for therapy. FGF2 is an angiogenic factor, dually expression by retinal microglia and vasculature making it a potential immunomodulatory target. The downregulation of FGF2 mRNA levels in the APB5 retinas and VEGF in PDGFB KO retinas shows that the minocycline not only dampens pro-inflammatory factors but also growth factors.

A common observation in both pharmacologic and genetic inhibition models was BRB breakdown as indicated by fluorescein leakage and ONL thinning in one eye but not the other in the same mouse. This phenotype is often observed in DR patients and has been described previously in the APB5 model of DR by Ogura and colleagues (Ogura et al., 2017). Here, we also report this phenotype in the PDGFB KO retinas and show that the vascular phenotype is more likely to occur in male mice than in female mice. Since these sexually divergent responses were not observed in the WT mice treated with tamoxifen, we suggest further investigation on the sex differences in *Pdgfb* gene deletion efficiency and disease progression to unravel the molecular basis for the present findings. Based on this observation we can confirm that postnatal inhibition of PDGFB/PDGFBRβ signalling reproduces key features of the human disease in adult mice. Therefore, these novel models are advanced in terms of disease reproducibility when compared to the hyperglycemic mice.

The failure of the BRB is a major characteristic of late-stage DR in mice and humans accompanied by thinning of the ONL (Duh et al., 2017; O'Leary & Campbell, 2023). Fluorescein angiography confirmed BRB breakdown with concomitant leakage of fluorescein dye in the APB5 and *Pdgfb*^{iECKO} mouse retinas. The breakdown of BRB is associated with loss of function of tight junction proteins and leakage of blood-derived components into the vitreous, leading to a chronic inflammation cycle. In the present study, minocycline downregulated mRNA levels of Endothelin 2, a potent vasoactive factor involved in the BRB breakdown that is known to override the effect of homeostatic regulators of angiogenesis in the retina (Alrashdi et al., 2018). Besides Edn2, the mRNA levels of Von willebrand Factor (VWF) were elevated in the PDGFB KO retinas. VWF promotes the recruitment of leukocytes to the endothelium and its downregulation by minocycline suggest reduced platelet and endothelial activation.

The discovery of Endothelin 2 in non-diabetic conditions further confirms its role in the development of DR complications. Under hyperglycemic conditions, elevated levels of Endothelin 2 mRNA and protein were reported in 24-week-old diabetic Akimba mice thus indicating Endothelin 2 as a marker for vascular alterations in DR (Binz et al., 2016). The vascular alterations including capillary dilation and leaky aneurysms in the APB5 and *Pdgfb*^{iECKO} retinas were abrogated by treatment with minocycline. Similar protective effects of minocycline have been reported in brain microvasculature in a rodent model of brain

subarachnoid hemorrhage (Gendosz de Carrillo et al., 2023). This suggests that minocycline, which can crosses the blood retina and brain barriers confers protection to the capillaries in the CNS.

The inflammatory responses that ensued at an early stage of the disease in the APB5 retinas were sustained in the adult retina. This inflammation is orchestrated by retinal microglia that become overtly activated due to perturbed retinal homeostasis due to infiltration of monocytes and angiogenic factors from the diseased and leaky vasculature. In this study, we have reported that activated microglia migrated from the plexiform layers towards nuclear layers where they participate in phagocytosis of healthy photoreceptors. Treatment with minocycline restored microglia homeostatic phenotype as shown by morphometric analyses and reduced migration of microglia into ONL and SRS in the adult retina. Additionally, minocycline protected the photoreceptors from the adverse effects of microgliosis through the downregulation of microglia activation markers *Fgf2*, *Lgals3*, *Tspo* and *Aif-1* in the APB5 and PDGFB KO retinas. These immune-dampening effects of minocycline at a cellular and molecular level conferred protection to the retinal microenvironment and helped in retention of photoreceptors. The present findings support previous studies that showed minocycline inhibited microgliosis and photoreceptor loss in mouse models of age-related retinal degeneration and P23H-1 (rhodopsin mutation) rat model of retinal degeneration (Di Pierdomenico et al., 2018; Du et al., 2022; Ozaki et al., 2022; Scholz et al., 2015).

Müller glia cells span the entire retina vertically thereby providing structural, neurotrophic and metabolomics support to the photoreceptors and processing visual information (Bringmann et al., 2006, 2009; Tomita et al., 2021). Although reactive Müller glia display protective roles in the retina by the release of antioxidants and neurotrophic factors to maintain tissue homeostasis, unresolved Müller cell gliosis may cause neurodegeneration (Bringmann et al., 2006). Müller cell gliosis, as marked by glial fibrillary acid protein (GFAP) expression by retinal Müller cells, is evident in nearly all retinal pathologies including AMD and DR. Herein, minocycline suppressed Müller cell gliosis and astrocytic stress that was observed in both the APB5 and *Pdgfb*^{iECKO} retinas. Gene expression results indicated that minocycline suppressed *Gfap* mRNA levels, consequently reducing the levels of GFAP in the diseased retinas and limiting reactive gliosis. Similar effects of minocycline on GFAP expression have been reported after subarachnoid hemorrhage (SAH) in mice (Blecharz-Lang et al., 2022; Gendosz de Carrillo et al., 2023).

Besides their supportive role, Müller cells are an important source of VEGF in the retina and play a critical role in modulating vascular function in diabetic retinopathy (Le, 2017). Indeed, Pierce and colleagues used ISH and immunohistochemistry to show that VEGF mRNA and

protein were localized to the cell bodies of Müller glia within the INL in the model of ROP (Pierce et al., 1995). Our findings on VEGF mRNA localized to the INL agree with the observations by Pierce and colleagues. Although VEGF mRNA levels were not altered among the IgG and APB5 groups with or without minocycline, the elevated levels of VEGF mRNA within the cell bodies of Müller glia in the *Pdgfb*^{iECKO} model were suppressed with minocycline. Therefore, we suggest that minocycline partly limits neovascularization and neovascular tuft formation in the *Pdgfb*^{iECKO} model of DR through inhibition of Müller glia-derived VEGF.

Herein, we have identified the molecular and cellular characteristics of retina inflammation following attenuation of PDGFB/PDGFRB signalling. The molecular signature confirms microglia-orchestrated inflammation as an early event that is sustained with the progression of the disease. Long-term treatment with minocycline suppressed inflammation, vascular collapse and ONL shrinkage in the mature retina. The present study identified FGF2 as a major factor associated with disease pathogenesis especially at the late stage in both APB5 and PDGFB-KO mice. The mammalian FGF family is composed of 18 secreted ligands that interact with four cell surface signalling tyrosine kinase receptors (FGFR1-4), regulated by protein cofactors (Ornitz & Itoh, 2015; Xie et al., 2020). Although ECs express FGFRs and are sensitive to FGF ligands, the deletion of *Fgfr1* and *Fgfr2* in cells of endothelial and hemapoietic origin in mice did not affect embryonic development and vascular integrity under physiological conditions but FGFR1/2 signalling was critical in injury-induced and pathological angiogenesis (House et al., 2016; Oladipupo et al., 2014). Despite the activation of multiple intracellular signalling pathways by FGF-FGFR signalling, FGF2 regulates pathogenic angiogenesis in CNV via Signal transducer and activator of transcription 3 (STAT3) activation in the retina (Dong et al., 2019). In addition, STAT proteins play critical roles in early DR and are potent proangiogenic factors in late stage DR (Hong et al., 2022). Besides FGF2, we show that minocycline suppressed STAT3 mRNA in the *Pdgfb*^{iECKO} mature mouse retinas. The protein levels of FGF2 and STAT3 were not investigated in the present study. FGF2 expression has been reported in retinal microglia where it was found to drive pathological angiogenesis in retinopathy via either hypoxia-triggered necroptosis or lactylation in microglia (He et al., 2021; X. Wang et al., 2023). Whether the neutralization or knockout of FGF2 would provide improved benefit and protect the retina from inflammation, vascular dysfunction and ONL shrinkage is yet to be elucidated.

5. CONCLUSION AND PERSPECTIVE

In conclusion, findings of the present study show that minocycline confers protective effects in the mouse retina upon attenuation of PDGFB/PDGFRβ signalling. We have shown that minocycline downregulates the inflammatory gene signature of microglia both at the postnatal stage and in the mature retina. In particular, we have shown that minocycline suppressed DAM signature, activation of microglia and secretion of angiogenic factors, VEGFA, PGF and ICAM-1 in the APB5 retina at the postnatal stage. In retinas of 4-week old mice, minocycline limited the migration of activated microglia into the nuclear layers and SRS and retained microglia in the homeostatic state. The immunomodulatory effect of minocycline in the mature retina was manifested at a molecular level by the decreased mRNA levels of Casp-1, AIF-1, TSPO and LGALS3 in mature retinas.

The present findings further identified FGF2, a growth factor that is upregulated in the APB5 retina besides VEGF. This shift in the expression of angiogenic factors seen in the APB5 retinas may partly explain the dynamics of DR, whereby anti-VEGF therapy is not fully effective in the management of the disease. Notably, minocycline suppressed the expression of both FGF2 and VEGF in the mature retinas. In regulating the expression of various angiogenic factors, we conclude that the effect of minocycline is not specific to CNS macrophages but extents to the endothelium. As the need for a safe treatment that is beneficial to the non-responders of anti-VEGF therapy is urgently needed, we suggest that minocycline may present an impactful therapy in the management of DR among human patients

Despite making a significant contribution to existing knowledge on the pathogenesis of DR, there were some limitations to the present study. Whereas depletion of pericytes or conditional knock out of PDGFB in the postnatal retina reproduces vascular complications similar to that of human disease, these models are non-diabetic and may not reflect the effect of hyperglycemia on retinal microglia. In addition, the retinal pathology in these mice progressed faster than in humans where DR pathology ensues after many years of diabetes mellitus.

While the present findings show a broad effect of minocycline and serve as a basis for the identification of signalling pathways through which these effects are exerted in the retina, they partially demonstrate how minocycline affects immune and non-immune cells and leave several questions to be addressed in the future. Examples of these questions include; i) What is the single molecular driver of disease and target of minocycline in this complex pathology in the retina? ii) To what extent are these findings translatable to human DR patients?

The transcriptome analyses in the present study can be used to answer some of these questions. In search for a single molecular target for minocycline, we propose targeting of

FGF2 by either inducible-gene deletion in the retinal endothelium or neutralization therapy in combination with minocycline to highlight the molecular basis for the current observations in our study. In addition, the expression of FGF2 should be investigated in patients of DR with the aim of exploring anti-FGF2 therapy involving FGF2 aptamers for *in vivo* testing and use in clinical trials. Furthermore, a co-culture system of retinal microglia and endothelial cells or single cell sorting techniques could be used to specifically study the effect of minocycline in these two types of cells. This would be vital in identifying molecular targets of minocycline in these cell types unlike in whole tissue where a repertoire factors from all retinal cells may be responding to minocycline.

Since minocycline is a FDA-approved drug for bacterial infections, we recommend the safety evaluation of minocycline-derived eye drops as an approach for translating the present findings. Local non-invasive administration of minocycline could be a better therapeutic option in comparison to the existing intravitreal injections in the management of retinal vascular diseases.

REFERENCES

Abraham, S., Yeo, M., Montero-Balaguer, M., Paterson, H., Dejana, E., Marshall, C. J., & Mavria, G. (2009). VE-Cadherin-mediated cell-cell interaction suppresses sprouting via signaling to MLC2 phosphorylation. *Current Biology : CB*, *19*(8), 668–674. https://doi.org/10.1016/j.cub.2009.02.057

Alrashdi, S. F., Deliyanti, D., Talia, D. M., & Wilkinson-Berka, J. L. (2018). Endothelin-2 Injures the Blood–Retinal Barrier and Macroglial Müller Cells: Interactions with Angiotensin II, Aldosterone, and NADPH Oxidase. *The American Journal of Pathology*, *188*(3), 805–817. https://doi.org/https://doi.org/10.1016/j.ajpath.2017.11.009

Andrae, J., Gallini, R., & Betsholtz, C. (2008). Role of platelet-derived growth factors in physiology and medicine. *Genes & Development*, *22*(10), 1276–1312. https://doi.org/10.1101/gad.1653708

Armulik, A., Abramsson, A., & Betsholtz, C. (2005). Endothelial/pericyte interactions. *Circulation Research*, *97*(6), 512–523. https://doi.org/10.1161/01.RES.0000182903.16652.d7

Arunagiri, A., Haataja, L., Cunningham, C. N., Shrestha, N., Tsai, B., Qi, L., Liu, M., & Arvan, P. (2018). Misfolded proinsulin in the endoplasmic reticulum during development of beta cell failure in diabetes. *Annals of the New York Academy of Sciences*, *1418*(1), 5–19. https://doi.org/10.1111/nyas.13531

Bai, Y., Ma, J., Guo, J., Wang, J., Zhu, M., Chen, Y., & Le, Y.-Z. (2009). Müller cell-derived VEGF is a significant contributor to retinal neovascularization. *The Journal of Pathology*, *219*(4), 446–454. https://doi.org/https://doi.org/10.1002/path.2611

Balser, C., Wolf, A., Herb, M., & Langmann, T. (2019). Co-inhibition of PGF and VEGF blocks their expression in mononuclear phagocytes and limits neovascularization and leakage in the murine retina. *Journal of Neuroinflammation*, *16*(1), 26. https://doi.org/10.1186/s12974-019-1419-2

Barber, A. J., Antonetti, D. A., Kern, T. S., Reiter, C. E. N., Soans, R. S., Krady, J. K., Levison, S. W., Gardner, T. W., & Bronson, S. K. (2005). The Ins2Akita mouse as a model of early retinal complications in diabetes. *Investigative Ophthalmology & Visual Science*, *46*(6), 2210–2218. https://doi.org/10.1167/iovs.04-1340

Barry-Carroll, L., Greulich, P., Marshall, A. R., Riecken, K., Fehse, B., Askew, K. E., Li, K., Garaschuk, O., Menassa, D. A., & Gomez-Nicola, D. (2023). Microglia colonize the

developing brain by clonal expansion of highly proliferative progenitors, following allometric scaling. *Cell Reports*, *42*(5), 112425. https://doi.org/10.1016/j.celrep.2023.112425

Binz, N., Rakoczy, E. P., Ali Rahman, I. S., Vagaja, N. N., & Lai, C.-M. (2016). Biomarkers for Diabetic Retinopathy - Could Endothelin 2 Be Part of the Answer? *PloS One*, *11*(8), e0160442. https://doi.org/10.1371/journal.pone.0160442

Blanco, R., & Gerhardt, H. (2013). VEGF and Notch in tip and stalk cell selection. *Cold Spring Harbor Perspectives in Medicine*, *3*(1), a006569. https://doi.org/10.1101/cshperspect.a006569

Blecharz-Lang, K. G., Patsouris, V., Nieminen-Kelhä, M., Seiffert, S., Schneider, U. C., & Vajkoczy, P. (2022). Minocycline Attenuates Microglia/Macrophage Phagocytic Activity and Inhibits SAH-Induced Neuronal Cell Death and Inflammation. *Neurocritical Care*, *37*(2), 410–423. https://doi.org/10.1007/s12028-022-01511-5

Bringmann, A., Iandiev, I., Pannicke, T., Wurm, A., Hollborn, M., Wiedemann, P., Osborne, N. N., & Reichenbach, A. (2009). Cellular signaling and factors involved in Müller cell gliosis: neuroprotective and detrimental effects. *Progress in Retinal and Eye Research*, *28*(6), 423–451. https://doi.org/10.1016/j.preteyeres.2009.07.001

Bringmann, A., Pannicke, T., Grosche, J., Francke, M., Wiedemann, P., Skatchkov, S. N., Osborne, N. N., & Reichenbach, A. (2006). Müller cells in the healthy and diseased retina. *Progress in Retinal and Eye Research*, *25*(4), 397–424. https://doi.org/10.1016/j.preteyeres.2006.05.003

Carmeliet, P., Ferreira, V., Breier, G., Pollefeyt, S., Kieckens, L., Gertsenstein, M., Fahrig, M., Vandenhoeck, A., Harpal, K., Eberhardt, C., Declercq, C., Pawling, J., Moons, L., Collen, D., Risau, W., & Nagy, A. (1996). Abnormal blood vessel development and lethality in embryos lacking a single VEGF allele. *Nature*, *380*(6573), 435–439. https://doi.org/10.1038/380435a0

Chan-Ling, T., Hu, P., Li Calzi, S., Warner, J., Uddin, N., DuPont, M., Neuringer, M., Kievit, P., Renner, L., Stoddard, J., Ryals, R., Boulton, M. E., McGill, T., & Grant, M. B. (2023). Glial, Neuronal, Vascular, Retinal Pigment Epithelium, and Inflammatory Cell Damage in a New Western Diet-Induced Primate Model of Diabetic Retinopathy. *The American Journal of Pathology*. https://doi.org/10.1016/j.ajpath.2023.02.019

Chang, R. C.-A., Shi, L., Huang, C. C.-Y., Kim, A. J., Ko, M. L., Zhou, B., & Ko, G. Y.-P. (2015). High-Fat Diet–Induced Retinal Dysfunction. *Investigative Ophthalmology & Visual*

Science, *56*(4), 2367–2380. https://doi.org/10.1167/iovs.14-16143

Checchin, D., Sennlaub, F., Levavasseur, E., Leduc, M., & Chemtob, S. (2006). Potential role of microglia in retinal blood vessel formation. *Investigative Ophthalmology & Visual Science*, *47*(8), 3595–3602. https://doi.org/10.1167/iovs.05-1522

Chen, D.-Y., Sun, N.-H., Chen, X., Gong, J.-J., Yuan, S.-T., Hu, Z.-Z., Lu, N.-N., Körbelin, J., Fukunaga, K., Liu, Q.-H., Lu, Y.-M., & Han, F. (2021). Endothelium-derived semaphorin 3G attenuates ischemic retinopathy by coordinating β-catenin-dependent vascular remodeling. *The Journal of Clinical Investigation*, *131*(4). https://doi.org/10.1172/JCI135296

Chen, H., Charlat, O., Tartaglia, L. A., Woolf, E. A., Weng, X., Ellis, S. J., Lakey, N. D., Culpepper, J., Moore, K. J., Breitbart, R. E., Duyk, G. M., Tepper, R. I., & Morgenstern, J. P. (1996). Evidence that the diabetes gene encodes the leptin receptor: identification of a mutation in the leptin receptor gene in db/db mice. *Cell*, *84*(3), 491–495. https://doi.org/10.1016/s0092-8674(00)81294-5

Chen, L., Yang, P., & Kijlstra, A. (2002). Distribution, markers, and functions of retinal microglia. *Ocular Immunology and Inflammation*, *10*(1), 27–39. https://doi.org/10.1076/ocii.10.1.27.10328

Chen, S., Tisch, N., Kegel, M., Yerbes, R., Hermann, R., Hudalla, H., Zuliani, C., Gülcüler, G. S., Zwadlo, K., von Engelhardt, J., Ruiz de Almodóvar, C., & Martin-Villalba, A. (2017). CNS Macrophages Control Neurovascular Development via CD95L. *Cell Reports*, *19*(7), 1378–1393. https://doi.org/10.1016/j.celrep.2017.04.056

Chen, Y., Peng, F., Xing, Z., Chen, J., Peng, C., & Li, D. (2022). Beneficial effects of natural flavonoids on neuroinflammation. *Frontiers in Immunology*, *13*, 1006434. https://doi.org/10.3389/fimmu.2022.1006434

Cheng, C.-Y., Barro, L., Tsai, S.-T., Feng, T.-W., Wu, X.-Y., Chao, C.-W., Yu, R.-S., Chin, T.-Y., & Hsieh, M. F. (2021). Epigallocatechin-3-Gallate-Loaded Liposomes Favor Anti-Inflammation of Microglia Cells and Promote Neuroprotection. *International Journal of Molecular Sciences*, *22*(6). https://doi.org/10.3390/ijms22063037

Cheung, A. K. H., Fung, M. K. L., Lo, A. C. Y., Lam, T. T. L., So, K. F., Chung, S. S. M., & Chung, S. K. (2005). Aldose reductase deficiency prevents diabetes-induced blood-retinal barrier breakdown, apoptosis, and glial reactivation in the retina of db/db mice. *Diabetes*, *54*(11), 3119–3125. https://doi.org/10.2337/diabetes.54.11.3119

Chopra, I., & Roberts, M. (2001). Tetracycline antibiotics: mode of action, applications,

molecular biology, and epidemiology of bacterial resistance. *Microbiology and Molecular Biology Reviews : MMBR*, *65*(2), 232-60 ; second page, table of contents. https://doi.org/10.1128/MMBR.65.2.232-260.2001

Chow, B. W., & Gu, C. (2017). Gradual Suppression of Transcytosis Governs Functional Blood-Retinal Barrier Formation. *Neuron*, *93*(6), 1325-1333.e3. https://doi.org/https://doi.org/10.1016/j.neuron.2017.02.043

Conway, D. E., Coon, B. G., Budatha, M., Arsenovic, P. T., Orsenigo, F., Wessel, F., Zhang, J., Zhuang, Z., Dejana, E., Vestweber, D., & Schwartz, M. A. (2017). VE-Cadherin Phosphorylation Regulates Endothelial Fluid Shear Stress Responses through the Polarity Protein LGN. *Current Biology : CB*, *27*(14), 2219-2225.e5. https://doi.org/10.1016/j.cub.2017.06.020

Crosby, C. V, Fleming, P. A., Argraves, W. S., Corada, M., Zanetta, L., Dejana, E., & Drake, C. J. (2005). VE-cadherin is not required for the formation of nascent blood vessels but acts to prevent their disassembly. *Blood*, *105*(7), 2771–2776. https://doi.org/10.1182/blood-2004-06-2244

Cukras, C. A., Petrou, P., Chew, E. Y., Meyerle, C. B., & Wong, W. T. (2012). Oral minocycline for the treatment of diabetic macular edema (DME): results of a phase I/II clinical study. *Investigative Ophthalmology & Visual Science*, *53*(7), 3865–3874. https://doi.org/10.1167/iovs.11-9413

De Bock, K., Georgiadou, M., Schoors, S., Kuchnio, A., Wong, B. W., Cantelmo, A. R., Quaegebeur, A., Ghesquière, B., Cauwenberghs, S., Eelen, G., Phng, L.-K., Betz, I., Tembuyser, B., Brepoels, K., Welti, J., Geudens, I., Segura, I., Cruys, B., Bifari, F., … Carmeliet, P. (2013). Role of PFKFB3-Driven Glycolysis in Vessel Sprouting. *Cell*, *154*(3), 651–663. https://doi.org/https://doi.org/10.1016/j.cell.2013.06.037

De, S., Van Deren, D., Peden, E., Hockin, M., Boulet, A., Titen, S., & Capecchi, M. R. (2018). Two distinct ontogenies confer heterogeneity to mouse brain microglia. *Development (Cambridge, England)*, *145*(13). https://doi.org/10.1242/dev.152306

De Schepper, S., Ge, J. Z., Crowley, G., Ferreira, L. S. S., Garceau, D., Toomey, C. E., Sokolova, D., Rueda-Carrasco, J., Shin, S.-H., Kim, J.-S., Childs, T., Lashley, T., Burden, J. J., Sasner, M., Sala Frigerio, C., Jung, S., & Hong, S. (2023). Perivascular cells induce microglial phagocytic states and synaptic engulfment via SPP1 in mouse models of Alzheimer's disease. *Nature Neuroscience*, *26*(3), 406–415. https://doi.org/10.1038/s41593-023-01257-z

Deczkowska, A., Amit, I., & Schwartz, M. (2018). Microglial immune checkpoint mechanisms. *Nature Neuroscience*, *21*(6), 779–786. https://doi.org/10.1038/s41593-018-0145-x

del Toro, R., Prahst, C., Mathivet, T., Siegfried, G., Kaminker, J. S., Larrivee, B., Breant, C., Duarte, A., Takakura, N., Fukamizu, A., Penninger, J., & Eichmann, A. (2010). Identification and functional analysis of endothelial tip cell–enriched genes. *Blood*, *116*(19), 4025–4033. https://doi.org/10.1182/blood-2010-02-270819

Di Pierdomenico, J., Scholz, R., Valiente-Soriano, F. J., Sánchez-Migallón, M. C., Vidal-Sanz, M., Langmann, T., Agudo-Barriuso, M., García-Ayuso, D., & Villegas-Pérez, M. P. (2018). Neuroprotective Effects of FGF2 and Minocycline in Two Animal Models of Inherited Retinal Degeneration. *Investigative Ophthalmology & Visual Science*, *59*(11), 4392–4403. https://doi.org/10.1167/iovs.18-24621

Dixon, K. C., King, A. J., & Malinin, T. (1960). Protein in Dying B-Cells of the Pancreatic Islets. *Quarterly Journal of Experimental Physiology and Cognate Medical Sciences*, *45*(2), 202–212. https://doi.org/10.1113/expphysiol.1960.sp001458

Dong, Z., Santeford, A., Ban, N., Lee, T. J., Smith, C., Ornitz, D. M., & Apte, R. S. (2019). FGF2-induced STAT3 activation regulates pathologic neovascularization. *Experimental Eye Research*, *187*, 107775. https://doi.org/10.1016/j.exer.2019.107775

Dorrell, M. I., Aguilar, E., & Friedlander, M. (2002). Retinal Vascular Development Is Mediated by Endothelial Filopodia, a Preexisting Astrocytic Template and Specific R-Cadherin Adhesion. *Investigative Ophthalmology & Visual Science*, *43*(11), 3500–3510.

Doyle, S. L., Campbell, M., Ozaki, E., Salomon, R. G., Mori, A., Kenna, P. F., Farrar, G. J., Kiang, A.-S., Humphries, M. M., Lavelle, E. C., O'Neill, L. A. J., Hollyfield, J. G., & Humphries, P. (2012). NLRP3 has a protective role in age-related macular degeneration through the induction of IL-18 by drusen components. *Nature Medicine*, *18*(5), 791–798. https://doi.org/10.1038/nm.2717

Du, X., Byrne, E. M., Chen, M., & Xu, H. (2022). Minocycline Inhibits Microglial Activation and Improves Visual Function in a Chronic Model of Age-Related Retinal Degeneration. *Biomedicines*, *10*(12). https://doi.org/10.3390/biomedicines10123222

Duh, E. J., Sun, J. K., & Stitt, A. W. (2017). Diabetic retinopathy: current understanding, mechanisms, and treatment strategies. *JCI Insight*, *2*(14). https://doi.org/10.1172/jci.insight.93751

Eid, S. A., O'Brien, P. D., Hinder, L. M., Hayes, J. M., Mendelson, F. E., Zhang, H., Narayanan, S., Abcouwer, S. F., Brosius, F. C. 3rd, Pennathur, S., Savelieff, M. G., & Feldman, E. L.

(2021). Differential effects of minocycline on microvascular complications in murine models of type 1 and type 2 diabetes. *Journal of Translational Science*, *7*(1). https://doi.org/10.15761/jts.1000431

Eleazu, C. O., Eleazu, K. C., Chukwuma, S., & Essien, U. N. (2013). Review of the mechanism of cell death resulting from streptozotocin challenge in experimental animals, its practical use and potential risk to humans. *Journal of Diabetes and Metabolic Disorders*, *12*(1), 60. https://doi.org/10.1186/2251-6581-12-60

Enge, M., Bjarnegård, M., Gerhardt, H., Gustafsson, E., Kalén, M., Asker, N., Hammes, H.-P., Shani, M., Fässler, R., & Betsholtz, C. (2002). Endothelium-specific platelet-derived growth factor-B ablation mimics diabetic retinopathy. *The EMBO Journal*, *21*(16), 4307–4316. https://doi.org/10.1093/emboj/cdf418

Fan, W., Huang, W., Chen, J., Li, N., Mao, L., & Hou, S. (2022). Retinal microglia: Functions and diseases. *Immunology*, *166*(3), 268–286. https://doi.org/10.1111/imm.13479

Fantin, A., Vieira, J. M., Gestri, G., Denti, L., Schwarz, Q., Prykhozhij, S., Peri, F., Wilson, S. W., & Ruhrberg, C. (2010). Tissue macrophages act as cellular chaperones for vascular anastomosis downstream of VEGF-mediated endothelial tip cell induction. *Blood*, *116*(5), 829–840. https://doi.org/10.1182/blood-2009-12-257832

Feit-Leichman, R. A., Kinouchi, R., Takeda, M., Fan, Z., Mohr, S., Kern, T. S., & Chen, D. F. (2005). Vascular damage in a mouse model of diabetic retinopathy: relation to neuronal and glial changes. *Investigative Ophthalmology & Visual Science*, *46*(11), 4281–4287. https://doi.org/10.1167/iovs.04-1361

Felcht, M., Luck, R., Schering, A., Seidel, P., Srivastava, K., Hu, J., Bartol, A., Kienast, Y., Vettel, C., Loos, E. K., Kutschera, S., Bartels, S., Appak, S., Besemfelder, E., Terhardt, D., Chavakis, E., Wieland, T., Klein, C., Thomas, M., … Augustin, H. G. (2012). Angiopoietin-2 differentially regulates angiogenesis through TIE2 and integrin signaling. *The Journal of Clinical Investigation*, *122*(6), 1991–2005. https://doi.org/10.1172/JCI58832

Ferrara, N., Carver-Moore, K., Chen, H., Dowd, M., Lu, L., O'Shea, K. S., Powell-Braxton, L., Hillan, K. J., & Moore, M. W. (1996). Heterozygous embryonic lethality induced by targeted inactivation of the VEGF gene. *Nature*, *380*(6573), 439–442. https://doi.org/10.1038/380439a0

Fong, G. H., Rossant, J., Gertsenstein, M., & Breitman, M. L. (1995). Role of the Flt-1 receptor tyrosine kinase in regulating the assembly of vascular endothelium. *Nature*, *376*(6535),

66–70. https://doi.org/10.1038/376066a0

Fraccaroli, A., Pitter, B., Taha, A. A., Seebach, J., Huveneers, S., Kirsch, J., Casaroli-Marano, R. P., Zahler, S., Pohl, U., Gerhardt, H., Schnittler, H.-J., & Montanez, E. (2015). Endothelial alpha-parvin controls integrity of developing vasculature and is required for maintenance of cell-cell junctions. *Circulation Research*, *117*(1), 29–40. https://doi.org/10.1161/CIRCRESAHA.117.305818

Fredriksson, L., Li, H., & Eriksson, U. (2004). The PDGF family: four gene products form five dimeric isoforms. *Cytokine & Growth Factor Reviews*, *15*(4), 197–204. https://doi.org/https://doi.org/10.1016/j.cytogfr.2004.03.007

Fruttiger, M. (2002). Development of the mouse retinal vasculature: angiogenesis versus vasculogenesis. *Investigative Ophthalmology & Visual Science*, *43*(2), 522–527.

Fruttiger, M. (2007). Development of the retinal vasculature. *Angiogenesis*, *10*(2), 77–88. https://doi.org/10.1007/s10456-007-9065-1

Garcia-Garcia, J., Usategui-Martin, R., Sanabria, M. R., Fernandez-Perez, E., Telleria, J. J., & Coco-Martin, R. M. (2022). Pathophysiology of Age-Related Macular Degeneration: Implications for Treatment. *Ophthalmic Research*, *65*(6), 615–636. https://doi.org/10.1159/000524942

Gardner, T. W., & Davila, J. R. (2017). The neurovascular unit and the pathophysiologic basis of diabetic retinopathy. *Graefe's Archive for Clinical and Experimental Ophthalmology = Albrecht von Graefes Archiv Fur Klinische Und Experimentelle Ophthalmologie*, *255*(1), 1–6. https://doi.org/10.1007/s00417-016-3548-y

Garrido-Mesa, N., Zarzuelo, A., & Gálvez, J. (2013). Minocycline: far beyond an antibiotic. *British Journal of Pharmacology*, *169*(2), 337–352. https://doi.org/10.1111/bph.12139

Gaucher, D., Chiappore, J. A., Pâques, M., Simonutti, M., Boitard, C., Sahel, J. A., Massin, P., & Picaud, S. (2007). Microglial changes occur without neural cell death in diabetic retinopathy. *Vision Research*, *47*(5), 612–623. https://doi.org/10.1016/j.visres.2006.11.017

Gavard, J. (2014). Endothelial permeability and VE-cadherin: a wacky comradeship. *Cell Adhesion & Migration*, *8*(2), 158–164. https://doi.org/10.4161/cam.29026

Gendosz de Carrillo, D., Student, S., Bula, D., Mielańczyk, Ł., Burek, M., Meybohm, P., & Jędrzejowska-Szypułka, H. (2023). The protective effect of low-dose minocycline on brain microvascular ultrastructure in a rodent model of subarachnoid hemorrhage.

Histochemistry and Cell Biology, *159*(1), 91–114. https://doi.org/10.1007/s00418-022-02150-9

Gerhardt, H., Golding, M., Fruttiger, M., Ruhrberg, C., Lundkvist, A., Abramsson, A., Jeltsch, M., Mitchell, C., Alitalo, K., Shima, D., & Betsholtz, C. (2003). VEGF guides angiogenic sprouting utilizing endothelial tip cell filopodia. *The Journal of Cell Biology*, *161*(6), 1163–1177. https://doi.org/10.1083/jcb.200302047

Giampietro, C., Disanza, A., Bravi, L., Barrios-Rodiles, M., Corada, M., Frittoli, E., Savorani, C., Lampugnani, M. G., Boggetti, B., Niessen, C., Wrana, J. L., Scita, G., & Dejana, E. (2015). The actin-binding protein EPS8 binds VE-cadherin and modulates YAP localization and signaling. *The Journal of Cell Biology*, *211*(6), 1177–1192. https://doi.org/10.1083/jcb.201501089

Giampietro, C., Taddei, A., Corada, M., Sarra-Ferraris, G. M., Alcalay, M., Cavallaro, U., Orsenigo, F., Lampugnani, M. G., & Dejana, E. (2012). Overlapping and divergent signaling pathways of N-cadherin and VE-cadherin in endothelial cells. *Blood*, *119*(9), 2159–2170. https://doi.org/10.1182/blood-2011-09-381012

Ginhoux, F., Greter, M., Leboeuf, M., Nandi, S., See, P., Gokhan, S., Mehler, M. F., Conway, S. J., Ng, L. G., Stanley, E. R., Samokhvalov, I. M., & Merad, M. (2010). Fate mapping analysis reveals that adult microglia derive from primitive macrophages. *Science*, *330*(6005), 841–845. https://doi.org/10.1126/science.1194637

Glassman, A. R., Wells, J. A. 3rd, Josic, K., Maguire, M. G., Antoszyk, A. N., Baker, C., Beaulieu, W. T., Elman, M. J., Jampol, L. M., & Sun, J. K. (2020). Five-Year Outcomes after Initial Aflibercept, Bevacizumab, or Ranibizumab Treatment for Diabetic Macular Edema (Protocol T Extension Study). *Ophthalmology*, *127*(9), 1201–1210. https://doi.org/10.1016/j.ophtha.2020.03.021

Gory, S., Vernet, M., Laurent, M., Dejana, E., Dalmon, J., & Huber, P. (1999). The vascular endothelial-cadherin promoter directs endothelial-specific expression in transgenic mice. *Blood*, *93*(1), 184–192.

Greenwald, R. A., Moak, S. A., Ramamurthy, N. S., & Golub, L. M. (1992). Tetracyclines suppress matrix metalloproteinase activity in adjuvant arthritis and in combination with flurbiprofen, ameliorate bone damage. *The Journal of Rheumatology*, *19*(6), 927–938.

Grimsley-Myers, C. M., Isaacson, R. H., Cadwell, C. M., Campos, J., Hernandes, M. S., Myers, K. R., Seo, T., Giang, W., Griendling, K. K., & Kowalczyk, A. P. (2020). VE-cadherin endocytosis controls vascular integrity and patterning during development. *The Journal*

of Cell Biology, *219*(5). https://doi.org/10.1083/jcb.201909081

Gupta, N., Brown, K. E., & Milam, A. H. (2003). Activated microglia in human retinitis pigmentosa, late-onset retinal degeneration, and age-related macular degeneration. *Experimental Eye Research*, *76*(4), 463–471. https://doi.org/https://doi.org/10.1016/S0014-4835(02)00332-9

Gurung, R. L., FitzGerald, L. M., Liu, E., McComish, B. J., Kaidonis, G., Ridge, B., Hewitt, A. W., Vote, B. J., Verma, N., Craig, J. E., & Burdon, K. P. (2023). Predictive factors for treatment outcomes with intravitreal anti-vascular endothelial growth factor injections in diabetic macular edema in clinical practice. *International Journal of Retina and Vitreous*, *9*(1), 23. https://doi.org/10.1186/s40942-023-00453-0

Han, Z., Guo, J., Conley, S. M., & Naash, M. I. (2013). Retinal angiogenesis in the Ins2(Akita) mouse model of diabetic retinopathy. *Investigative Ophthalmology & Visual Science*, *54*(1), 574–584. https://doi.org/10.1167/iovs.12-10959

Hattori, Y. (2023). The microglia-blood vessel interactions in the developing brain. *Neuroscience Research*, *187*, 58–66. https://doi.org/10.1016/j.neures.2022.09.006

He, C., Liu, Y., Huang, Z., Yang, Z., Zhou, T., Liu, S., Hao, Z., Wang, J., Feng, Q., Liu, Y., Cao, Y., & Liu, X. (2021). A specific RIP3+ subpopulation of microglia promotes retinopathy through a hypoxia-triggered necroptotic mechanism. *Proceedings of the National Academy of Sciences*, *118*(11), e2023290118. https://doi.org/10.1073/pnas.2023290118

Heberle, H., Meirelles, G. V., da Silva, F. R., Telles, G. P., & Minghim, R. (2015). InteractiVenn: a web-based tool for the analysis of sets through Venn diagrams. *BMC Bioinformatics*, *16*(1), 169. https://doi.org/10.1186/s12859-015-0611-3

Hellgren, G., Löfqvist, C., Hansen-Pupp, I., Gram, M., Smith, L. E., Ley, D., & Hellström, A. (2018). Increased postnatal concentrations of pro-inflammatory cytokines are associated with reduced IGF-I levels and retinopathy of prematurity. *Growth Hormone & IGF Research*, *39*, 19–24. https://doi.org/https://doi.org/10.1016/j.ghir.2017.11.006

Hellström, M., Kalén, M., Lindahl, P., Abramsson, A., & Betsholtz, C. (1999). Role of PDGF-B and PDGFR-beta in recruitment of vascular smooth muscle cells and pericytes during embryonic blood vessel formation in the mouse. *Development (Cambridge, England)*, *126*(14), 3047–3055. https://doi.org/10.1242/dev.126.14.3047

Hill, R. A., Tong, L., Yuan, P., Murikinati, S., Gupta, S., & Grutzendler, J. (2015). Regional Blood Flow in the Normal and Ischemic Brain Is Controlled by Arteriolar Smooth Muscle

Cell Contractility and Not by Capillary Pericytes. *Neuron*, *87*(1), 95–110. https://doi.org/10.1016/j.neuron.2015.06.001

Hong, L., Lin, Y., Yang, X., Wu, T., Zhang, Y., Xie, Z., Yu, J., Zhao, H., Yi, G., & Fu, M. (2022). A Narrative Review of STAT Proteins in Diabetic Retinopathy: From Mechanisms to Therapeutic Prospects. *Ophthalmology and Therapy*, *11*(6), 2005–2026. https://doi.org/10.1007/s40123-022-00581-0

House, S. L., Castro, A. M., Lupu, T. S., Weinheimer, C., Smith, C., Kovacs, A., & Ornitz, D. M. (2016). Endothelial fibroblast growth factor receptor signaling is required for vascular remodeling following cardiac ischemia-reperfusion injury. *American Journal of Physiology. Heart and Circulatory Physiology*, *310*(5), H559-71. https://doi.org/10.1152/ajpheart.00758.2015

Hu, Z., Mao, X., Chen, M., Wu, X., Zhu, T., Liu, Y., Zhang, Z., Fan, W., Xie, P., Yuan, S., & Liu, Q. (2022). Single-Cell Transcriptomics Reveals Novel Role of Microglia in Fibrovascular Membrane of Proliferative Diabetic Retinopathy. *Diabetes*, *71*(4), 762–773. https://doi.org/10.2337/db21-0551

Huang, D. W., Sherman, B. T., & Lempicki, R. A. (2009). Systematic and integrative analysis of large gene lists using DAVID bioinformatics resources. *Nature Protocols*, *4*(1), 44–57. https://doi.org/10.1038/nprot.2008.211

Huang, Z., Liang, J., Chen, S., Ng, T. K., Brelén, M. E., Liu, Q., Yang, R., Xie, B., Ke, S., Chen, W., & Huang, D. (2023). RIP3-mediated microglial necroptosis promotes neuroinflammation and neurodegeneration in the early stages of diabetic retinopathy. *Cell Death & Disease*, *14*(3), 227. https://doi.org/10.1038/s41419-023-05660-z

Huang, Z., Zhou, T., Sun, X., Zheng, Y., Cheng, B., Li, M., Liu, X., & He, C. (2018). Necroptosis in microglia contributes to neuroinflammation and retinal degeneration through TLR4 activation. *Cell Death and Differentiation*, *25*(1), 180–189. https://doi.org/10.1038/cdd.2017.141

Hummel, K. P., Dickie, M. M., & Coleman, D. L. (1966). Diabetes, a New Mutation in the Mouse. *Science*, *153*(3740), 1127–1128. https://doi.org/10.1126/science.153.3740.1127

Huxlin, K. R., Sefton, A. J., & Furby, J. H. (1992). The origin and development of retinal astrocytes in the mouse. *Journal of Neurocytology*, *21*(7), 530–544. https://doi.org/10.1007/BF01186955

Hyun, J., Lee, M., Rehman, J., Pajcini, K. V, & Malik, A. B. (2022). Notch1 promotes ordered revascularization through Semaphorin 3g modulation of downstream vascular patterning

signalling factors. *The Journal of Physiology*, *600*(3), 509–530. https://doi.org/https://doi.org/10.1113/JP282286

Izumi, T., Yokota-Hashimoto, H., Zhao, S., Wang, J., Halban, P. A., & Takeuchi, T. (2003). Dominant Negative Pathogenesis by Mutant Proinsulin in the Akita Diabetic Mouse . *Diabetes*, *52*(2), 409–416. https://doi.org/10.2337/diabetes.52.2.409

Jain, A., Saxena, S., Khanna, V. K., Shukla, R. K., & Meyer, C. H. (2013). Status of serum VEGF and ICAM-1 and its association with external limiting membrane and inner segment-outer segment junction disruption in type 2 diabetes mellitus. *Molecular Vision*, *19*, 1760–1768.

Jin, Y., Ding, Y., Richards, M., Kaakinen, M., Giese, W., Baumann, E., Szymborska, A., Rosa, A., Nordling, S., Schimmel, L., Akmeriç, E. B., Pena, A., Nwadozi, E., Jamalpour, M., Holstein, K., Sáinz-Jaspeado, M., Bernabeu, M. O., Welsh, M., Gordon, E., … Claesson-Welsh, L. (2022). Tyrosine-protein kinase Yes controls endothelial junctional plasticity and barrier integrity by regulating VE-cadherin phosphorylation and endocytosis. *Nature Cardiovascular Research*, *1*(12), 1156–1173. https://doi.org/10.1038/s44161-022-00172-z

Jonsson, K. B., Frydkjaer-Olsen, U., & Grauslund, J. (2016). Vascular Changes and Neurodegeneration in the Early Stages of Diabetic Retinopathy: Which Comes First? *Ophthalmic Research*, *56*(1), 1–9. https://doi.org/10.1159/000444498

Joussen, A. M., Doehmen, S., Le, M. L., Koizumi, K., Radetzky, S., Krohne, T. U., Poulaki, V., Semkova, I., & Kociok, N. (2009). TNF-alpha mediated apoptosis plays an important role in the development of early diabetic retinopathy and long-term histopathological alterations. *Molecular Vision*, *15*, 1418–1428.

Karlstetter, M., Scholz, R., Rutar, M., Wong, W. T., Provis, J. M., & Langmann, T. (2015). Retinal microglia: Just bystander or target for therapy? *Progress in Retinal and Eye Research*, *45*, 30–57. https://doi.org/10.1016/j.preteyeres.2014.11.004

Keren-Shaul, H., Spinrad, A., Weiner, A., Matcovitch-Natan, O., Dvir-Szternfeld, R., Ulland, T. K., David, E., Baruch, K., Lara-Astaiso, D., Toth, B., Itzkovitz, S., Colonna, M., Schwartz, M., & Amit, I. (2017). A Unique Microglia Type Associated with Restricting Development of Alzheimer's Disease. *Cell*, *169*(7), 1276-1290.e17. https://doi.org/10.1016/j.cell.2017.05.018

Kierdorf, K., Erny, D., Goldmann, T., Sander, V., Schulz, C., Perdiguero, E. G., Wieghofer, P., Heinrich, A., Riemke, P., Hölscher, C., Müller, D. N., Luckow, B., Brocker, T., Debowski,

K., Fritz, G., Opdenakker, G., Diefenbach, A., Biber, K., Heikenwalder, M., … Prinz, M. (2013). Microglia emerge from erythromyeloid precursors via Pu.1- and Irf8-dependent pathways. *Nature Neuroscience*, *16*(3), 273–280. https://doi.org/10.1038/nn.3318

Kim, M. E., Park, P. R., Na, J. Y., Jung, I., Cho, J. H., & Lee, J. S. (2019). Anti-neuroinflammatory effects of galangin in LPS-stimulated BV-2 microglia through regulation of IL-1β production and the NF-κB signaling pathways. *Molecular and Cellular Biochemistry*, *451*(1–2), 145–153. https://doi.org/10.1007/s11010-018-3401-1

Kinuthia, U. M., Wolf, A., & Langmann, T. (2020). Microglia and Inflammatory Responses in Diabetic Retinopathy. In *Frontiers in Immunology* (Vol. 11, p. 2888). https://doi.org/10.3389/fimmu.2020.564077

Kloppenburg, M., Dijkmans, B. A., Verweij, C. L., & Breedveld, F. C. (1996). Inflammatory and immunological parameters of disease activity in rheumatoid arthritis patients treated with minocycline. *Immunopharmacology*, *31*(2–3), 163–169. https://doi.org/10.1016/0162-3109(95)00041-0

Krady, J. K., Basu, A., Allen, C. M., Xu, Y., LaNoue, K. F., Gardner, T. W., & Levison, S. W. (2005). Minocycline reduces proinflammatory cytokine expression, microglial activation, and caspase-3 activation in a rodent model of diabetic retinopathy. *Diabetes*, *54*(5), 1559–1565. https://doi.org/10.2337/diabetes.54.5.1559

Kubota, Y., Takubo, K., Shimizu, T., Ohno, H., Kishi, K., Shibuya, M., Saya, H., & Suda, T. (2009). M-CSF inhibition selectively targets pathological angiogenesis and lymphangiogenesis. *The Journal of Experimental Medicine*, *206*(5), 1089–1102. https://doi.org/10.1084/jem.20081605

Lagendijk, A. K., & Hogan, B. M. (2015). VE-cadherin in vascular development: a coordinator of cell signaling and tissue morphogenesis. *Current Topics in Developmental Biology*, *112*, 325–352. https://doi.org/10.1016/bs.ctdb.2014.11.024

Lauro, C., Chece, G., Monaco, L., Antonangeli, F., Peruzzi, G., Rinaldo, S., Paone, A., Cutruzzolà, F., & Limatola, C. (2019). Fractalkine Modulates Microglia Metabolism in Brain Ischemia. In *Frontiers in Cellular Neuroscience* (Vol. 13, p. 414). https://doi.org/10.3389/fncel.2019.00414

Le May, C., Chu, K., Hu, M., Ortega, C. S., Simpson, E. R., Korach, K. S., Tsai, M.-J., & Mauvais-Jarvis, F. (2006). Estrogens protect pancreatic beta-cells from apoptosis and prevent insulin-deficient diabetes mellitus in mice. *Proceedings of the National Academy of Sciences of the United States of America*, *103*(24), 9232–9237.

https://doi.org/10.1073/pnas.0602956103

Le, Y.-Z. (2017). VEGF production and signaling in Müller glia are critical to modulating vascular function and neuronal integrity in diabetic retinopathy and hypoxic retinal vascular diseases. *Vision Research*, *139*, 108–114. https://doi.org/https://doi.org/10.1016/j.visres.2017.05.005

Lee, H., Jang, H., Choi, Y. A., Kim, H. C., & Chung, H. (2018). Association Between Soluble CD14 in the Aqueous Humor and Hyperreflective Foci on Optical Coherence Tomography in Patients With Diabetic Macular Edema. *Investigative Ophthalmology & Visual Science*, *59*(2), 715–721. https://doi.org/10.1167/iovs.17-23042

Lenzen, S. (2008). The mechanisms of alloxan- and streptozotocin-induced diabetes. *Diabetologia*, *51*(2), 216–226. https://doi.org/10.1007/s00125-007-0886-7

Li, C. R., & Sun, S. G. (2010). VEGF expression and cell apoptosis in NOD mouse retina. *International Journal of Ophthalmology*, *3*(3), 224–227. https://doi.org/10.3980/j.issn.2222-3959.2010.03.10

Li, S., & Jakobs, T. C. (2022). Secreted phosphoprotein 1 slows neurodegeneration and rescues visual function in mouse models of aging and glaucoma. *Cell Reports*, *41*(13), 111880. https://doi.org/https://doi.org/10.1016/j.celrep.2022.111880

Lindahl, P., Johansson, B. R., Levéen, P., & Betsholtz, C. (1997). Pericyte loss and microaneurysm formation in PDGF-B-deficient mice. *Science (New York, N.Y.)*, *277*(5323), 242–245. https://doi.org/10.1126/science.277.5323.242

Lindblom, P., Gerhardt, H., Liebner, S., Abramsson, A., Enge, M., Hellström, M., Bäckström, G., Fredriksson, S., Landegren, U., Nyström, H. C., Bergström, G., Dejana, E., Östman, A., Lindahl, P., & Betsholtz, C. (2003). Endothelial PDGF-B retention is required for proper investment of pericytes in the microvessel wall. *Genes and Development*, *17*(15), 1835–1840. https://doi.org/10.1101/gad.266803

Lobov, I. B., Rao, S., Carroll, T. J., Vallance, J. E., Ito, M., Ondr, J. K., Kurup, S., Glass, D. A., Patel, M. S., Shu, W., Morrisey, E. E., McMahon, A. P., Karsenty, G., & Lang, R. A. (2005). WNT7b mediates macrophage-induced programmed cell death in patterning of the vasculature. *Nature*, *437*(7057), 417–421. https://doi.org/10.1038/nature03928

Lynch, S. K., & Abràmoff, M. D. (2017). Diabetic retinopathy is a neurodegenerative disorder. *Vision Research*, *139*, 101–107. https://doi.org/https://doi.org/10.1016/j.visres.2017.03.003

Martin, P. M., Roon, P., Van Ells, T. K., Ganapathy, V., & Smith, S. B. (2004). Death of retinal neurons in streptozotocin-induced diabetic mice. *Investigative Ophthalmology & Visual Science*, *45*(9), 3330–3336. https://doi.org/10.1167/iovs.04-0247

Masland, R. H. (2001). The fundamental plan of the retina. *Nature Neuroscience*, *4*(9), 877–886. https://doi.org/10.1038/nn0901-877

McCrea, P. D., Maher, M. T., & Gottardi, C. J. (2015). Nuclear signaling from cadherin adhesion complexes. *Current Topics in Developmental Biology*, *112*, 129–196. https://doi.org/10.1016/bs.ctdb.2014.11.018

McLenachan, S., Magno, A. L., Ramos, D., Catita, J., McMenamin, P. G., Chen, F. K., Rakoczy, E. P., & Ruberte, J. (2015). Angiography reveals novel features of the retinal vasculature in healthy and diabetic mice. *Experimental Eye Research*, *138*, 6–21. https://doi.org/10.1016/j.exer.2015.06.023

McLetchie, N. G. (2002). Alloxan diabetes: a discovery, albeit a minor one. *The Journal of the Royal College of Physicians of Edinburgh*, *32*(2), 134–142.

Mengstie, M. A., Chekol Abebe, E., Behaile Teklemariam, A., Tilahun Mulu, A., Agidew, M. M., Teshome Azezew, M., Zewde, E. A., & Agegnehu Teshome, A. (2022). Endogenous advanced glycation end products in the pathogenesis of chronic diabetic complications . In *Frontiers in Molecular Biosciences* (Vol. 9). https://www.frontiersin.org/articles/10.3389/fmolb.2022.1002710

Metea, M. R., & Newman, E. A. (2007). Signalling within the neurovascular unit in the mammalian retina. *Experimental Physiology*, *92*(4), 635–640. https://doi.org/10.1113/expphysiol.2006.036376

Montanez, E., Wickström, S. A., Altstätter, J., Chu, H., & Fässler, R. (2009). Alpha-parvin controls vascular mural cell recruitment to vessel wall by regulating RhoA/ROCK signalling. *The EMBO Journal*, *28*(20), 3132–3144. https://doi.org/10.1038/emboj.2009.295

Nikodemova, M., Kimyon, R. S., De, I., Small, A. L., Collier, L. S., & Watters, J. J. (2015). Microglial numbers attain adult levels after undergoing a rapid decrease in cell number in the third postnatal week. *Journal of Neuroimmunology*, *278*, 280–288. https://doi.org/10.1016/j.jneuroim.2014.11.018

O'Koren, E. G., Yu, C., Klingeborn, M., Wong, A. Y. W., Prigge, C. L., Mathew, R., Kalnitsky, J., Msallam, R. A., Silvin, A., Kay, J. N., Bowes Rickman, C., Arshavsky, V. Y., Ginhoux, F., Merad, M., & Saban, D. R. (2019). Microglial Function Is Distinct in Different

Anatomical Locations during Retinal Homeostasis and Degeneration. *Immunity*, *50*(3), 723-737.e7. https://doi.org/10.1016/j.immuni.2019.02.007

O'Leary, F., & Campbell, M. (2023). The blood–retina barrier in health and disease. *The FEBS Journal*, *290*(4), 878–891. https://doi.org/https://doi.org/10.1111/febs.16330

Ogura, S., Kurata, K., Hattori, Y., Takase, H., Ishiguro-Oonuma, T., Hwang, Y., Ahn, S., Park, I., Ikeda, W., Kusuhara, S., Fukushima, Y., Nara, H., Sakai, H., Fujiwara, T., Matsushita, J., Ema, M., Hirashima, M., Minami, T., Shibuya, M., … Uemura, A. (2017). Sustained inflammation after pericyte depletion induces irreversible blood-retina barrier breakdown. *JCI Insight*, *2*(3), e90905. https://doi.org/10.1172/jci.insight.90905

Okabe, K., Kobayashi, S., Yamada, T., Kurihara, T., Tai-Nagara, I., Miyamoto, T., Mukouyama, Y., Sato, T. N., Suda, T., Ema, M., & Kubota, Y. (2014). Neurons limit angiogenesis by titrating VEGF in retina. *Cell*, *159*(3), 584–596. https://doi.org/10.1016/j.cell.2014.09.025

Okamoto, N., Tobe, T., Hackett, S. F., Ozaki, H., Vinores, M. A., LaRochelle, W., Zack, D. J., & Campochiaro, P. A. (1997). Transgenic mice with increased expression of vascular endothelial growth factor in the retina: a new model of intraretinal and subretinal neovascularization. *The American Journal of Pathology*, *151*(1), 281–291.

Oladipupo, S. S., Smith, C., Santeford, A., Park, C., Sene, A., Wiley, L. A., Osei-Owusu, P., Hsu, J., Zapata, N., Liu, F., Nakamura, R., Lavine, K. J., Blumer, K. J., Choi, K., Apte, R. S., & Ornitz, D. M. (2014). Endothelial cell FGF signaling is required for injury response but not for vascular homeostasis. *Proceedings of the National Academy of Sciences of the United States of America*, *111*(37), 13379–13384. https://doi.org/10.1073/pnas.1324235111

Olivares, A. M., Althoff, K., Chen, G. F., Wu, S., Morrisson, M. A., DeAngelis, M. M., & Haider, N. (2017). Animal Models of Diabetic Retinopathy. *Current Diabetes Reports*, *17*(10), 93. https://doi.org/10.1007/s11892-017-0913-0

Ornitz, D. M., & Itoh, N. (2015). The Fibroblast Growth Factor signaling pathway. *Wiley Interdisciplinary Reviews. Developmental Biology*, *4*(3), 215–266. https://doi.org/10.1002/wdev.176

Orsenigo, F., Giampietro, C., Ferrari, A., Corada, M., Galaup, A., Sigismund, S., Ristagno, G., Maddaluno, L., Koh, G. Y., Franco, D., Kurtcuoglu, V., Poulikakos, D., Baluk, P., McDonald, D., Grazia Lampugnani, M., & Dejana, E. (2012). Phosphorylation of VE-cadherin is modulated by haemodynamic forces and contributes to the regulation of

vascular permeability in vivo. *Nature Communications*, *3*, 1208. https://doi.org/10.1038/ncomms2199

Ozaki, E., Delaney, C., Campbell, M., & Doyle, S. L. (2022). Minocycline suppresses disease-associated microglia (DAM) in a model of photoreceptor cell degeneration. *Experimental Eye Research*, *217*, 108953. https://doi.org/https://doi.org/10.1016/j.exer.2022.108953

Paolicelli, R. C., Sierra, A., Stevens, B., Tremblay, M.-E., Aguzzi, A., Ajami, B., Amit, I., Audinat, E., Bechmann, I., Bennett, M., Bennett, F., Bessis, A., Biber, K., Bilbo, S., Blurton-Jones, M., Boddeke, E., Brites, D., Brône, B., Brown, G. C., … Wyss-Coray, T. (2022). Microglia states and nomenclature: A field at its crossroads. *Neuron*, *110*(21), 3458–3483. https://doi.org/10.1016/j.neuron.2022.10.020

Park, D. Y., Lee, J., Kim, J., Kim, K., Hong, S., Han, S., Kubota, Y., Augustin, H. G., Ding, L., Kim, J. W., Kim, H., He, Y., Adams, R. H., & Koh, G. Y. (2017). Plastic roles of pericytes in the blood–retinal barrier. *Nature Communications*, *8*(1), 15296. https://doi.org/10.1038/ncomms15296

Park, Y.-G., Jee, D., & Kwon, J.-W. (2019). Aqueous Humor Cytokine Levels in Diabetic Macular Edema Patients with Cotton-Wool Spots. *Journal of Diabetes Research*, *2019*, 8137417. https://doi.org/10.1155/2019/8137417

Perry, E. A., Bennett, C. F., Luo, C., Balsa, E., Jedrychowski, M., O'Malley, K. E., Latorre-Muro, P., Ladley, R. P., Reda, K., Wright, P. M., Gygi, S. P., Myers, A. G., & Puigserver, P. (2021). Tetracyclines promote survival and fitness in mitochondrial disease models. *Nature Metabolism*, *3*(1), 33–42. https://doi.org/10.1038/s42255-020-00334-y

Pfister, F., Przybyt, E., Harmsen, M. C., & Hammes, H.-P. (2013). Pericytes in the eye. *Pflügers Archiv - European Journal of Physiology*, *465*(6), 789–796. https://doi.org/10.1007/s00424-013-1272-6

Phng, L.-K., & Gerhardt, H. (2009). Angiogenesis: a team effort coordinated by notch. *Developmental Cell*, *16*(2), 196–208. https://doi.org/10.1016/j.devcel.2009.01.015

Pierce, E. A., Avery, R. L., Foley, E. D., Aiello, L. P., & Smith, L. E. (1995). Vascular endothelial growth factor/vascular permeability factor expression in a mouse model of retinal neovascularization. *Proceedings of the National Academy of Sciences*, *92*(3), 905–909. https://doi.org/10.1073/pnas.92.3.905

Pitter, B., Werner, A.-C., & Montanez, E. (2018). Parvins Are Required for Endothelial Cell-Cell Junctions and Cell Polarity During Embryonic Blood Vessel Formation. *Arteriosclerosis, Thrombosis, and Vascular Biology*, *38*(5), 1147–1158.

https://doi.org/10.1161/ATVBAHA.118.310840

Potter, M. D., Barbero, S., & Cheresh, D. A. (2005). Tyrosine Phosphorylation of VE-cadherin Prevents Binding of p120- and β-Catenin and Maintains the Cellular Mesenchymal State*. *Journal of Biological Chemistry*, *280*(36), 31906–31912. https://doi.org/https://doi.org/10.1074/jbc.M505568200

Provis, J. M., Leech, J., Diaz, C. M., Penfold, P. L., Stone, J., & Keshet, E. (1997). Development of the human retinal vasculature: cellular relations and VEGF expression. *Experimental Eye Research*, *65*(4), 555–568. https://doi.org/10.1006/exer.1997.0365

Qi, Y., Liang, X., Dai, F., Guan, H., Sun, J., & Yao, W. (2020). RhoA/ROCK Pathway Activation is Regulated by AT1 Receptor and Participates in Smooth Muscle Migration and Dedifferentiation via Promoting Actin Cytoskeleton Polymerization. *International Journal of Molecular Sciences*, *21*(15). https://doi.org/10.3390/ijms21155398

Radice, G. L., Rayburn, H., Matsunami, H., Knudsen, K. A., Takeichi, M., & Hynes, R. O. (1997). Developmental defects in mouse embryos lacking N-cadherin. *Developmental Biology*, *181*(1), 64–78. https://doi.org/10.1006/dbio.1996.8443

Rajagopal, R., Bligard, G. W., Zhang, S., Yin, L., Lukasiewicz, P., & Semenkovich, C. F. (2016). Functional Deficits Precede Structural Lesions in Mice With High-Fat Diet-Induced Diabetic Retinopathy. *Diabetes*, *65*(4), 1072–1084. https://doi.org/10.2337/db15-1255

Rakoczy, E. P., Ali Rahman, I. S., Binz, N., Li, C.-R., Vagaja, N. N., de Pinho, M., & Lai, C.-M. (2010). Characterization of a mouse model of hyperglycemia and retinal neovascularization. *The American Journal of Pathology*, *177*(5), 2659–2670. https://doi.org/10.2353/ajpath.2010.090883

Rashid, K., Akhtar-Schaefer, I., & Langmann, T. (2019). Microglia in Retinal Degeneration . In *Frontiers in Immunology* (Vol. 10). https://www.frontiersin.org/articles/10.3389/fimmu.2019.01975

Rathi, S., Jalali, S., Patnaik, S., Shahulhameed, S., Musada, G. R., Balakrishnan, D., Rani, P. K., Kekunnaya, R., Chhablani, P. P., Swain, S., Giri, L., Chakrabarti, S., & Kaur, I. (2017). Abnormal Complement Activation and Inflammation in the Pathogenesis of Retinopathy of Prematurity . In *Frontiers in Immunology* (Vol. 8). https://www.frontiersin.org/articles/10.3389/fimmu.2017.01868

Rathnasamy, G., Foulds, W. S., Ling, E.-A., & Kaur, C. (2019). Retinal microglia – A key player in healthy and diseased retina. *Progress in Neurobiology*, *173*, 18–40.

https://doi.org/https://doi.org/10.1016/j.pneurobio.2018.05.006

Rivera, J. C., Sitaras, N., Noueihed, B., Hamel, D., Madaan, A., Zhou, T., Honoré, J. C., Quiniou, C., Joyal, J. S., Hardy, P., Sennlaub, F., Lubell, W., & Chemtob, S. (2013). Microglia and interleukin-1β in ischemic retinopathy elicit microvascular degeneration through neuronal semaphorin-3A. *Arteriosclerosis, Thrombosis, and Vascular Biology*, *33*(8), 1881–1891. https://doi.org/10.1161/ATVBAHA.113.301331

Roca, C., & Adams, R. H. (2007). Regulation of vascular morphogenesis by Notch signaling. *Genes & Development*, *21*(20), 2511–2524. https://doi.org/10.1101/gad.1589207

Rocha, S. F., Schiller, M., Jing, D., Li, H., Butz, S., Vestweber, D., Biljes, D., Drexler, H. C. A., Nieminen-Kelhä, M., Vajkoczy, P., Adams, S., Benedito, R., & Adams, R. H. (2014). Esm1 modulates endothelial tip cell behavior and vascular permeability by enhancing VEGF bioavailability. *Circulation Research*, *115*(6), 581–590. https://doi.org/10.1161/CIRCRESAHA.115.304718

Rupp, P. A., & Little, C. D. (2001). Integrins in vascular development. *Circulation Research*, *89*(7), 566–572. https://doi.org/10.1161/hh1901.097747

Saeedi, P., Petersohn, I., Salpea, P., Malanda, B., Karuranga, S., Unwin, N., Colagiuri, S., Guariguata, L., Motala, A. A., Ogurtsova, K., Shaw, J. E., Bright, D., & Williams, R. (2019). Global and regional diabetes prevalence estimates for 2019 and projections for 2030 and 2045: Results from the International Diabetes Federation Diabetes Atlas, 9(th) edition. *Diabetes Research and Clinical Practice*, *157*, 107843. https://doi.org/10.1016/j.diabres.2019.107843

Saharinen, P., Eklund, L., & Alitalo, K. (2017). Therapeutic targeting of the angiopoietin–TIE pathway. *Nature Reviews Drug Discovery*, *16*(9), 635–661. https://doi.org/10.1038/nrd.2016.278

Santos, A. M., Calvente, R., Tassi, M., Carrasco, M.-C., Martín-Oliva, D., Marín-Teva, J. L., Navascués, J., & Cuadros, M. A. (2008). Embryonic and postnatal development of microglial cells in the mouse retina. *The Journal of Comparative Neurology*, *506*(2), 224–239. https://doi.org/10.1002/cne.21538

Schlamp, C. L., Montgomery, A. D., Mac Nair, C. E., Schuart, C., Willmer, D. J., & Nickells, R. W. (2013). Evaluation of the percentage of ganglion cells in the ganglion cell layer of the rodent retina. *Molecular Vision*, *19*, 1387–1396.

Schlecht, A., Zhang, P., Wolf, J., Thien, A., Rosmus, D.-D., Boneva, S., Schlunck, G., Lange, C., & Wieghofer, P. (2020). Secreted Phosphoprotein 1 Expression in Retinal

Mononuclear Phagocytes Links Murine to Human Choroidal Neovascularization. *Frontiers in Cell and Developmental Biology*, *8*, 618598. https://doi.org/10.3389/fcell.2020.618598

Scholz, R., Sobotka, M., Caramoy, A., Stempfl, T., Moehle, C., & Langmann, T. (2015). Minocycline counter-regulates pro-inflammatory microglia responses in the retina and protects from degeneration. *Journal of Neuroinflammation*, *12*(1), 209. https://doi.org/10.1186/s12974-015-0431-4

Scott, I. U., Jackson, G. R., Quillen, D. A., Larsen, M., Klein, R., Liao, J., Holfort, S., Munch, I. C., & Gardner, T. W. (2014). Effect of Doxycycline vs Placebo on Retinal Function and Diabetic Retinopathy Progression in Patients With Severe Nonproliferative or Non–High-Risk Proliferative Diabetic Retinopathy: A Randomized Clinical Trial. *JAMA Ophthalmology*, *132*(5), 535–543. https://doi.org/10.1001/jamaophthalmol.2014.93

Sernagor, E., Eglen, S. J., & Wong, R. O. (2001). Development of retinal ganglion cell structure and function. *Progress in Retinal and Eye Research*, *20*(2), 139–174. https://doi.org/10.1016/s1350-9462(00)00024-0

Serreze, D. V, Chapman, H. D., Varnum, D. S., Gerling, I., Leiter, E. H., & Shultz, L. D. (1997). Initiation of autoimmune diabetes in NOD/Lt mice is MHC class I-dependent. *Journal of Immunology (Baltimore, Md. : 1950)*, *158*(8), 3978–3986.

Sherman, B. T., Hao, M., Qiu, J., Jiao, X., Baseler, M. W., Lane, H. C., Imamichi, T., & Chang, W. (2022). DAVID: a web server for functional enrichment analysis and functional annotation of gene lists (2021 update). *Nucleic Acids Research*, *50*(W1), W216-21. https://doi.org/10.1093/nar/gkac194

Shiraya, T., Araki, F., Ueta, T., Fukunaga, H., Totsuka, K., Arai, T., Uemura, A., Moriya, K., & Kato, S. (2020). Ursodeoxycholic Acid Attenuates the Retinal Vascular Abnormalities in Anti-PDGFR-β Antibody-Induced Pericyte Depletion Mouse Models. *Scientific Reports*, *10*(1), 977. https://doi.org/10.1038/s41598-020-58039-x

Sohn, E. H., Van Dijk, H. W., Jiao, C., Kok, P. H. B., Jeong, W., Demirkaya, N., Garmager, A., Wit, F., Kucukevcilioglu, M., Van Velthoven, M. E. J., DeVries, J. H., Mullins, R. F., Kuehn, M. H., Schlingemann, R. O., Sonka, M., Verbraak, F. D., & Abràmoff, M. D. (2016). Retinal neurodegeneration may precede microvascular changes characteristic of diabetic retinopathy in diabetes mellitus. *Proceedings of the National Academy of Sciences of the United States of America*, *113*(19), E2655–E2664. https://doi.org/10.1073/pnas.1522014113

Sörensen, I., Adams, R. H., & Gossler, A. (2009). DLL1-mediated Notch activation regulates endothelial identity in mouse fetal arteries. *Blood*, *113*(22), 5680–5688. https://doi.org/10.1182/blood-2008-08-174508

Stahl, A., Connor, K. M., Sapieha, P., Chen, J., Dennison, R. J., Krah, N. M., Seaward, M. R., Willett, K. L., Aderman, C. M., Guerin, K. I., Hua, J., Löfqvist, C., Hellström, A., & Smith, L. E. H. (2010). The mouse retina as an angiogenesis model. *Investigative Ophthalmology & Visual Science*, *51*(6), 2813–2826. https://doi.org/10.1167/iovs.10-5176

Strasser, G. A., Kaminker, J. S., & Tessier-Lavigne, M. (2010). Microarray analysis of retinal endothelial tip cells identifies CXCR4 as a mediator of tip cell morphology and branching. *Blood*, *115*(24), 5102–5110. https://doi.org/https://doi.org/10.1182/blood-2009-07-230284

Su, L., Ji, J., Bian, J., Fu, Y., Ge, Y., & Yuan, Z. (2012). Tacrolimus (FK506) prevents early retinal neovascularization in streptozotocin-induced diabetic mice. *International Immunopharmacology*, *14*(4), 606–612. https://doi.org/10.1016/j.intimp.2012.09.010

Sun, H., Saeedi, P., Karuranga, S., Pinkepank, M., Ogurtsova, K., Duncan, B. B., Stein, C., Basit, A., Chan, J. C. N., Mbanya, J. C., Pavkov, M. E., Ramachandaran, A., Wild, S. H., James, S., Herman, W. H., Zhang, P., Bommer, C., Kuo, S., Boyko, E. J., & Magliano, D. J. (2022). IDF Diabetes Atlas: Global, regional and country-level diabetes prevalence estimates for 2021 and projections for 2045. *Diabetes Research and Clinical Practice*, *183*, 109119. https://doi.org/10.1016/j.diabres.2021.109119

Taddei, A., Giampietro, C., Conti, A., Orsenigo, F., Breviario, F., Pirazzoli, V., Potente, M., Daly, C., Dimmeler, S., & Dejana, E. (2008). Endothelial adherens junctions control tight junctions by VE-cadherin-mediated upregulation of claudin-5. *Nature Cell Biology*, *10*(8), 923–934. https://doi.org/10.1038/ncb1752

Tee, L. B. G., Penrose, M. A., O'Shea, J. E., Lai, C. M., Rakoczy, E. P., & Dunlop, S. A. (2008). VEGF-induced choroidal damage in a murine model of retinal neovascularisation. *British Journal of Ophthalmology*, *92*(6), 832–838. https://doi.org/10.1136/bjo.2007.130898

Teo, Z. L., Tham, Y.-C., Yu, M., Chee, M. L., Rim, T. H., Cheung, N., Bikbov, M. M., Wang, Y. X., Tang, Y., Lu, Y., Wong, I. Y., Ting, D. S. W., Tan, G. S. W., Jonas, J. B., Sabanayagam, C., Wong, T. Y., & Cheng, C.-Y. (2021). Global Prevalence of Diabetic Retinopathy and Projection of Burden through 2045: Systematic Review and Meta-analysis. *Ophthalmology*, *128*(11), 1580–1591. https://doi.org/10.1016/j.ophtha.2021.04.027

Tomita, Y., Qiu, C., Bull, E., Allen, W., Kotoda, Y., Talukdar, S., Smith, L. E. H., & Fu, Z. (2021). Müller glial responses compensate for degenerating photoreceptors in retinitis pigmentosa. *Experimental & Molecular Medicine*, *53*(11), 1748–1758. https://doi.org/10.1038/s12276-021-00693-w

Trost, A., Bruckner, D., Rivera, F. J., & Reitsamer, H. A. (2019). *Pericytes in the Retina BT - Pericyte Biology in Different Organs* (A. Birbrair (ed.); pp. 1–26). Springer International Publishing. https://doi.org/10.1007/978-3-030-11093-2_1

Trost, A., Schroedl, F., Lange, S., Rivera, F. J., Tempfer, H., Korntner, S., Stolt, C. C., Wegner, M., Bogner, B., Kaser-Eichberger, A., Krefft, K., Runge, C., Aigner, L., & Reitsamer, H. A. (2013). Neural crest origin of retinal and choroidal pericytes. *Investigative Ophthalmology & Visual Science*, *54*(13), 7910–7921. https://doi.org/10.1167/iovs.13-12946

Truett, G. E., Heeger, P., Mynatt, R. L., Truett, A. A., Walker, J. A., & Warman, M. L. (2000). Preparation of PCR-quality mouse genomic DNA with hot sodium hydroxide and tris (HotSHOT). *BioTechniques*, *29*(1), 52,54. https://doi.org/10.2144/00291bm09

Uemura, A., Ogawa, M., Hirashima, M., Fujiwara, T., Koyama, S., Takagi, H., Honda, Y., Wiegand, S. J., Yancopoulos, G. D., & Nishikawa, S.-I. (2002). Recombinant angiopoietin-1 restores higher-order architecture of growing blood vessels in mice in the absence of mural cells. *The Journal of Clinical Investigation*, *110*(11), 1619–1628. https://doi.org/10.1172/JCI15621

van Eeden, P. E., Tee, L. B. G., Lukehurst, S., Lai, C.-M., Rakoczy, E. P., Beazley, L. D., & Dunlop, S. A. (2006). Early vascular and neuronal changes in a VEGF transgenic mouse model of retinal neovascularization. *Investigative Ophthalmology & Visual Science*, *47*(10), 4638–4645. https://doi.org/10.1167/iovs.06-0251

Vecino, E., Rodriguez, F. D., Ruzafa, N., Pereiro, X., & Sharma, S. C. (2016). Glia–neuron interactions in the mammalian retina. *Progress in Retinal and Eye Research*, *51*, 1–40. https://doi.org/https://doi.org/10.1016/j.preteyeres.2015.06.003

Vestweber, D. (2008). VE-cadherin: the major endothelial adhesion molecule controlling cellular junctions and blood vessel formation. *Arteriosclerosis, Thrombosis, and Vascular Biology*, *28*(2), 223–232. https://doi.org/10.1161/ATVBAHA.107.158014

Vishwakarma, S., Gupta, R. K., Jakati, S., Tyagi, M., Pappuru, R. R., Reddig, K., Hendricks, G., Volkert, M. R., Khanna, H., Chhablani, J., & Kaur, I. (2020). Molecular Assessment of Epiretinal Membrane: Activated Microglia, Oxidative Stress and Inflammation.

Antioxidants (Basel, Switzerland), *9*(8). https://doi.org/10.3390/antiox9080654

Vittet, D., Buchou, T., Schweitzer, A., Dejana, E., & Huber, P. (1997). Targeted null-mutation in the vascular endothelial-cadherin gene impairs the organization of vascular-like structures in embryoid bodies. *Proceedings of the National Academy of Sciences of the United States of America*, *94*(12), 6273–6278. https://doi.org/10.1073/pnas.94.12.6273

Volland, S., Esteve-Rudd, J., Hoo, J., Yee, C., & Williams, D. S. (2015). A comparison of some organizational characteristics of the mouse central retina and the human macula. *PloS One*, *10*(4), e0125631. https://doi.org/10.1371/journal.pone.0125631

Vujosevic, S., Micera, A., Bini, S., Berton, M., Esposito, G., & Midena, E. (2016). Proteome analysis of retinal glia cells-related inflammatory cytokines in the aqueous humour of diabetic patients. *Acta Ophthalmologica*, *94*(1), 56–64. https://doi.org/10.1111/aos.12812

Wallez, Y., Cand, F., Cruzalegui, F., Wernstedt, C., Souchelnytskyi, S., Vilgrain, I., & Huber, P. (2007). Src kinase phosphorylates vascular endothelial-cadherin in response to vascular endothelial growth factor: identification of tyrosine 685 as the unique target site. *Oncogene*, *26*(7), 1067–1077. https://doi.org/10.1038/sj.onc.1209855

Wang, J., Xu, E., Elliott, M. H., Zhu, M., & Le, Y. Z. (2010). Müller cell-derived VEGF is essential for diabetes-induced retinal inflammation and vascular leakage. *Diabetes*, *59*(9), 2297–2305. https://doi.org/10.2337/db09-1420

Wang, L., Zhou, X., Yin, Y., Mai, Y., Wang, D., & Zhang, X. (2018). Hyperglycemia Induces Neutrophil Extracellular Traps Formation Through an NADPH Oxidase-Dependent Pathway in Diabetic Retinopathy. *Frontiers in Immunology*, *9*, 3076. https://doi.org/10.3389/fimmu.2018.03076

Wang, X., Fan, W., Li, N., Ma, Y., Yao, M., Wang, G., He, S., Li, W., Tan, J., Lu, Q., & Hou, S. (2023). YY1 lactylation in microglia promotes angiogenesis through transcription activation-mediated upregulation of FGF2. *Genome Biology*, *24*(1), 87. https://doi.org/10.1186/s13059-023-02931-y

Watanabe, T., & Raff, M. C. (1988). Retinal astrocytes are immigrants from the optic nerve. *Nature*, *332*(6167), 834–837. https://doi.org/10.1038/332834a0

Weerasekera, L. Y., Balmer, L. A., Ram, R., & Morahan, G. (2015). Characterization of Retinal Vascular and Neural Damage in a Novel Model of Diabetic Retinopathy. *Investigative Ophthalmology & Visual Science*, *56*(6), 3721–3730. https://doi.org/10.1167/iovs.14-16289

Wells, J. A., Glassman, A. R., Ayala, A. R., Jampol, L. M., Bressler, N. M., Bressler, S. B., Brucker, A. J., Ferris, F. L., Hampton, G. R., Jhaveri, C., Melia, M., & Beck, R. W. (2016). Aflibercept, Bevacizumab, or Ranibizumab for Diabetic Macular Edema: Two-Year Results from a Comparative Effectiveness Randomized Clinical Trial. *Ophthalmology*, *123*(6), 1351–1359. https://doi.org/10.1016/j.ophtha.2016.02.022

Wessel, F., Winderlich, M., Holm, M., Frye, M., Rivera-Galdos, R., Vockel, M., Linnepe, R., Ipe, U., Stadtmann, A., Zarbock, A., Nottebaum, A. F., & Vestweber, D. (2014). Leukocyte extravasation and vascular permeability are each controlled in vivo by different tyrosine residues of VE-cadherin. *Nature Immunology*, *15*(3), 223–230. https://doi.org/10.1038/ni.2824

Winkler, E. A., Bell, R. D., & Zlokovic, B. V. (2011). Central nervous system pericytes in health and disease. *Nature Neuroscience*, *14*(11), 1398–1405. https://doi.org/10.1038/nn.2946

Wisniewska-Kruk, J., Klaassen, I., Vogels, I. M. C., Magno, A. L., Lai, C.-M., Van Noorden, C. J. F., Schlingemann, R. O., & Rakoczy, E. P. (2014). Molecular analysis of blood-retinal barrier loss in the Akimba mouse, a model of advanced diabetic retinopathy. *Experimental Eye Research*, *122*, 123–131. https://doi.org/10.1016/j.exer.2014.03.005

Wolf, Y., Yona, S., Kim, K. W., & Jung, S. (2013). Microglia, seen from the CX3CR1 angle. *Frontiers in Cellular Neuroscience*, *7*(MAR), 26. https://doi.org/10.3389/fncel.2013.00026

Xie, Y., Su, N., Yang, J., Tan, Q., Huang, S., Jin, M., Ni, Z., Zhang, B., Zhang, D., Luo, F., Chen, H., Sun, X., Feng, J. Q., Qi, H., & Chen, L. (2020). FGF/FGFR signaling in health and disease. *Signal Transduction and Targeted Therapy*, *5*(1), 181. https://doi.org/10.1038/s41392-020-00222-7

Xu, J., Chen, L. J., Yu, J., Wang, H. J., Zhang, F., Liu, Q., & Wu, J. (2018). Involvement of Advanced Glycation End Products in the Pathogenesis of Diabetic Retinopathy. *Cellular Physiology and Biochemistry*, *48*(2), 705–717. https://doi.org/10.1159/000491897

Yamamoto, H., Ehling, M., Kato, K., Kanai, K., van Lessen, M., Frye, M., Zeuschner, D., Nakayama, M., Vestweber, D., & Adams, R. H. (2015). Integrin β1 controls VE-cadherin localization and blood vessel stability. *Nature Communications*, *6*(1), 6429. https://doi.org/10.1038/ncomms7429

Yu, Y., Shen, Q., Lai, Y., Park, S. Y., Ou, X., Lin, D., Jin, M., & Zhang, W. (2018). Anti-inflammatory Effects of Curcumin in Microglial Cells. *Frontiers in Pharmacology*, *9*, 386. https://doi.org/10.3389/fphar.2018.00386

Yu, Z., Zhang, T., Gong, C., Sheng, Y., Lu, B., Zhou, L., Ji, L., & Wang, Z. (2016). Erianin

inhibits high glucose-induced retinal angiogenesis via blocking ERK1/2-regulated HIF-1α-VEGF/VEGFR2 signaling pathway. *Scientific Reports*, *6*(1), 34306. https://doi.org/10.1038/srep34306

Zeng, H. Y., Green, W. R., & Tso, M. O. M. (2008). Microglial activation in human diabetic retinopathy. *Archives of Ophthalmology*, *126*(2), 227–232. https://doi.org/10.1001/archophthalmol.2007.65

Zhang, T., Ouyang, H., Mei, X., Lu, B., Yu, Z., Chen, K., Wang, Z., & Ji, L. (2019). Erianin alleviates diabetic retinopathy by reducing retinal inflammation initiated by microglial cells via inhibiting hyperglycemia-mediated ERK1/2–NF-κB signaling pathway. *FASEB Journal*, *33*(11), 11776–11790. https://doi.org/10.1096/fj.201802614RRR

Zudaire, E., Gambardella, L., Kurcz, C., & Vermeren, S. (2011). A computational tool for quantitative analysis of vascular networks. *PloS One*, *6*(11), e27385. https://doi.org/10.1371/journal.pone.0027385

APPENDIX

Supplementary figures

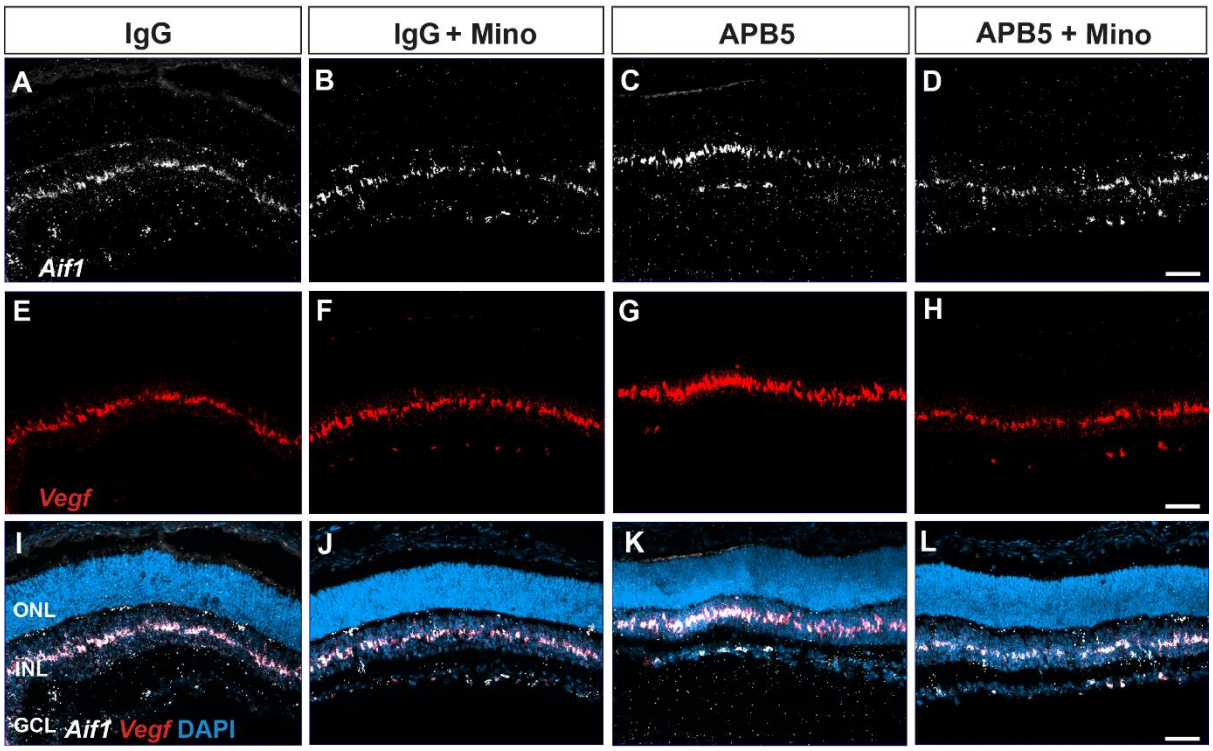

Supplementary figure 1: In situ hybridization of *Aif* and *Vegf* mRNAs in P10 retinas. Retina sections from IgG, IgG+Mino, APB5 and APB5+Mino showing in situ hybridization for *Aif1* (A-D) and *Vegf* (E-H). Merged channels showing *Vegf* mRNA and its colocalization with *Aif1* mRNA in the INL of APB5 retinas (I-L). The *Vegf* signal was reduced by minocycline (H). ONL, outer nuclear layer; INL, inner nuclear layer; GCL, ganglion cell layer; *Aif1*, Allograft inflammatory factor-1; *Vegf*, Vascular endothelial growth factor. The scale bar is 50µm.

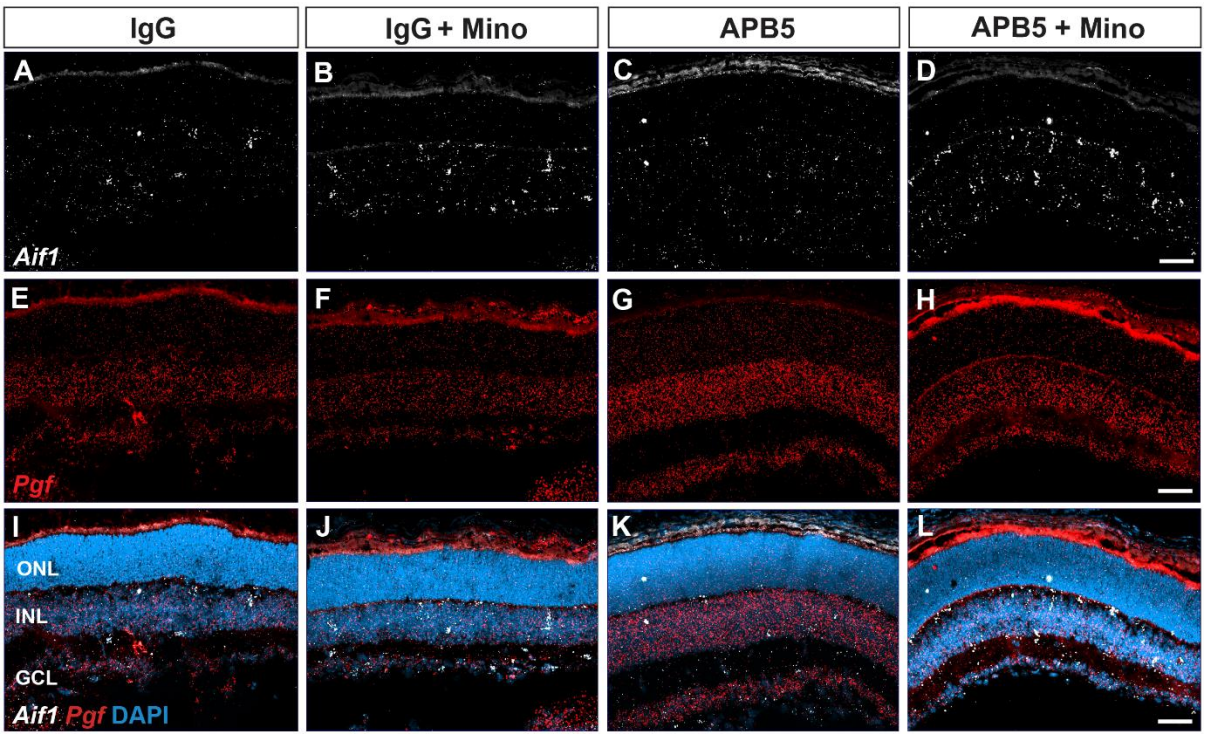

Supplementary figure 2: In situ hybridization of *Aif1* and *Pgf* in P10 retinas. Retina sections from IgG, IgG+Mino, APB5 and APB5+Mino showing ISH for *Aif1* (A-D) and *Pgf* (E-H) mRNA (A-D). Images showing abundant *Pgf* mRNA within the INL and GCL of APB5 retinas (G). The *Pgf* signal was reduced by minocycline (L). ONL, outer nuclear layer; INL, inner nuclear layer; GCL, ganglion cell layer; *Aif1*, allograft inflammatory factor-1; *Pgf*, Placental growth factor. The scale bar is 50µm.

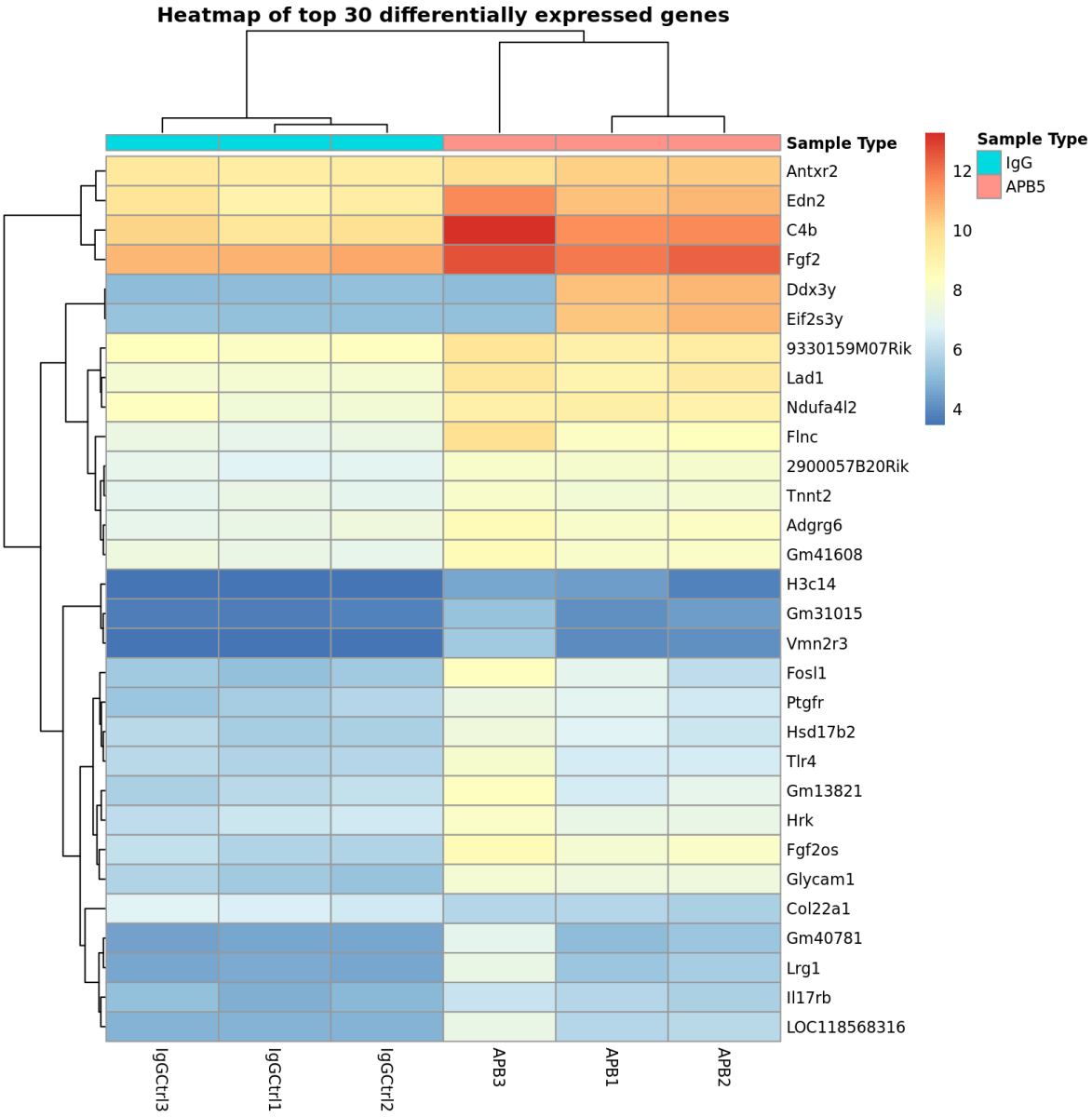

Supplementary figure 3: Heat map of top 30 differentially expressed **genes comparing APB5 versus IgG control**. Heat map generated from DRAGEN software on the Illumina Basespace sequence hub.

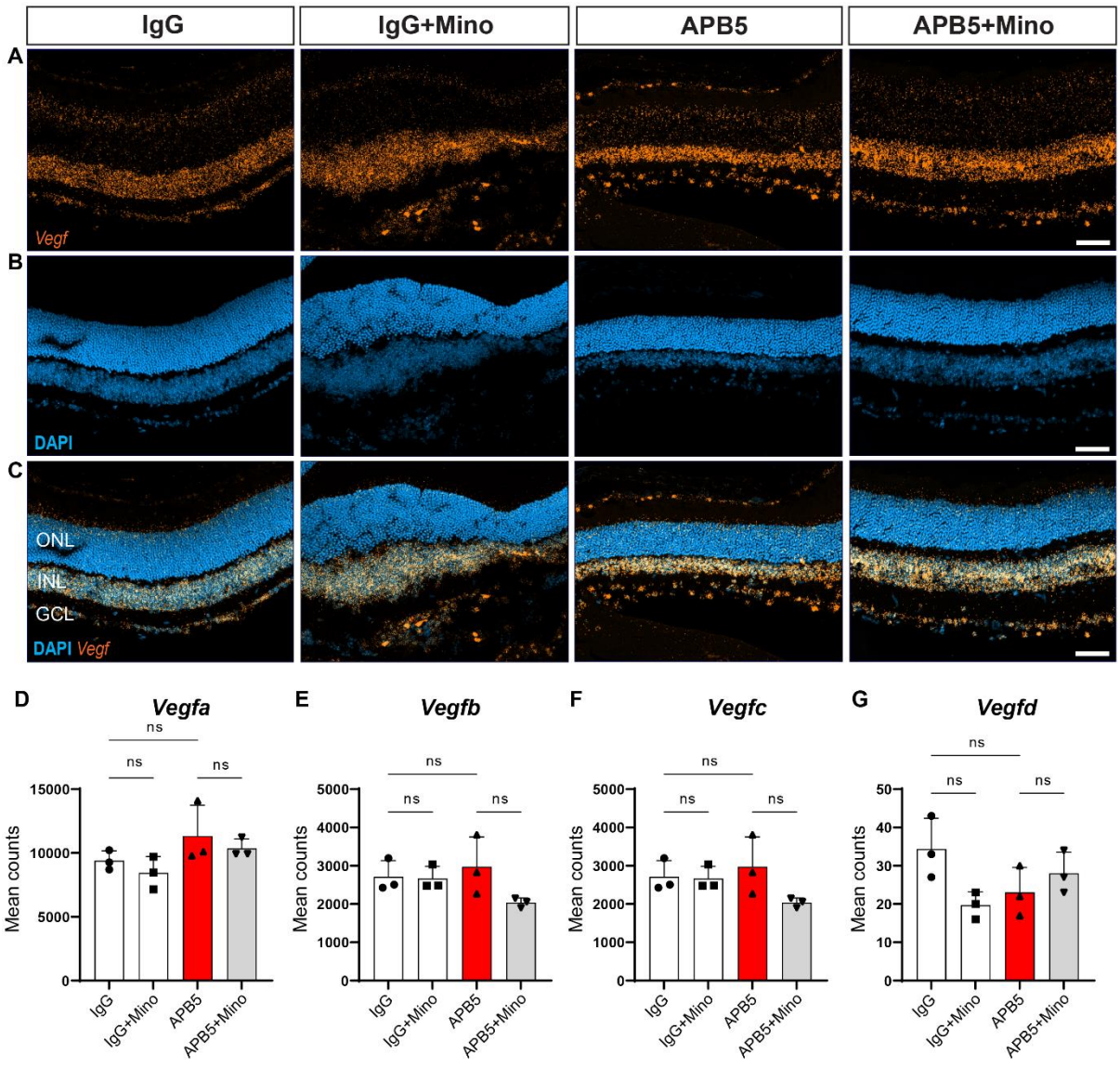

Supplementary figure 4: RNAscope in situ hybridization of *Vegf* mRNA on retinal sections and quantification of mRNA mean counts of *Vegf* isoforms. Representative images of *Vegf* mRNA expression on cross sections from the four treatment groups (A). DAPI stained nuclei (B). Merged channel images of *Vegf* and DAPI. Quantification of mRNA mean counts of *Vegfa* (D), *Vegfb* (E), V*egfc* (F) and *Vegfd* (G). n = 3 samples. Scale bar is 50µm. Vegf is vascular endothelial growth factor.

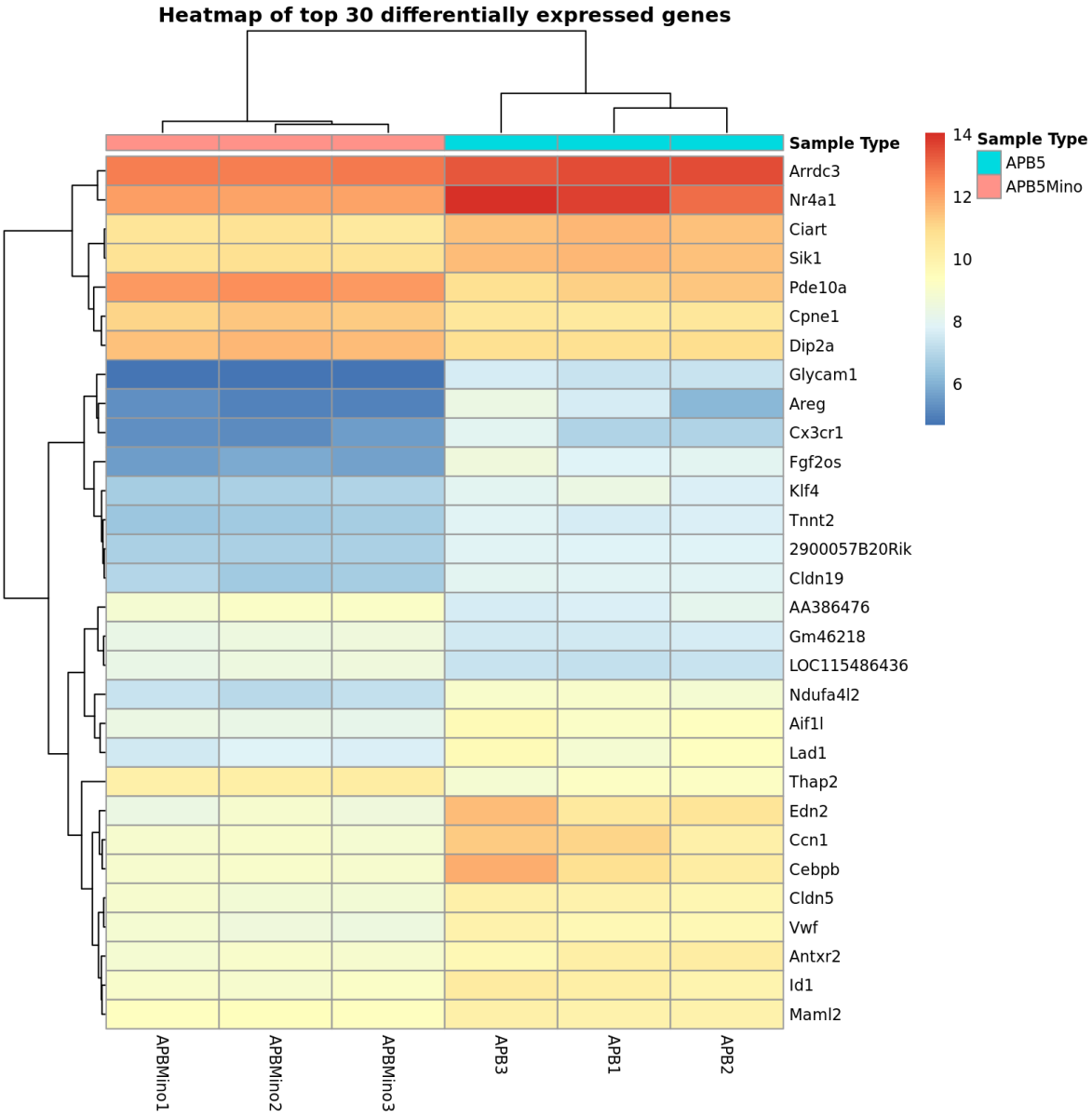

Supplementary figure 5: Heatmap of the top 30 differentially expressed genes comparing APB5 and APB5 plus minocycline treatment. Heatmap generated using the DRAGEN software on the Illumina Basespace sequence hub.

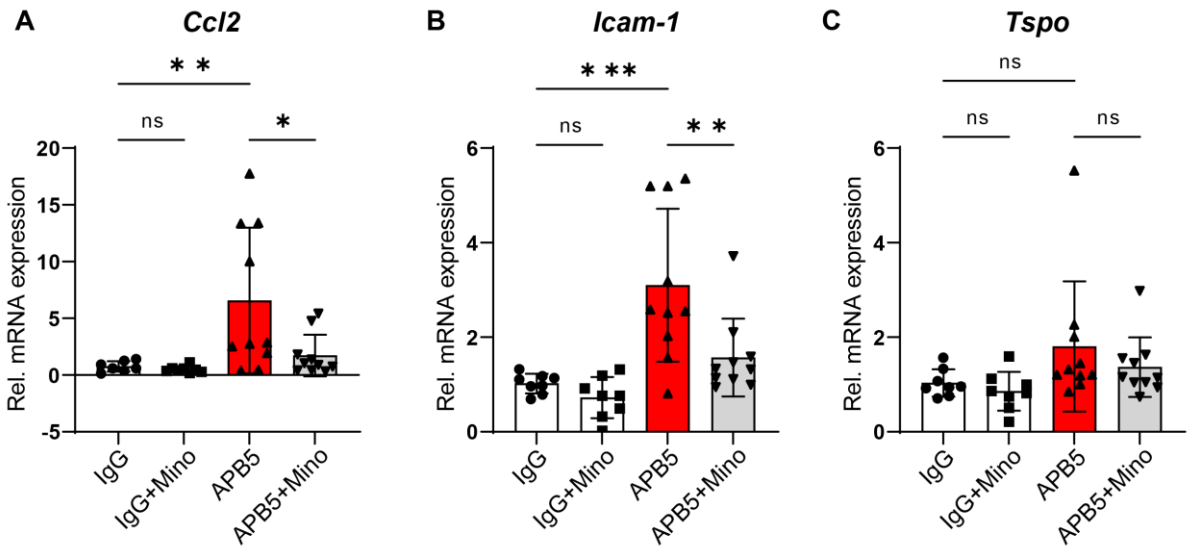

Supplementary figure 6: qRT-PCR analyses of mRNA expression levels in retina of four weeks old mice. IgG; n = 8, IgG + Mino; n = 8, APB5; n = 10, APB5 + Mino; n = 10

Supplementary Table 1: Differentially upregulated genes (top 103) comparing APB5-treated retinas versus IgG control retinas

Gene	log2 fold change	P adjusted value
Ddx3y	12.85938	0.001881307
Eif2s3y	12.64723	0.001075839
Uty	10.22883	0.005905699
Vmn2r3	8.348869	4.34E-05
H3c14	7.775865	5.34E-05
Sprr1a	7.299948	0.048696609
Cd300lb	6.993955	0.030723449
Slpi	6.938336	0.044551073
Prn	6.862709	0.002630255
Wfdc17	5.520339	0.008721363
Gxylt2	4.988019	0.0218396
Lyz2	4.986955	0.038666105
Enpp6	4.921765	0.033563533
Areg	4.535303	0.01250414
Lrg1	4.488597	1.58E-05
Soat2	4.457842	0.021052087
Fgf2os	4.388568	6.64E-19

Glycam1	4.31493	7.95E-17
Cnn1	4.297153	0.008721363
Bcl3	4.045244	0.016434285
Fosl1	4.029248	2.46E-05
LOC118568316	3.917305	1.76E-06
Lbp	3.854217	0.01743479
Slc6a2	3.81252	0.008103107
C4b	3.801303	0.000811651
Abcc3	3.729689	0.003335587
Top2a	3.718493	0.048696609
LOC118568080	3.502471	0.003335587
Casp1	3.454944	0.010323326
Lilrb4a	3.39317	0.026359884
P2rx7	3.032464	0.006740444
Flnc	2.921504	4.90E-05
Ptgfr	2.903212	2.41E-05
Cxcl10	2.863705	0.038666105
Fxyd3	2.827552	0.040531311
Myc	2.678229	0.015760567
Tlr4	2.661704	0.001881307
Edn2	2.62482	1.52E-06
Il17rb	2.621284	0.001742722
Hsd17b2	2.612157	0.000811651
Apobec1	2.611253	0.002836918
Mdfi	2.582201	0.043939328
Lad1	2.424671	1.21E-12
Vax1	2.399705	0.033563533
Hrk	2.398579	0.00012734
Emp1	2.361051	0.021052087
H2-Ab1	2.345915	0.010323326
H19	2.326723	0.017596399
Gadl1	2.303683	0.019770513
Plekhf1	2.292664	0.006676265
Trim30d	2.284837	0.026617927
Tcim	2.277115	0.006676265

Cfi	2.172074	0.01743479
Fgf2	2.159185	2.68E-11
Icam1	2.139372	0.004513865
Tnfrsf1b	2.13051	0.036204974
Bag3	2.125258	0.001881307
Tgm2	2.11116	0.014741037
Lsp1	2.097451	0.01146823
Hmox1	2.017286	0.006573006
Zbtb7c	2.016111	0.016920465
Cryzl2	2.003084	0.003335587
Ccnd2	1.966931	0.03435203
Cd44	1.955744	0.029250064
Tagln2	1.953078	0.036204974
Egln3	1.936901	0.046226618
Eif4ebp1	1.926455	0.026567481
Cdkn1a	1.925383	0.021623906
Plin4	1.91977	0.002730909
Nr4a3	1.910954	0.014250671
Fosl2	1.854783	0.004513865
B2m	1.843805	0.036204974
Cebpd	1.84357	0.03435203
Ndufa4l2	1.837025	0.000281005
F3	1.833221	0.018661143
Ifitm3	1.826835	0.048696609
Nfkb2	1.810736	0.038445541
2900057B20Rik	1.73897	3.39E-08
Isg15	1.738131	0.021452104
Pdlim3	1.717471	0.004513865
Adgrg6	1.699271	0.001197181
Samd4	1.675397	0.010273172
9330159M07Rik	1.660667	1.15E-05
Jak3	1.63525	0.044551073
Pdgfra	1.631516	0.010559449
Rhoj	1.587146	0.02191912
Gbp9	1.551564	0.016920465

Gpx3	1.524564	0.033164946
Smco3	1.50133	0.016920465
Fmod	1.493619	0.036204974
Stc2	1.473412	0.022092441
BC055402	1.428368	0.008721363
Tnnt2	1.386095	0.00013576
Gadd45b	1.373351	0.043939328
Zfp992	1.361492	0.037612097
Igfbp5	1.316104	0.015228443
Antxr2	1.315718	0.00063183
Tmem26	1.292073	0.039181618
Siah3	1.231923	0.033563533
Scn7a	1.225117	0.048696609
Vwf	1.194071	0.006740444
Apln	1.080632	0.009121617

Supplementary Table 2: List of top 103 differentially downregulated genes comparing APB5 versus APB5 plus minocycline treatment

Gene	log2 fold change	P adjusted value
Sprr1a	-9.04199	0.008846
Vmn2r3	-8.21658	1.10E-05
Clec4n	-7.93958	0.000155
Cxcl2	-7.70488	0.000155
Glycam1	-7.38102	3.83E-22
Ereg	-7.15842	0.000371
Cyp4f18	-7.04414	0.001217
Slamf7	-7.01013	0.001791
Wfdc17	-6.44013	0.024246
Lyz2	-6.38848	0.000135
Actg2	-6.27565	0.020973
Apoc2	-6.18156	0.043713
Slpi	-5.84138	0.016696
Trem1	-5.82867	0.02281
Inmt	-5.81387	0.024832
Soat2	-5.72717	0.000905

Lilrb4a	-5.6799	0.002422
Top2a	-5.42154	0.000857
Clec7a	-5.22439	0.001141
Enpp6	-5.13961	7.67E-06
Bik	-5.1275	2.72E-05
Areg	-5.08831	4.07E-10
Cd22	-4.92606	0.001874
Casp12	-4.84015	5.87E-05
Akr1c18	-4.81805	0.038006
Plbd1	-4.79994	0.001481
Treml2	-4.71769	0.008672
H2-Aa	-4.65372	0.006165
Eda2r	-4.64961	0.001485
Cytip	-4.62403	0.000199
Fgf2os	-4.62044	2.45E-24
Tnfaip2	-4.61227	0.009537
Ccdc194	-4.59453	0.000306
Lbp	-4.58184	0.000325
LOC118567872	-4.49609	0.00424
H19	-4.4488	8.20E-09
Fcgr2b	-4.42321	2.36E-05
Abcc3	-4.38651	6.66E-05
Il21r	-4.25619	0.004192
Lgals3	-4.22586	0.009793
Pqlc3	-4.15152	0.001555
Rgs1	-4.11876	0.000169
Clec5a	-4.11843	0.009742
Bcl3	-4.11425	0.00082
Mlana	-4.10862	0.005985
Ms4a6d	-4.10825	0.002443
Ccdc3	-4.08665	5.78E-05
Cnn1	-4.07914	0.002092
Ptgs2	-4.07723	0.004003
C4b	-4.05976	5.28E-06
Cxcl10	-4.04516	4.99E-05

Gxylt2	-4.03876	0.016791
Angptl7	-4.03437	0.022161
Mki67	-4.0156	0.008243
Egr1	-4.01029	0.000224
Myo1f	-3.99374	0.000642
Cd84	-3.98818	0.000901
Adam7	-3.97974	0.005904
Adgre1	-3.9483	6.47E-05
Bcl2a1b	-3.94629	0.000738
Tnfaip8l2	-3.94087	0.010085
Cx3cr1	-3.93583	1.35E-09
Arhgap30	-3.92584	0.000972
Csn3	-3.89477	0.027176
Ccrl2	-3.86785	7.17E-06
Runx3	-3.86476	0.001038
Fbln5	-3.83064	0.001786
Fgl2	-3.80279	0.019472
Vav1	-3.79572	0.002371
Cd48	-3.79474	0.015795
Gfap	-3.76046	0.002843
Plau	-3.74519	0.000209
Casp1	-3.72425	0.000662
Cfi	-3.7125	7.63E-07
Was	-3.68196	0.001201
LOC118567857	-3.66537	0.00147
Cd300lg	-3.63171	0.009537
Egr3	-3.61914	0.015673
Glipr1	-3.61654	0.029819
Ikzf1	-3.60794	0.001182
Il17rb	-3.60512	2.00E-08
Pcolce	-3.59858	0.001054
Nnmt	-3.59808	0.038667
Cdk1	-3.58806	0.004192
Fxyd3	-3.57383	0.000556
Edn2	-3.56104	8.02E-14

Sash3	-3.54485	0.008409
H2-Ob	-3.50961	0.01212
Il1b	-3.49283	0.035553
Ms4a4a	-3.49268	0.00157
LOC118568080	-3.48311	0.001784
Ptafr	-3.48025	0.014526
Lif	-3.47604	0.008664
Cyb5r2	-3.47411	0.007518
Cd52	-3.46403	0.000189
Stx11	-3.46344	0.005694
Aplnr	-3.45651	0.002024
H2-Ab1	-3.45586	3.58E-06
Socs3	-3.45044	0.009606
S100a9	-3.44621	0.016312
Aif1	-3.44478	0.000556
Lyz1	-3.44444	0.001981
Cyp21a2-ps	-3.42018	0.007871

Supplementary Table 3: Scoring of vascular anomalies and fluorescein leakage in the *Pdgfb*^{iECKO} mice at four weeks of age using Fluorescein angiography

	Fluorescein leakage		
MALES	**Right eye**	**Left eye**	**Both eyes**
M	yes	yes	yes
M	no	yes	no
M	no	yes	no
M	no	no	no
M	no	yes	no
M	yes	yes	yes
M	yes	yes	yes
M	yes	yes	yes
M	no	yes	no
M	yes	no	no
% occurrence	**50**	**80**	**40**
FEMALES			

F	yes	no	no
F	no	yes	no
F	no	yes	no
F	yes	optimal	no
F	no	yes	no
F	yes	yes	yes
F	yes	no	no
F	no	no	no
% occurrence	**50**	**50**	**12.5**

ACKNOWLEDGEMENT

I wish to express my deepest gratitude to my supervisor, Prof. Dr. Thomas Langmann for the opportunity to work together and for his supervision, mentorship and motivation for the entire duration of my doctoral studies. This endeavor would not have been possible without Dr. Rashid Khalid who introduced me to Prof. Dr. Langmann when I was looking for an opportunity to advance my studies. I am extremely grateful to my doctoral thesis tutors, Prof. Dr. Gunther Döhlemann and Prof. Dr. Henning Walczak for their incredible advice and input during my research. I could not have taken this journey without the research funding of the Center for Molecular Medicine Cologne (CMMC) and the academic mentorship within the Interdisciplinary Program Molecular Medicine (IPMM).

I would like to thank the past and present members of Prof. Dr. Langmann's working group. Special thanks to Dr. Khalid, Dr. Khan, Dr. Taiwo, Dr. Benke, and Dr. Tabel for their advice and encouragement. I am also thankful to Dr. Anne Wolf for advice and scientific support during my Ph.D. Thanks should go to Dr. Keihani, Dr. Melis and Julia for being wonderful office mates. Thanks to Mandy Hector, Justus and Anna.

To my good and learned friend, Dr. Nils Laudenberg, thank you for the exciting discussions, inspiring stories and fun days outside the lab! Indeed, physical exercises keeps the mind younger! In the words of William Shakespeare, "*To me, fair friend, you can never be forgotten*."

Special thanks to Anja Volkmann and Eva Scheiffert for the administrative and technical assistance, respectively, during my studies.

I would like to acknowledge my parents, Boniface Kinuthia and Teresia Mutanu for their tremendous support since my childhood. I thank my brother, Joseph and sister, Ann.

All glory to God.

ERKLÄRUNG

Ich versichere, dass ich die von mir vorgelegte Dissertation selbstständig angefertigt, die benutzten Quellen und Hilfsmittel vollständig angegeben und die Stellen der Arbeit - einschließlich Tabellen, Karten und Abbildungen -, die anderen Werken im Wortlaut oder dem Sinn nach entnommen sind, in jedem Einzelfall als Entlehnung kenntlich gemacht habe; dass diese Dissertation noch keiner anderen Fakultät oder Universität zur Prüfung vorgelegen hat; dass sie - abgesehen von unten angegebenen Teilpublikationen - noch nicht veröffentlicht worden ist sowie, dass ich eine solche Veröffentlichung vor Abschluss des Promotionsverfahrens nicht vornehmen werde. Die Bestimmungen dieser Promotionsordnung sind mir bekannt. Die von mir vorgelegte Dissertation ist von Herrn Prof. Dr. Thomas Langman betreut worden.

Ich versichere, dass ich alle Angaben wahrheitsgemäß nach bestem Wissen und Gewissen gemacht habe und verpflichte mich, jedmögliche, die obigen Angaben betreffenden Veränderungen, dem Promotionsausschuss unverzüglich mitzuteilen.

Köln, den 29.04.2024 Urbanus Muthai Kinuthia